Doctoral Dissertation

Effects of substrate microstructure and composition on the growth of anodic oxide layers on Ti and its alloys in fluoride-containing electrolytes

(フッ化物含有溶液中にて Ti および Ti 合金に生成する陽極酸化皮膜の成長挙動に及ぼす基板性状の影響)

Min-Su Kim

December 2015

Division of Materials and Manufacturing Science

Graduate School of Engineering,

Osaka University

Contents

Chapter 1 General introduction

1.1 Anodization

Anodization is one of the most investigated electrochemical processes due to ease of operation and low cost. In anodization metal surface is electrochemically oxidized to form oxide layers. Anodic oxide layers can improve corrosion resistance and provides superior design to metal surface. It is well-known that anodization in suitable electrolytes forms nano-structured oxide layers on the surface of metal substrate. Two examples of nano-structured oxide layer formed by anodization are presented in Fig. 1-1; nanoporous oxide on Al and nanotubular oxide on Ti[1, 2)]. Anodic nanoporous oxide layers on Al possess longer history compared to nanotubular oxide layers on Ti.

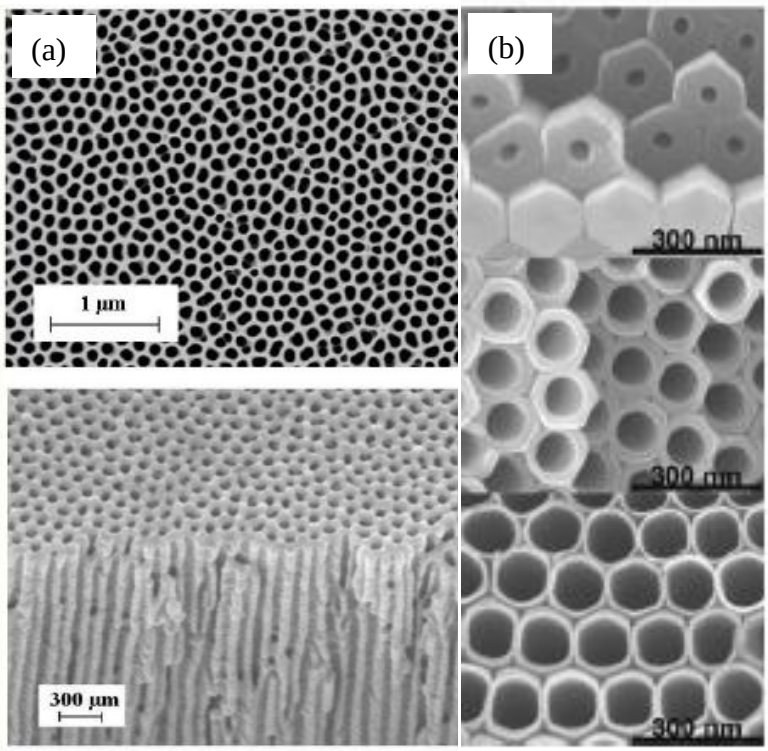

Fig. 1-1 Different morphologies of nanostructures obtained by electrochemical anodization : (a) Aluminum and (b) Titanium[1, 2)].

The fundamental model for nanoporous oxide layers was reported already in 1953 by Keller et al.[3]. Significant progress of pore arrangement in nanoporous oxide layer was achieved by Masuda et al. in 1995[4]. They successfully fabricated highly ordered nanoporous oxide layers on Al. It was reported that these structures can be used as templates for the fabrication of nanostructures such as nanowires, nanorods and nanotubes.

On the other hand, the formation of nanotubular oxide layers on Ti and Ti alloys was firstly reported by Assefpour-Dezfuly et al. in 1984[5] and Zwilling et al. in 1999[6, 7]. Since then, numerous research efforts have been dedicated for anodic TiO_2 nanotubular layer as TiO_2 can be used in various fields such as photocatalyst, dye-sensitized solar cells, gas sensors and electrochromic devices[8-11].

So far, in addition to Al and Ti, the formation of nanoporous and nanotubular oxide layers has been reported for various valve metals such as Zr[12-14], Nb[15-17], W[18-20], Ta[21-23], Hf[24-26], V[27] as well as several different Ti-based alloys[28-34].

1.2 Growth of nanotubular oxide layer on Ti

It is reported that nanoporous Al_2O_3 layer is often formed in "fluoride-free" acidic electrolytes such as phosphoric[35], chromic[36] and sulfuric acid[37]. On the other hand, anodization in the acidic electrolytes forms a flat compact oxide layer on Ti as illustrated in Fig. 1-2 (a)[38]. The formation of TiO_2 layer can be described by the following anodic reactions;

$$Ti + 2H_2O \rightarrow TiO_2 + 4H^+ + 4e^- \quad (1\text{-}1)$$

The corresponding cathodic reaction occurs at the counter electrode;

$$4H_2O + 4e^- \rightarrow 4H_2 + 4OH^- \quad (1\text{-}2)$$

The applied potential builds an electric field across the oxide, which causes inward transport of O^{2-} ions and outward transport of Ti^{4+} ions in the oxide. This leads to the

formation of compact TiO_2 layer.

TiO_2 nanotubular layer is essentially formed in fluoride-containing electrolytes such as HF and NH_4F. With fluorides, water-soluble $[TiF_6]^{2-}$ complex is formed in addition to the above-mentioned anodic reaction as illustrated in Fig. 1-2 (b). The complexation occurs with ejected Ti^{4+} ions at the interface between oxide and electrolyte;

$$Ti^{4+} + 6F^- \rightarrow [TiF_6]^{2-} \quad (1\text{-}3)$$

The chemical dissolution of formed oxide also occurs;

$$TiO_2 + 6HF \rightarrow [TiF_6]^{2-} + 2H_2O + 2H^+ \quad (1\text{-}4)$$

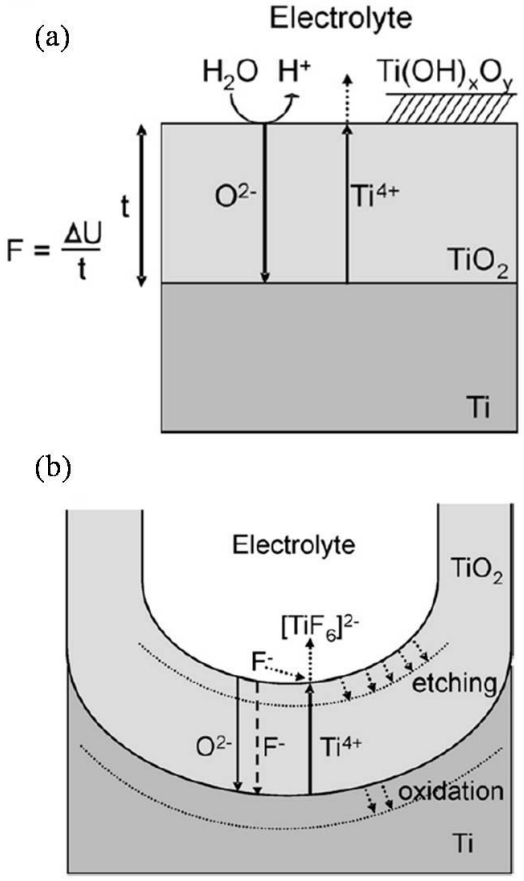

Fig. 1-2 Growth of TiO_2 layer (a) without fluoride ions and (b) in presence of fluoride ions[38].

A typical current-time curve for nanotube formation is illustrated in Fig. 1-3 (a)[38] as

the red solid line. The curve can be devided into three stages. In the first stage, a compact TiO_2 layer is formed according to a classic high field model. The current exhibits significant decay due to increasing TiO_2 layer. In the second stage, nanoscopic pores are formed in the initial compact TiO_2 layer and form nanotubes from the initial compact TiO_2 layer (defined as initiation layer and described in the chapter 2). In the third stage a steady state situation is established where TiO_2 nanotubular layer continuously grows with a certain speed. The formation and growth of TiO_2 nanotubular layer are affected by electrochemical parameters. More detail information on the parameters is provided in the next section.

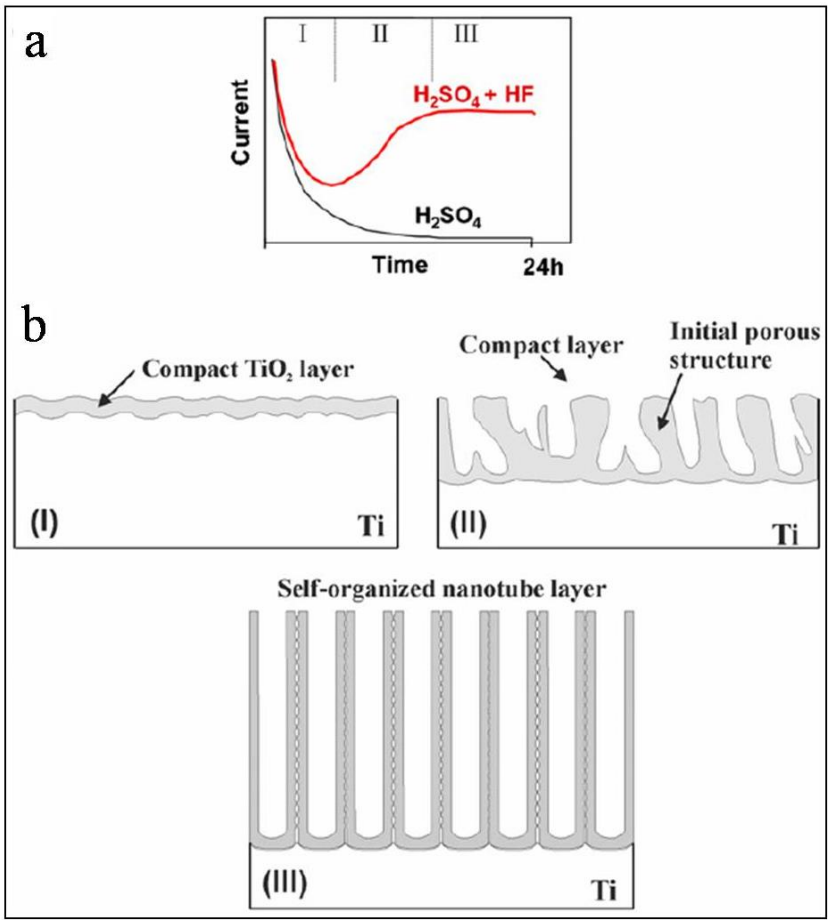

Fig. 1-3 (a) Characteristic of current-time curves for Ti anodization with and without fluoride ions in the electrolyte, (b) corresponding variation of TiO_2 morphology[38].

1.3 Effect of anodization parameters

1.3.1 Applied voltage

One of the most straightforward electrochemical parameters that are variable for anodization is applied voltage. As mentioned above anodic oxides formed in fluoride-free electrolytes exhibit flat and compact structure. It is well-known that the thickness of compact oxide layers formed on Ti increases with increasing applied voltage and the color of anodizaed surfaces changes depending on the thickness of compact oxide layer, as listed in Table 1-1[39]. The color of the surface is attributed to the interference of light through the oxide layer. On the other hand, the thickness of TiO_2 nanotubular layer also increases with increasing applied voltage. Macak et al. reported the effect of applied potential on the growth of TiO_2 nanotubular layer[40]. Figure 1-4 shows the thickness of TiO_2 nanotubular layers formed in a glycerol based electrolyte. The thickness of the layer clearly increases with increasing applied potential upto 20 V and then remains constant for higher potentials. They ascribed non-potential dependence of the thickness to significant thinning of nanotube walls due to chemical dissolution of the oxide. On the one hand, the chemical dissolution of formed TiO_2 is one of the important factors for nanotube formation as explained above. On the other hand, the chemical dissolution strongly restricts the thickness of TiO_2 nanotubular layers. Both chemical dissolutions continuously take place during anodization and affect the morphology of TiO_2 nanotubular layer. In other words, the morphology of TiO_2 nanotubular layer can be affected by chemical reaction. The effect is discussed in terms of anodization time.

Table 1-1 Color of oxide layers formed by anodization at different voltages. The data are taken from Ref [39] and re-arranged.

Applied voltage (V)	Color
2	Silver
6	Light brown
10	Golden brown
15	Purple blue
20	Dark blue
25	Sky blue
30	Pale blue
35	Steel blue
40	Light olive
45	Greenish yellow
50	Lemon yellow
55	Golden
60	Pink
65	Light purple
75	Blue

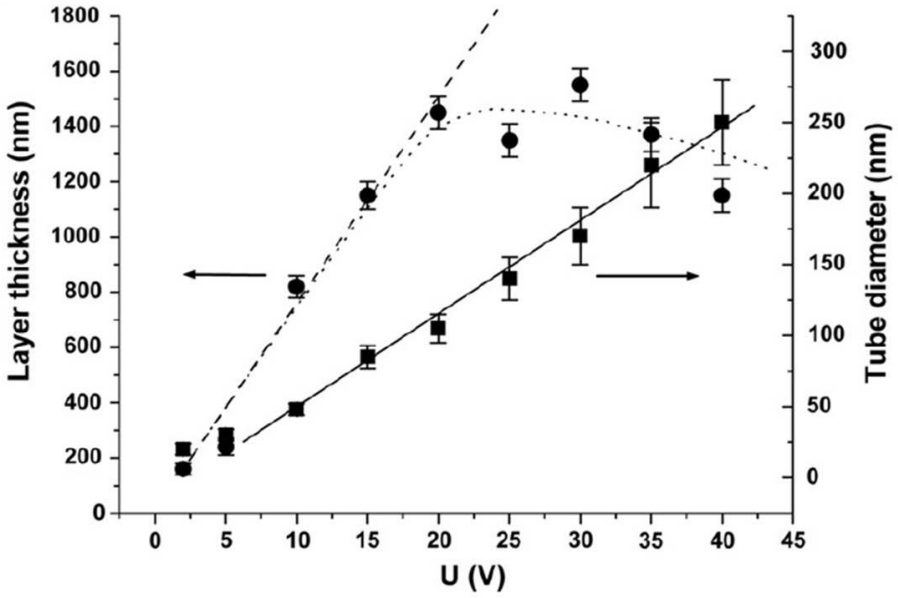

Fig. 1-4 Variation of tube diameter and thickness in dependence of the anodization potential in a glycerol containing 0.27 M NH_4F and deionized water[40].

1.3.2 Anodization time

Figure 1-5 shows the thickness of TiO_2 nanotubular layer formed in glycerol

containing water and ammonium fluoride[40] as a function of anodization time. The thickness steeply increases with time until 8 hours. Then it levels off at a constant value, that is, extended anodization does not increase the thickness of TiO_2 nanotubular layer. This can be explained in terms of the chemical dissolution of formed TiO_2 nanotubular layer. As described in 1.2, the chemical dissolution of formed TiO_2 layer at the bottom of nanotubes by fluorides is prerequisite for the growth of nanotubes. As the chemical dissolution occurs not only at nanotube bottoms but also at nanotube walls, the thickness of nanotube wall becomes thinner with time. After a certain time, nanotube walls near the top surface of nanotubular layer is dissolved completely, implying that the nanotube layer thickness is determined by the competition between the nanotube growth rate at nanotube bottom and the chemical dissolution rate at the top surface of nanotube layer. That is, in the early stage of anodization, the nanotube growth rate is faster compared to the chemical dissolution, leading to the steady growth of nanotubes that increases the thickness of TiO_2 nanotubular layer. On the growth process of nanotubes, the growth rate becomes decreased due to the increasing diffusion path of fluoride species to the nanotube bottom, causing the increase in layer thickness slower and slower. The increase in layer thickness becomes terminated when a steady-state situation – the nanotube growth rate and the chemical dissolution rate are balanced – is established. As described here, the chemical dissolution strongly affects the growth and morphology of TiO_2 nanotubular layer. The finding provides the strategy to control the morphology of nanotubular layer that is discussed next.

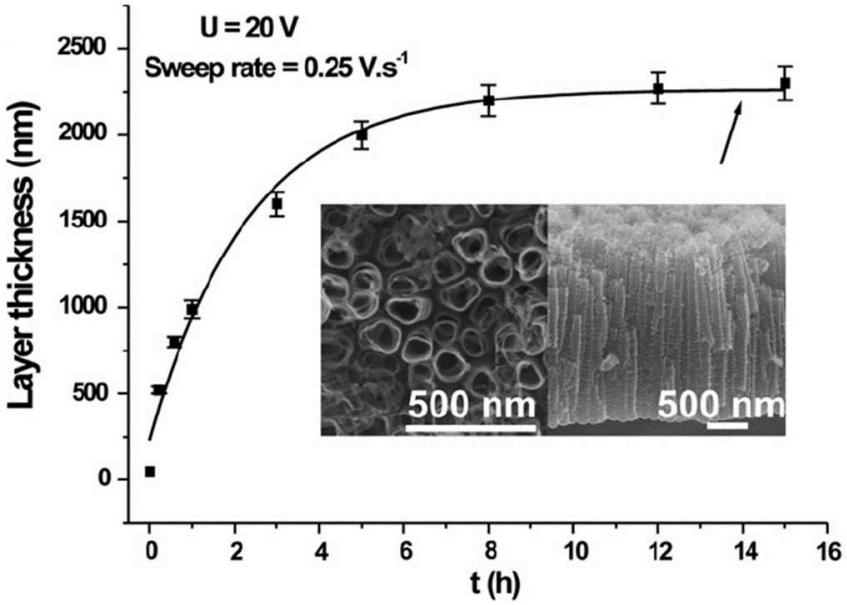

Fig. 1-5 Thickness evolution of TiO_2 nanotubular layer formed in glycerol containing 0.27M NH_4F and deionized water with time[40].

1.3.3 Effect of electrolytes

As described in 1.3.2, the chemical dissolution is the important factor to control the morphology of TiO_2 nanotubular layer. The present section reviews how the chemical dissolution has been controlled. As described in 1-1, the formation of TiO_2 nanotubular layer was firstly reported by Assefpour-Dezfuly et al. and Zwilling et al.[5-7]. They anodized Ti and Ti alloy in fluoride-containing aqueous electrolytes. Then Gong et al[41]. and Beranek et al[42]. also showed anodization of Ti in fluoride-containing aqueous electrolytes to form nanotubular oxide layers. In all cases, however, the thickness of TiO_2 nanotubular layer was limited upto several hundred nanometers. The electrolytes used for the anodization are in acidic state. Figure 1-6 demonstrated how pH of electrolyte affects the chemical dissolution of TiO_2 in fluoride-containing electrolyte[43]. It is clear that the dissolution rate decreases with increasing pH. Therefore using electrolyte with high pH can suppress the dissolution, which can result in the increase of layer thickness. Figure 1-7 presents SEM image of a TiO_2 nanotubular layer formed in neutral ammonium sulfate

electrolyte containing ammonium fluoride[44]. It is noted that the anodization was carried out at the same potential as that performed in an acidic sulfuric acid electrolyte containing a small amount of hydrofluoric acid where TiO_2 nanotubular layer with the thickness of approximately 500 nm was grown.

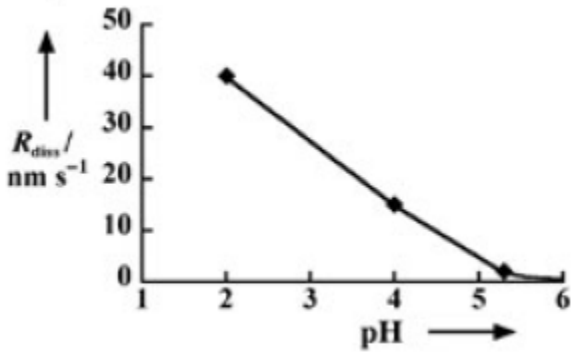

Fig. 1-6 Variation of chemical dissolution rate of TiO_2 layer in fluoride-containing electrolyte[43].

It is obvious that TiO_2 nanotubular layer formed in the neutral electrolyte show in Fig. 1-7 is around 2.5 μm thick, that is, the nanotubular layer in the neutral electrolyte is thicker compared to that in the acidic electrolyte. In neutral electrolyte, the chemical dissolution at the top surface of TiO_2 nanotubular layer is suppressed due to high pH of bulk electrolyte. At nanotube bottoms, on the other hand, pH of electrolyte becomes lower due to formed H^+ according to equations (1-1). This creates pH gradient within nanotubes as shown in Fig. 1-8; higher pH is kept near nanotube mouth while lower pH is established near nanotube bottom. Therefore the dissolution of TiO_2 at nanotube bottoms occurs at a relatively higher rate, which helps to keep barrier layer at nanotube bottom at a moderate thickness. This contributes the continuous growth at nanotube bottom in neutral electrolyte.

For both cases as acidic and neutral electrolytes, the important key to grow nanotubular oxide layers on Ti is the diffusion of fluoride ions to the bottom of nanotubes.

Macak et al. achieved higher aspect ratio of nanotubes in viscous glycerol containing ammonium fluoride compared to in the neutral ammonium sulfate electrolyte containing ammonium fluoride[45]. Albu et al. also reported the growth of 250 μm long TiO_2 nanotubes under an optimized condition in ethylene glycol based electrolyte[46]. These results demonstrate the importance of the diffusion of fluoride species. The authors also investigated the influence of the type of organic electrolyte on the growth of TiO_2 nanotubes[47] and revealed that the growth rate of nanotubes is strongly affected by the type of ethylene glycol, that is, the growth is significantly suppressed in diethylene glycol, triethylene glycol, tetraethylene glycol and polyethylene glycol compared to ethylene glycol. Furthermore, the authors carried out anodization of Ti in ethylene glycol containing ammonium hexafluoro-titanate or ammonium hezafluoro-zirconate instead of ammonium fluoride and showed that the type of fluoride also strongly affects the growth of TiO_2 nanotubes. As the author has described in the present section, the electrochemistry has the great impact on the growth of TiO_2 nanotubes.

As mentioned above, the electrochemical parameters affect the growth of nanotubular oxide layers. However, electrochemical reactions occurred during the anodization are the interaction between electrolyte and metallic substrate. Therefore, substrates used for anodization can affect the growth of nanotubes. In the next section, the researches that examined the effect of substrate are reviewed.

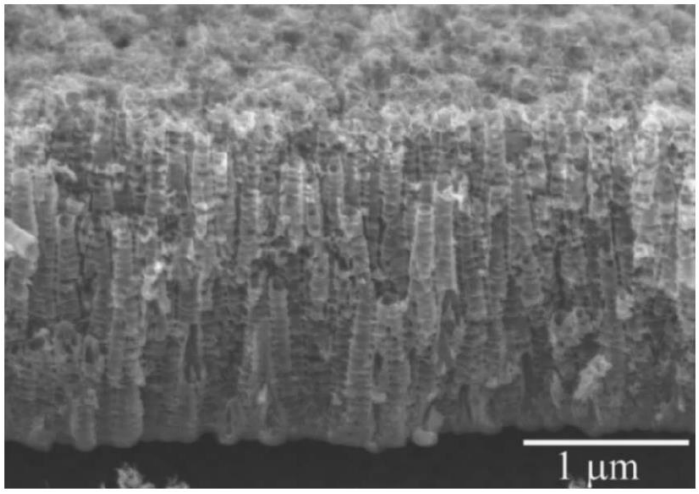

Fig. 1-7 Cross-sectional SEM image of TiO_2 layers formed on Ti at 20 V for 2 hours in 1 M $(NH_4)_2SO_4$ and 0.5 wt. % NH_4F[44].

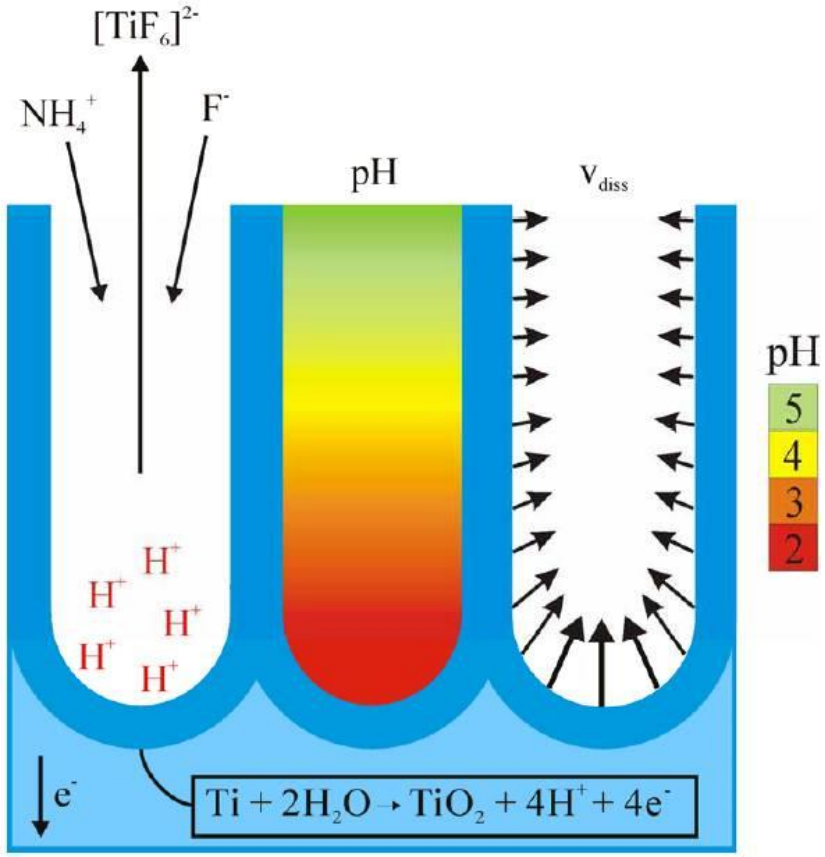

Fig. 1-8 Schematic illustration on oxidation and dissolution reactions occur at the tube bottom (left), the pH variation in a tube (middle) and dissolution rates in the tube wall[43].

1.4 Effect of alloying element in Ti-based alloys

The fabrication of nanotubular oxide layers in fluoride-containing electrolytes has been achieved not only on Ti but also the other metals such as Zr[12-14], Nb[15-17], W[18-20], Ta[21-23], Hf[24-26], Fe[48, 49] and Co[50]. On the other hand, alloys are also concerned as substrates for anodization. Alloy anodization was carried out by Macak et al. for commercial Ti6Al4V and Ti6Al7Nb[51]. They reported that inhomogeneous oxide layers are formed on the alloys due to selective dissolution of one phase or different reaction rates on different phases. Since then, the alloy anodization has been tried using commercial and designed Ti alloys.

Tsuchiya et al.[52] studied nanotubular oxide layers formed on Ti-Zr alloys with various Zr contents. The tube diameter decreases with increasing Zr content whereas the length of tube increases with Zr content. Jang et al.[53] reported nanotubular oxide layers formed on Ti-Nb alloys with different Nb contents. In the Ti-Nb alloy the crystal structure changed from α-phase to β-phase with increasing Nb content, which led to the inhomogeneous growth of oxide layer[51] although nanotubular oxide layers were formed on all substrates. Furthermore, it was reported that the thickness of nanotubular oxide layer on Ti-Nb alloy increased with increasing Nb content in substrate. Alloy anodization has been considered not only to examine how the chemical composition of alloy affect the morphology of anodic oxide layer but also to improve the properties of TiO_2 nanotubular layer by doping of secondary element. Nah et al.[54] reported the formation of W-doped TiO_2 nanotubular layers on Ti-W alloys. The nanotubular oxide layer thickness did not significantly increase with increasing W content from 0.2 at.% to 9 at.%. However, W-doped TiO_2 nanotubular layer improved electrochromic properties of TiO_2 nanotubular oxide layers with increasing W content.

Although nanotube oxide growth has been investigated mainly for alloys consisting of

titanium and the other valve metal, recently the alloys consisting of titanium and transition metal have also been used for anodization.

Mohapatra et al.[55] studied the nanotubular oxide layers formed on Ti-8Mn alloy in various electrolytes. The Ti-Mn alloy consisted of two different phases; α-phase and β-phase. Anodization of the alloy in fluoride-containing ethylene glycol resulted in the formation of nanotubular oxide layer on both phases whereas in the other electrolytes no nanotubes were formed. Ma et al.[56] reported that anodization of binary Ti-Cu alloy led to different nanotubular structures; highly ordered nanotube array on Cu-rich phase and disordered nanotube bundles on Ti-rich phase. Compared to alloys consisting of valve metals, however, the anodization of the alloys that contain transition metal has not been fully examined yet.

1.5 The purpose and structure of this thesis

Research on nanotubular oxide layers has been developed around TiO_2 nanotubular layer due to various applications, such as photocatalysis, dye-sensitized solar cells, gas sensors, electrochromic devices and surface coatings on biomedical implants[8-11), 57]. In order to improve the properties, the control of the morphology of TiO_2 nanotubular layer should be desired. Therefore electrochemical parameters have been extensively tailored to optimize the morphology. Instead, the effect of substrate microstructure on the morphology and growth of nanotubular oxide layer has not been fully focused. Furthermore, although alloy anodization is often examined recently, almost all works target alloys consisting of valve metals. In other words, alloys containing transition metal have not been studied well. In the present work the author examined the effect of substrate microstructure and composition on the growth of anodic oxide layers on pure Ti and various Ti alloys that contain the transition metals such as Fe, Co and Ni.

This thesis consists of 7 chapters.

Chapter 1 gives the background and purpose of this study.

In chapter 2, the effects of substrate microstructure on the growth of TiO_2 nanotubular layer are examined.

Chapter 3 shows how Ni content in Ti-Ni alloy strongly affects the growth and morphology of anodic oxide layers.

Chapter 4 provides the growth behavior of anodic oxide layers on Ti-Fe alloys and demonstrates how electrochemistry has strong influences on the growth and morphology of anodic oxide layers.

Chapter 5 give a comparison on the morphology of anodic oxide layer on Ti alloys with different alloying elements.

Chapter 6 presents the effect of Ti-Ni alloy microstructure on the growth of anodic oxide layers.

In chapter 7 the findings of this thesis are summarized.

References:

1) G.E. J. Poinern, X. Le, M. Hager, T. Becker, D. Fawcett, Am. J. Biomed. Eng., **3** (2013) 119.

2) D. Kowalski, D. Kim, P. Schmuki, Nano Today, **8** (2013) 235.

3) F. Keller, M. S. Hunter, and D. L. Robinson, J. Electrochem. Soc., **100** (1953) 411.

4) H. Masuda, K. Fukuda, Science, **268** (1995) 1466.

5) M. Assefpour-Dezfuly, C. Vlachos, E. H. Andrews, J. Mater. Sci., **19** (1984) 3626.

6) V. Zwilling, M. Aucouturier, E. Darque-Ceretti, Electrochim. Acta, **45** (1999) 921.

7) V. Zwilling, E. Darque-Ceretti, A. Boutry-Forveille, D. David, M. Y. Perrin1, M. Aucouturier, Surf. Interface Anal., **27** (1999) 629.

8) J.G. Yu, G.P. Dai, B. Cheng, J. Phys. Chem. C, **114** (2010) 19378.

9) G.K. Mor, K. Shankar, M. Paulose, O. K. Varghese and C. A. Grimes, Nano Lett., **6** (2006) 215.

10) H.F. Lu, F. Li, G. Liu, Z. Chen, D. Wang, H. Fang, G. Lu, Z. Jiang, H. Cheng, Nanotechnology, **19** (2008) 405504.

11) S. Berger, A. Ghicov, Y.C. Nah, P. Schmuki, Langmuir, **25** (2009) 4841.

12) J. Zhao, X. Wang, R. Xu, F. Meng, L. Guo, Y. Li, Mat. Lett., **62** (2008) 4428.

13) S. Berger, J. Faltenbacher, S. Bauer, P. Schmuki, Phys. Stat. Sol. RRL, **2** (2008) 102.

14) L. Guo, J. Zhao, X. Wang, X. Xu, H. Liu, Y. Li, Int. J. Appl. Ceram. Technol., **6** (2009) 636.

15) J. Choi, J.H. Lim, J. Lee, K.J. Kim, Nanotechnology, **18** (2007) 055603.

16) W. Wei, S. Berger, C. Hauser, K. Meyer, M. Yang, P. Schmuki, Electrochem. Commun., **12** (2010) 1184.

17) I. Sieber, H. Hildebrand, A. Friedrich, P. Schmuki, Electrochem. Commun., **7** (2005) 97.

18) N.R. de Tacconi, C.R. Chenthamarakshan, G. Yogeeswaran, A. Watcharenwong, R.S. de Zoysa, N.A. Basit, K. Rajeshwar, J. Phys Chem. B, **110** (2006) 25347.

19) H. Tsuchiya, J.M. Macak, I. Sieber, L. Taveira, A. Ghicov, K. Sirotna, P. Schmuki, Electrochem. Commun., **7** (2005) 295.

20) M. Yang, N.K. Shrestha, P. Schmuki, Electrochem. Commun., **11** (2009) 1908.

21) N.K. Allam, X.J. Feng, C.A. Grimes, Chem. Mater., **20** (2008) 6477.

22) W. Wei, J.M. Macak, P. Schmuki, Electrochem. Commun., **10** (2008) 428.

23) I. Sieber, P. Schmuki, J. Electrochem. Soc., **152** (2005) C639.

24) S. Berger, F. Jakubka, P. Schmuki, Electrochem. Sol. State Lett., **12** (2009) K45.

25) X. Qiu, J. Howe, M. Cardoso, O. Polat, W. Heller, M. Paranthaman, Nanotechnology, **20** (2009) 455601.

26) H. Tsuchiya, P. Schmuki, Electrochem. Commun., **7** (2005) 49.

27) Y. Yang, S.P. Albu, D. Kim, P. Schmuki, Angew. Chem. Int. Ed., **50** (2011) 9071.

28) S. Grigorescu, C. Ungureanu, R. Kirchgeorg, P. Schmuki, I. Demetrescu, Appl. Surf. Sci., **270** (2013) 190.

29) B. Luo, H. Yang, S. Liu, W. Fu, P. Sun, M. Yuan, Y. Zhang, Z. Liu, Mater. Lett., **62** (2008) 4512.

30) V.S. Saji, H.C. Choe, W.A. Brantley, Acta Biomaterialia, **5** (2009) 2303.

31) B. Luo, H. Yang, S. Liu, W. Fu, P. Sun, M. Yuan, Y. Zhang, Z. Liu, Mater. Lett., **62** (2008) 4512.

32) E. Matykina, J.M. Hernandez-López, A. Conde, C. Domingo, J. De Damborenea, M.A. Arenas, Electrochim. Acta, **56** (2011) 2221.

33) Y.Q. Liang, X.J. Yang, Z.D. Cui, S.L. Zhu, J. Mater. Res., **24** (2009) 3647.

34) K. Lee, W.G. Kim, J.Y. Cho, S.W. Eun, H.C. Choe, Trans. Nonferrous Met. Soc. China, **19** (2009) 857.

35) H. Masuda, K. Yada, A. Osaka, Jpn. J. Appl. Phys., **37** (1998) L1340.

36) W.J. Stępniowski, M. Michalska-Domańska, M. Norek, T. Czujko, Mater Lett, **117** (2014) 69.

37) G.D. Sulka, S. Stroobants, V. Moshchalkov, G. Borghs, J.P. Celis, J. Electrochem. Soc., **149** (2002) D97.

38) J.M. Macak, H. Tsuchiya, A. Ghicov, K. Yasuda, R. Hahn, S. Bauer, P. Schmuki, Curr. Opin. Solid State Mater., **11** (2007) 3.

39) A.K. Sharma, Thin Solid Films, **208** (1992) 48.

40) J.M. Macak, H. Hildebrand, U. Marten-Jahns, P. Schmuki, J. Electroanal. Chem., **621** (2008) 254.

41) D.W. Gong, C.A. Grimes, O.K. Varghese, W. Hu, R.S. Singh, Z. Chen, E.C. Dickey, J. Mater. Res., **16** (2001) 3331.

42) R. Beranek, H. Hildebrand, P. Schmuki, Electrochem. Solid-State Lett., **6** (2003) B12.

43) J.M. Macak, H. Tsuchiya, P. Schmuki, Angew. Chem. Int. Ed., **44** (2005) 2100.

44) V. Taveira, J.M. Macak, H. Tsuchiya, L.F.P. Dick, P. Schmuki, J. Electrochem. Soc., **152** (2005) B405.

45) J.M. Macak, H. Tsuchiya, L. Taveira, S. Aldabergerova, P. Schmuki, Angew. Chem. Int. Ed. **44** (2008) 7463.

46) S.P. Albu, A. Ghicov, J.M. Macak, P. Schmuki, phys. stat. sol. (RRL), **1** (2007) R65.

47) H. Tsuchiya, M.-S. Kim, Y. Otani, Y. Shimizu, S. Fujimoto, Proc. Of 24th Int. Symp. Proc. Fab. Adv. Mater. (2015) 722.

48) S.P. Albu, A. Ghicov, P. Schmuki, Phys. Stat. Sol. (RRL), **3** (2009) 64.

49) Z. Zhang, M.F. Hossain, T. Takahashi, Mater. Lett., **64** (2010) 435.

50) C.Y. Lee, K. Lee, P. Schmuki, Angew. Chem.-Int. Ed., **52** (2013) 2077.

51) J.M. Macak, H. Tsuchiya, L. Taveira, A. Ghicov, P. Schmuki, J. Biomed. Mater. Res. A,

75 (2005) 928.

52) H. Tsuchiya, T. Akaki, J. Nakata, D. Terada, N. Tsuji, Y. Koizumi, Y. Minamino, P. Schmuki, S. Fujimoto, Electrochim. Acta, **54** (2009) 5155.

53) S.H. Jang, H.C. Choe, Y.M. Ko, W.A. Brantley, Thin Solid Films, **517** (2009) 5038.

54) Y.C. Nah, A. Ghicov, D. Kim, S. Berger, P. Schmuki, J. Am. Chem. Soc., **130** (2008) 16154.

55) S.K. Mohapatra, K.S. Raja, M. Misra, V.K. Mahajan, M. Ahmadian, Electrochim. Acta, **53** (2007) 590.

56) Q. Ma, S.J. Liu, L.Q. Weng, Y. Liu, B. Liu, J. Alloys Compd., **501** (2010) 333.

57) K. Das, S. Bose, A. Bandyopadhyay, J. Biomed. Mater. Res. A, **90** (2009) 225.

Chapter 2 Growth of TiO_2 nanotubular layers on Ti substrates with different microstructures

2.1 Introduction

Nanoporous aluminum oxide layers formed by anodization have been widely studied for more than a half century[1, 2] and used as templates for the fabrication of nanostructured materials such as nanowires, nanorods, nanotubes, nanodots[3, 4]. More recently the formation of self-organized anodic nanotubular oxide layers on Ti and Ti alloys in fluoride containing electrolytes was reported by Assefpour-Dezfuly et al and Zwilling et al[5-7]. Since then, nanotubular oxide layers have been formed on various valve metals such as Zr[8], Nb[9], W[10], Ta[11], Hf[12], Co[13] as well as several Ti alloys[14-18] and various applications of the nanotubular oxide layers have been proposed due to their excellent physical and chemical properties. Extensive research efforts have revealed that anodization parameters such as temperature, applied voltage and electrolyte can strongly affect the growth and morphology of anodic nanotubular oxide layers. For examples, the thickness and diameter of nanotubular oxide layers increased with increasing anodization temperatures. The increased H_2O concentration in organic electrolytes decreased the thickness of oxide layers while it increased the diameter of nanotubular oxide layers. Additionally, it was reported that the tube diameter and thickness have increased with increasing applied voltage[19]. Recently not only the anodization parameters but also microstructures of substrate have attracted much attention[20, 21].

In the present chapter, the author examined the morphology and growth of anodic oxide layers on pure Ti with different microstructures controlled by accumulative roll-bonding (ARB) process and various heat-treatments in order to clarify the effect of

substrate microstructure on the growth of TiO_2 nanotubular layer.

2.2 Experimental

Materials used were pure Ti sheets (purity : 99.5%). Prior to the ARB process or heat-treatment, all samples were homogenized at 500 ℃ for 12 hours under an air atmosphere. Figure 2-1 schematically presents the ARB process[22]. As proposed in the literature, two Ti sheets were ground and then degreased with acetone. The Ti sheets were stacked and rolled with 50% reduction in thickness at room temperature by a conventional rolling process. After the 50% reduction, the roll-bonded sheet was cut in half-length. The sectioned samples were again surface-treated, stacked and roll-bonded. This process was repeated upto 6 cycles. On the other hand, some samples were heat-treated at 500 ℃ and 900 ℃ for various durations in different atmospheres after the homogenization.

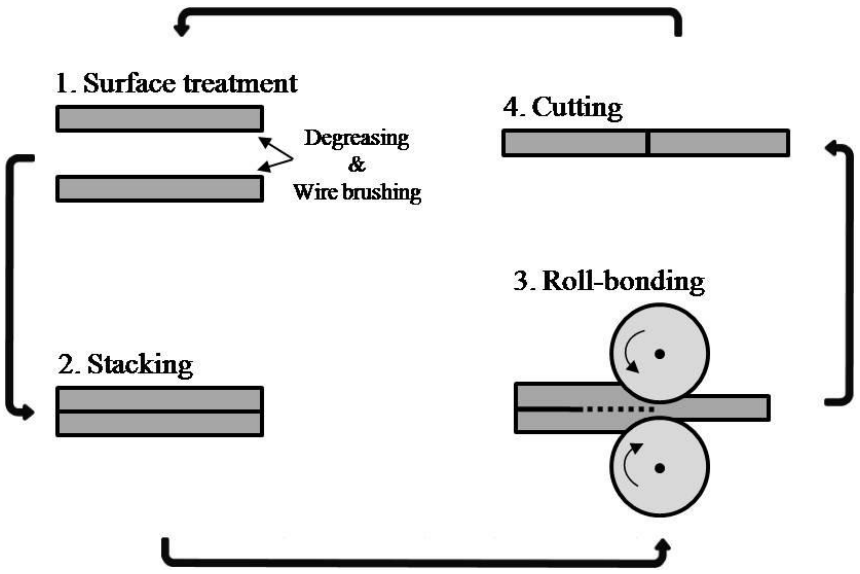

Fig. 2-1 Schematic illustration of the accumulative roll-bonding (ARB) process[22].

After the ARB process or heat-treatment, all samples were ground with SiC abrasive paper and then, mirror-finished with diamond paste. Prior to electrochemical anodization,

the samples were ultra-sonicated in acetone, isopropanol and methanol, successively, finally followed by rinsing with deionized water. The electrochemical setup consisted of a two-electrode configuration with the treated Ti substrate as a working electrode and a platinum plate as a counter electrode. The anodization was carried out in an ethylene glycol electrolyte containing 0.05 M NH_4F and 2.0 wt.% H_2O at 50 V for 3 hours. For anodization voltage increased from 0 V to a desired voltage with the voltage ramp rate of 1 Vs^{-1} and then was kept at the voltage. After the anodization, the samples were washed with ethanol. The surface morphology of anodized samples was investigated with field-emission scanning electron microscope (FE-SEM, JEOL JSM-7001FA). Cross-sectional images were taken from mechanically scratched samples where several pieces of formed oxide layers lifted off at the interface between the substrate / oxide layer.

2.3 Results and discussion

2.3.1 Growth of anodic oxide layer on heat-treated Ti substrate

In the present work, TiO_2 nanotubular oxide layers were formed in a fluoride-containing ethylene glycol electrolyte by anodization of Ti substrates with different microstructures that were controlled by the heat-treatment or the ARB process. The author describes the effects of heat-treatment in different atmospheres on the morphology and growth of TiO_2 nanotubular layers in the present section. Figure 2-2 exhibits the microstructures of Ti substrates heat-treated in an air atmosphere at 500 ℃ and 900 ℃ for various durations. It is clear that at 500 ℃ the average grain size slightly increased with heat-treatment duration while at 900 ℃ the grain growth clearly occurred, that is, the average grain size drastically increased at 900 ℃ with time.

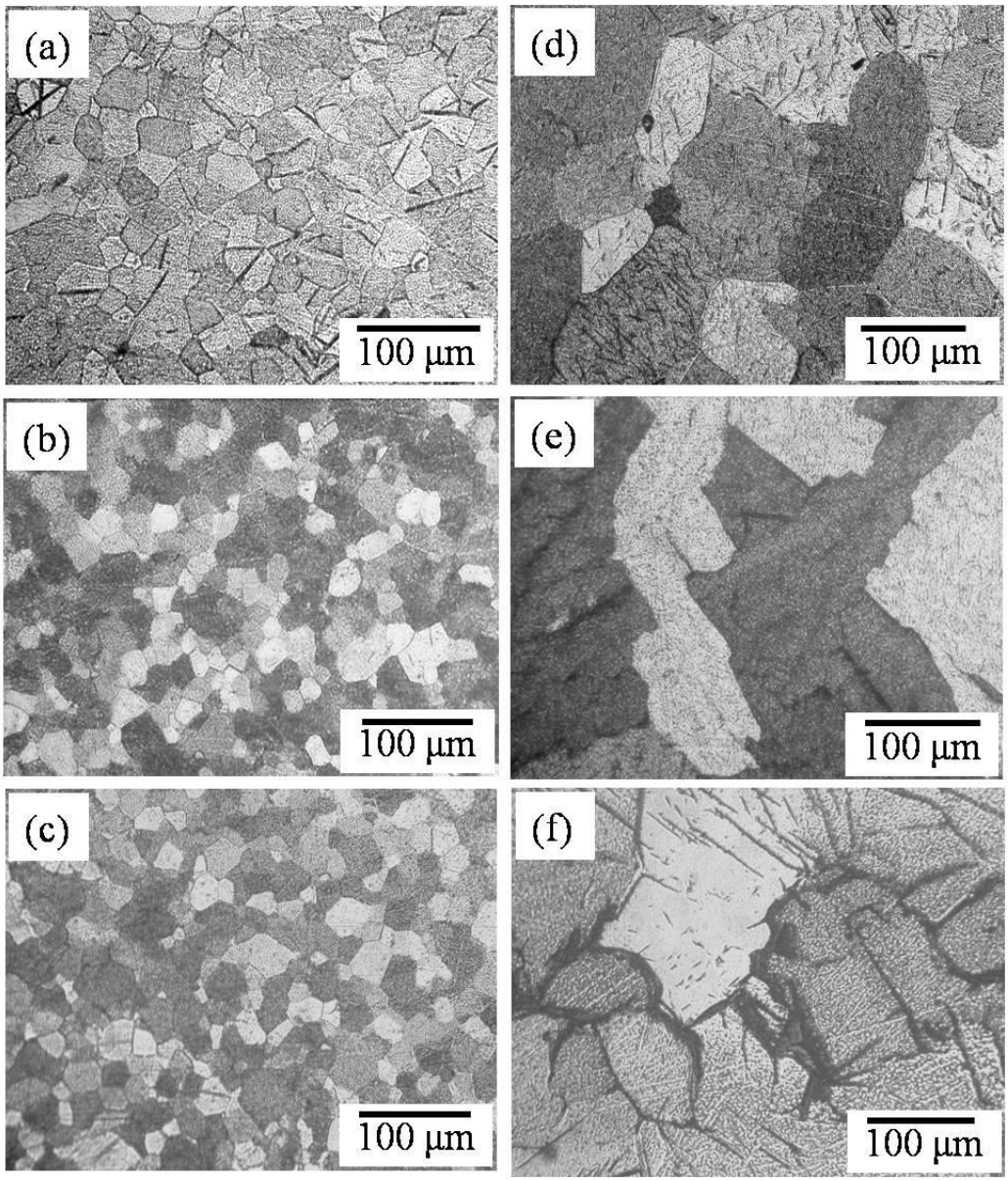

Fig. 2-2 Microstructures of Ti substrates after heat-treatment in an air atmosphere at (a, b, c) 500 ℃ and (d, e, f) 900 ℃. The heat-treatment durations were (a, d) 3 h, (b, e) 12 h and (c, f) 48 h.

Figure 2-3 shows the current-time curves recorded for the air heat-treated Ti substrates at 50 V for 3 hours in the ethylene glycol containing 0.05 M NH_4F and 2.0 wt.% H_2O. As apparent from Fig. 2-3, similar current behavior is observed for all Ti substrates; the current drastically decreases in the early stage of anodization, then increases once and finally decreases again to a steady state current. This current behavior is typical for

nanotubular anodic oxide formation[23]. Furthermore, the current varies depending on the heat-treatment conditions, indicating that the growth of anodic oxide layer is affected by the heat-treatment conditions.

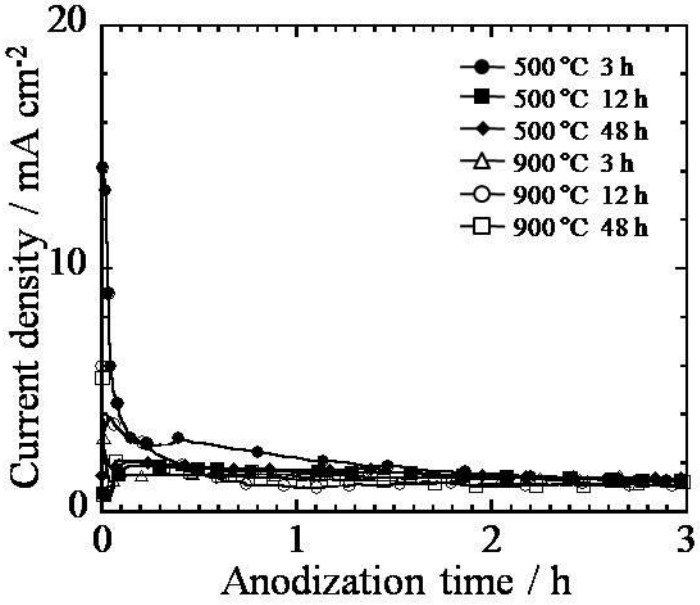

Fig. 2-3 Current-time curves recorded at 50 V for 3 h in the ethylene glycol containing 0.05 M NH_4F and 2.0 wt.% H_2O on air heat-treated Ti substrates.

Top-view and cross-sectional morphologies of resulting oxide layers are presented in Figs. 2-4 and 2-5, respectively. It is obvious from the cross-sectional images that the oxide layers exhibit nanotubular morphology although such nanotubular structure is not observed from the top-views due to the remaining initiation layer as described in the chapter 1. The pore diameter on the initiation layers is slightly different depending on the heat-treatment conditions. However, much larger difference can be observed in the thickness of anodic oxide layer. The thickness of the oxide layers is estimated from the cross-sections and summarized in Fig. 2-6. The thickness of nanotubular oxide layers formed on Ti substrates heat-treated at 500 ℃ is larger compared to those heat-treated at 900 ℃. Furthermore, the thickness decreases with increasing the heat-treatment duration for both cases. The

thickness variations follow the electric charge generated during anodization; higher charge leads to higher thickness.

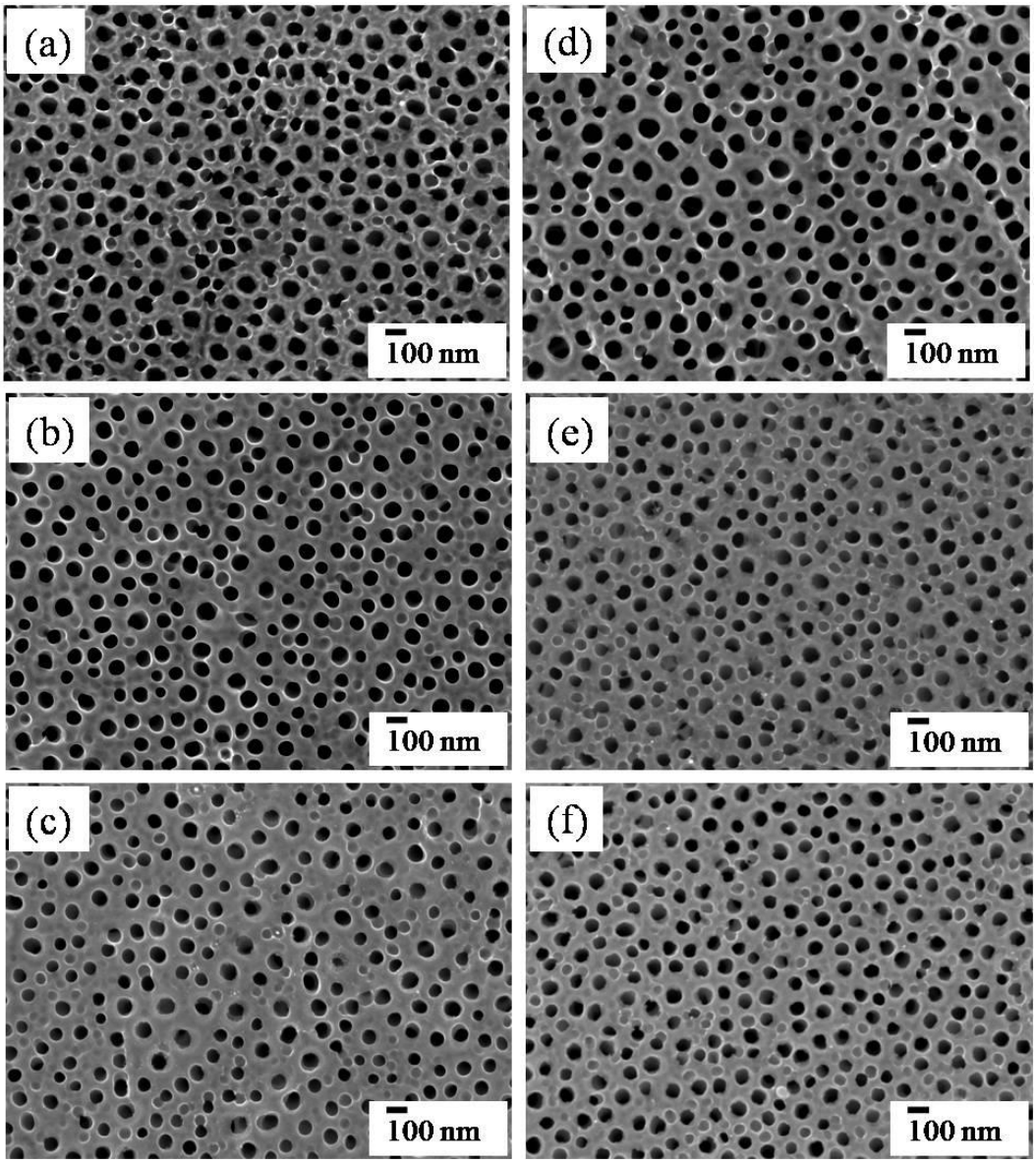

Fig. 2-4 Top-view SEM images of oxide layers formed on air heat-treated Ti substrates in the ethylene glycol containing 0.05 M NH_4F and 2.0 wt.% H_2O; (a, b, c) 500 ℃ for 3 h, 12 h and 48 h, (d, e ,f) 900 ℃ for 3 h, 12 h and 48 h.

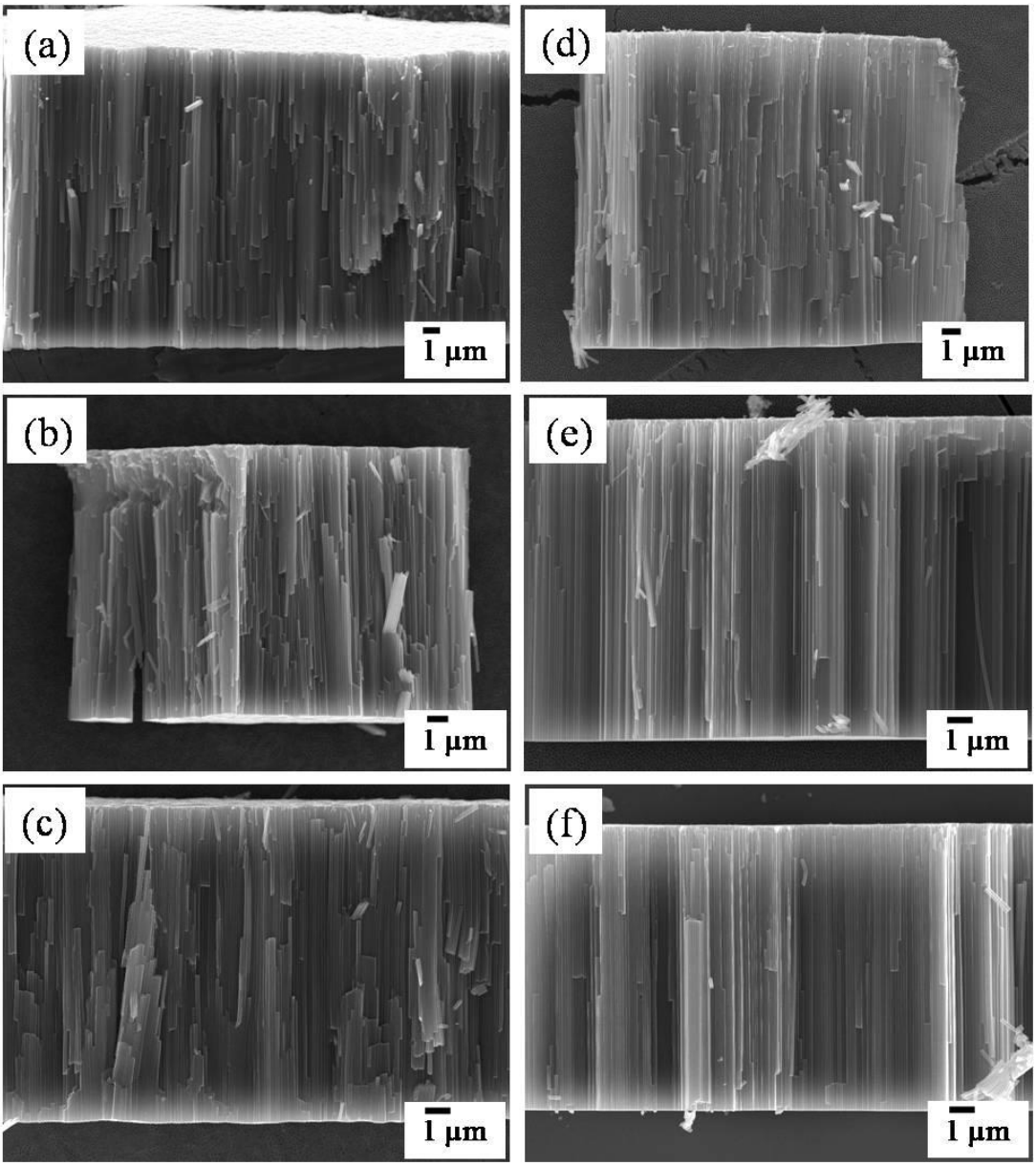

Fig. 2-5 Cross-sectional SEM images of oxide layers formed on air heat-treated Ti substrates in the ethylene glycol containing 0.05 M NH_4F and 2.0 wt.% H_2O; (a, b, c) 500 ℃ for 3 h, 12 h and 48 h, (d, e ,f) 900 ℃ for 3 h, 12 h and 48 h.

In order to examine the effect of heat-treatment atmosphere, some Ti substrates were subjected to the heat-treatment in Ar. Figure 2-7 presents the microstructures of Ti substrates heat-treated in the Ar atmosphere at 500 ℃ and 900 ℃ for various durations. Similar to the heat-treatment in the air atmosphere, the heat-treatment in the Ar atmosphere increases slightly the grain size with heat-treatment duration at 500 ℃ while at 900 ℃

grains drastically grow with time.

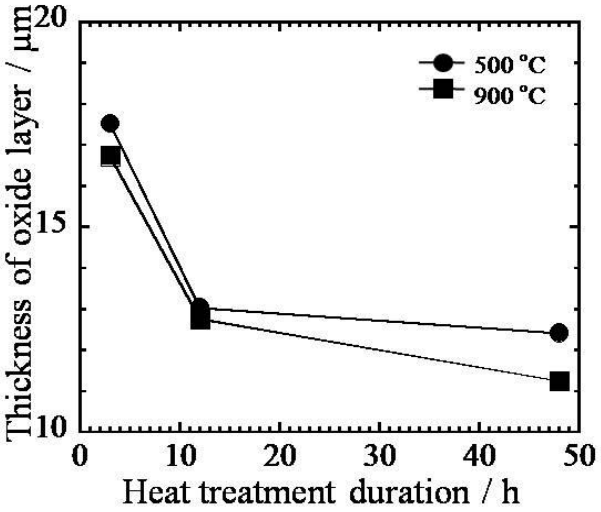

Fig. 2-6 Variation of oxide layer thickness estimated from nanotubular oxide layers on Ti substrates heat-treated in the air with different conditions.

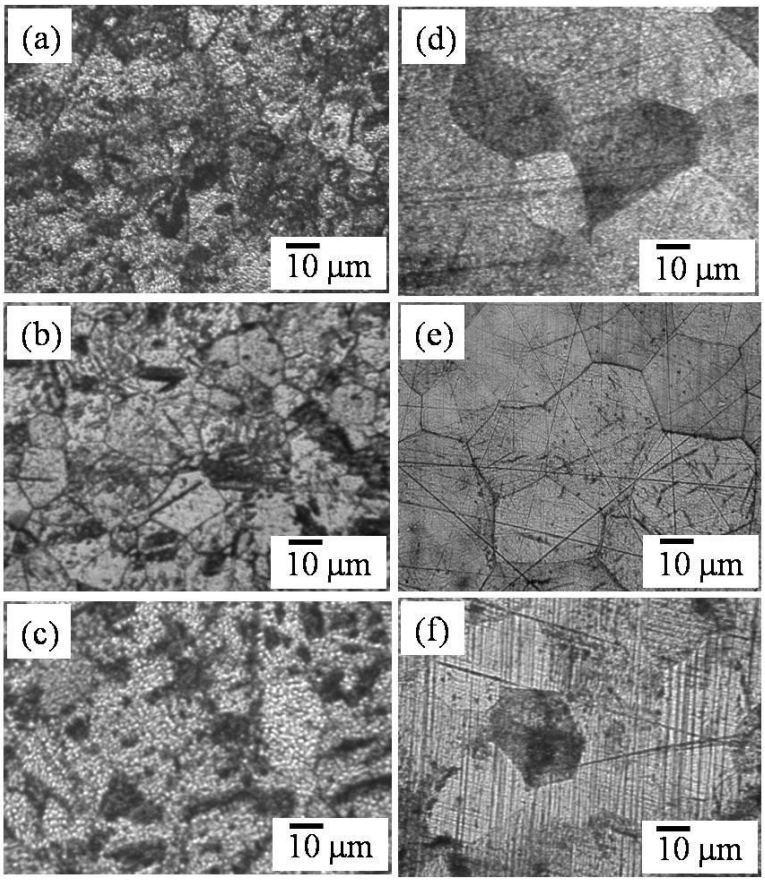

Fig. 2-7 Microstructures of Ti substrates after heat-treatment in Ar ; (a, b, c) 500 ℃ for 3 h, 12 h and 48 h, (d, e, f) 900 ℃ for 3 h, 12 h and 48 h.

Figure 2-8 shows current behavior during the anodization of the substrates heat-treated in the Ar atmosphere. The anodization for the Ar heat-treated substrates was carried out under the same condition as the air heat-treated substrates. The current behavior obtained for Ti substrates heat-treated in the Ar atmosphere is similar to that for substrates treated in the air atmosphere.

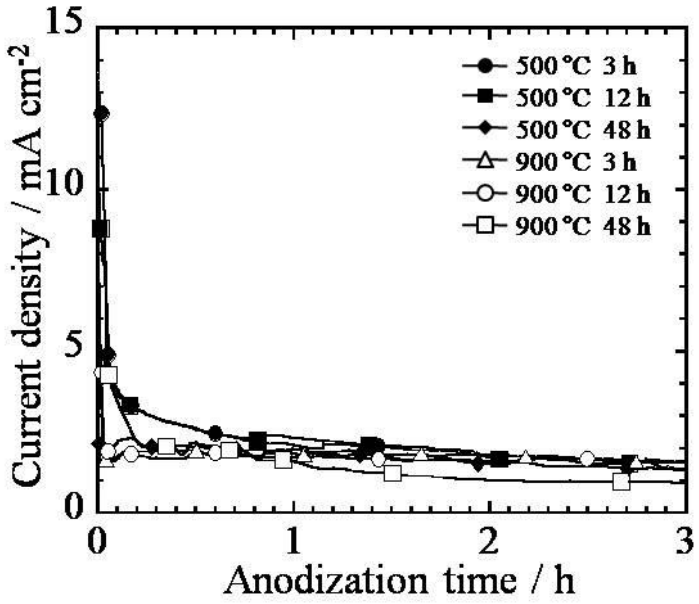

Fig. 2-8 Current-time curves recorded at 50 V for 3 h in the ethylene glycol containing 0.05 M NH_4F + 2.0 wt.% H_2O on Ar heat-treated Ti substrates.

Figures 2-9 and 2-10 show SEM images of resulting anodic oxide layers and the thickness of the oxide layers is summarized in Fig. 2-11. It is clear from Fig. 2-10 that nanotubular oxide layers were formed on all substrates. Similar to the heat-treatments in the air atmosphere, for the heat-treatment in the Ar atmosphere, obtained nanotubular oxide thickness for the substrates heat-treated at 500 ℃ is larger compared to that for the substrates treated at 900 ℃ and furthermore, the thickness decreases with increasing heat-treatment time. In addition, it is indicated that the nanotubular oxide thickness obtained on the air heat-treated Ti substrate is thicker than that obtained for the Ar

heat-treated Ti substrate.

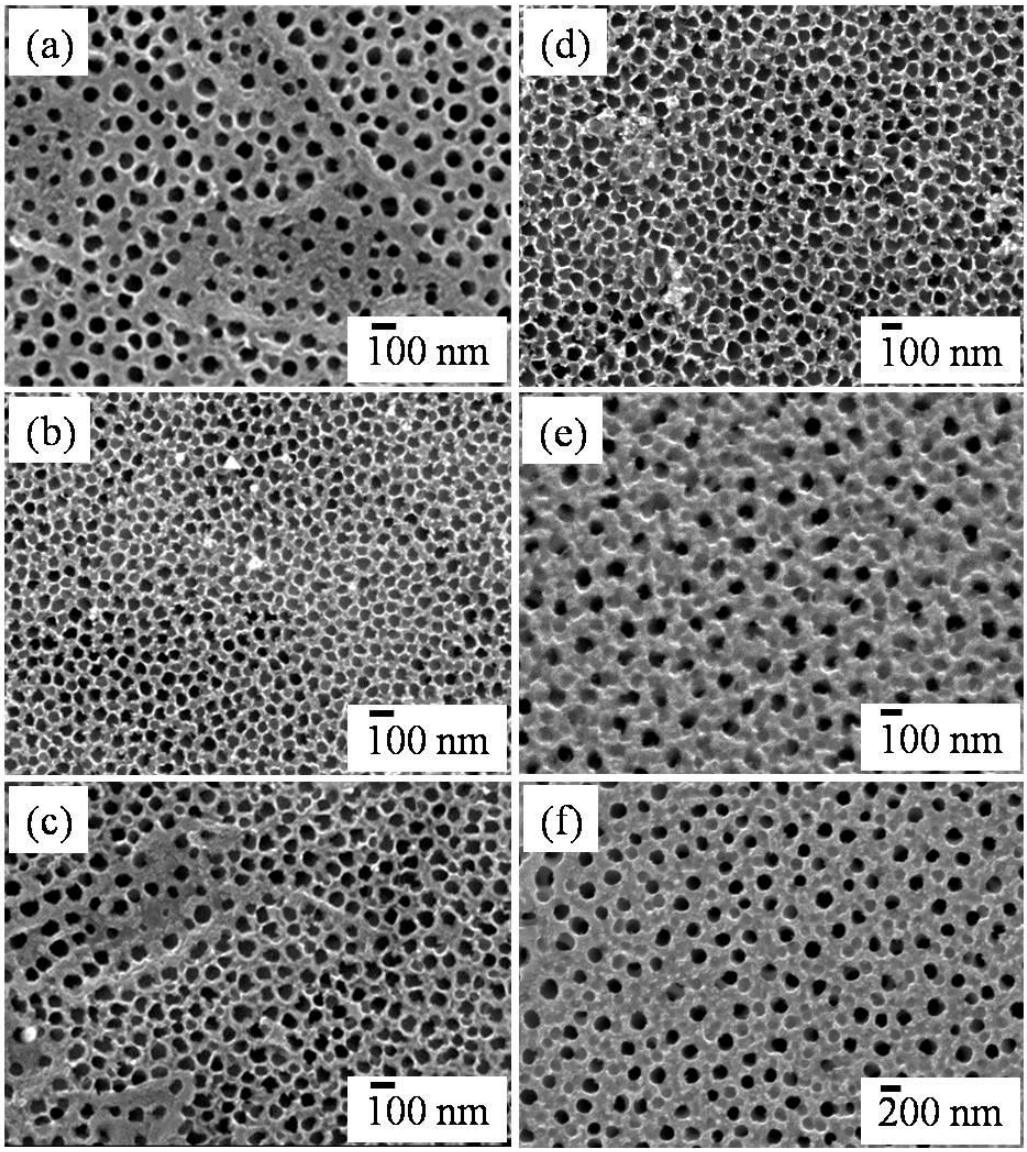

Fig. 2-9 Top-view SEM images of oxide layers formed on Ar heat-treated Ti substrates in the ethylene glycol containing 0.05 M NH_4F and 2.0 wt.% H_2O; (a, b, c) 500 ℃ for 3 h, 12 h and 48 h, (d, e, f) 900 ℃ for 3 h, 12 h and 48 h.

From these results one may deduce the microstructure of Ti substrates clearly affects the growth of nanotubular oxide layers although the effect of the heat-treatment atmosphere is not clear at the moment; the electric charge generated during anodization of the air heat-treatment Ti substrates is higher compared to the Ar heat-treated substrates,

leading to higher thickness of TiO_2 nanotubular layer on the air heat-treated substrates as indicated in Figs. 2-6 and 2-11.

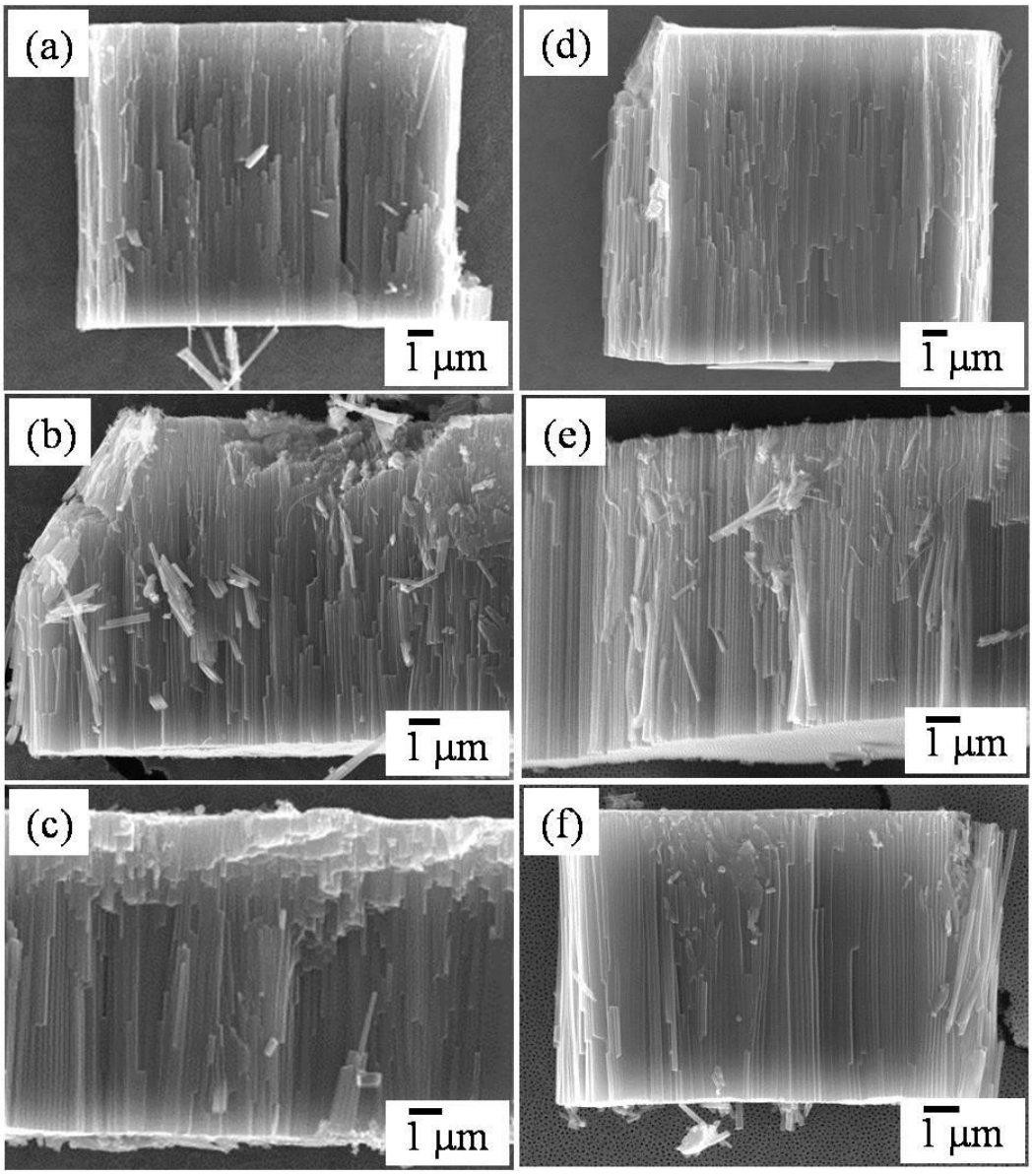

Fig. 2-10 Cross-sectional SEM images of oxide layers formed on Ar heat-treated Ti substrates in the ethylene glycol containing 0.05 M NH_4F and 2.0 wt.% H_2O; (a, b, c) 500 ℃ for 3 h, 12 h and 48 h, (d, e, f) 900 ℃ for 3 h, 12 h and 48 h.

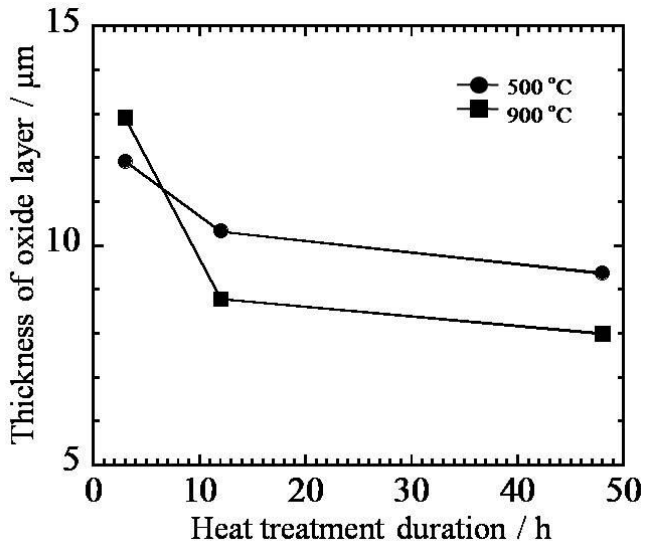

Fig. 2-11 Variation of oxide layer thickness formed on Ti substrates heat-treated in Ar with different conditions.

2.3.2 Growth of anodic oxide layer on ARB processed Ti substrate

In the present section, the microstructure of Ti substrate was controlled with the ARB process. The microstructure of Ti substrate subjected to the ARB process was already examined by Terada at al[24]. It was reported in the literature that after 2 cycles, initial grains were elongated with complex deformation microstructures and after 4 cycles elongated grains became very fine with many shear bands. Therefore, the different microstructures achieved by the ARB process will affect anodization behavior and resulting anodic oxide layers.

Figure 2-12 shows the current-time curves of ARB processed Ti substrates in an ethylene glycol containing 0.05 M NH_4F and 2.0 wt.% H_2O. “0 cycle” indicates as-homogenized Ti substrate, which was used as a starting substrate for the ARB process. In the ARB process, as already explained, 50% reduction in thickness was performed in each cycle, meaning that for ARB 6 cycles, the 50% reduction was repeated 6 times. This indicates that more defects such as dislocation are introduced with increasing ARB cycle. It is clear from Fig. 2-12 that the current-time curves obtained for ARB-processed substrates

are similar to those shown in Figs. 2-3 and 2-8 for the heat-treated substrates, but the steady state current slightly increased with increasing ARB cycle. Figures 2-13 and 2-14 show top-view and cross-sectional SEM images of anodic oxide layers formed on ARB processed samples. It is clear that similar structures were obtained to those formed on the heat-treated substrates; nanotubular oxide layers were grown also on ARB-processed substrates. This means that the microstructure of Ti substrate does not change the morphology of anodic oxide layer under the present anodization condition, that is, nanotubular oxide layers were formed on all Ti substrates that possess different microstructures. Fig. 2-15 summarizes the layer thickness as a function of ARB cycle. It is obvious that the thickness increases with increasing ARB cycle. This indicates that the introduction and increment of defects into Ti substrate facilitates the growth of nanotubular oxide layers.

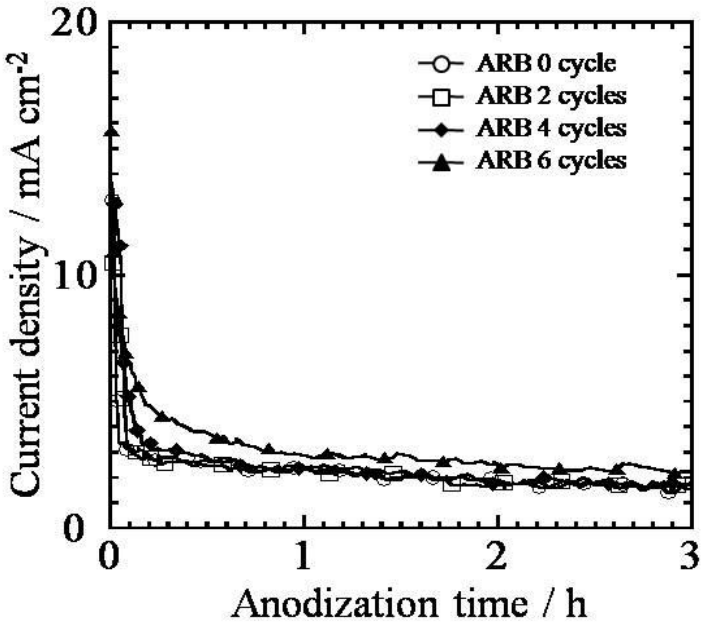

Fig. 2-12 Current-time curves recorded at 50 V for 3 h in the ethylene glycol containing 0.05 M NH_4F + 2.0 wt.% H_2O on the ARB treated Ti substrates.

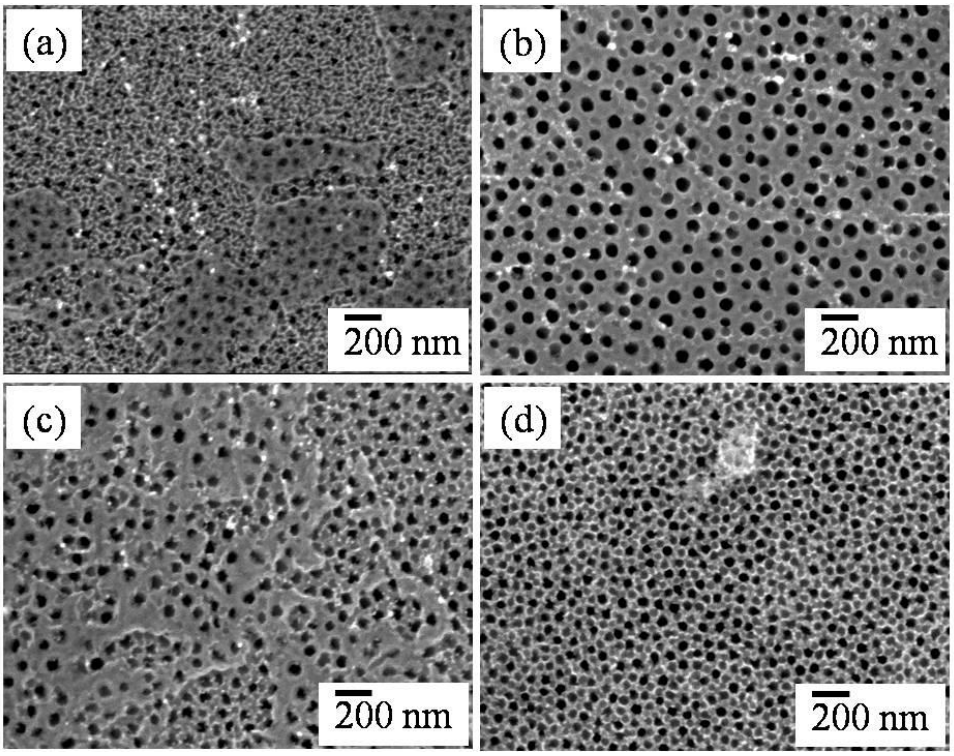

Fig. 2-13 Top-view SEM images of oxide layers formed on ARB treated Ti substrates; (a) 0 cycle, (b) 2 cycles, (c) 4 cycles and (d) 6 cycles.

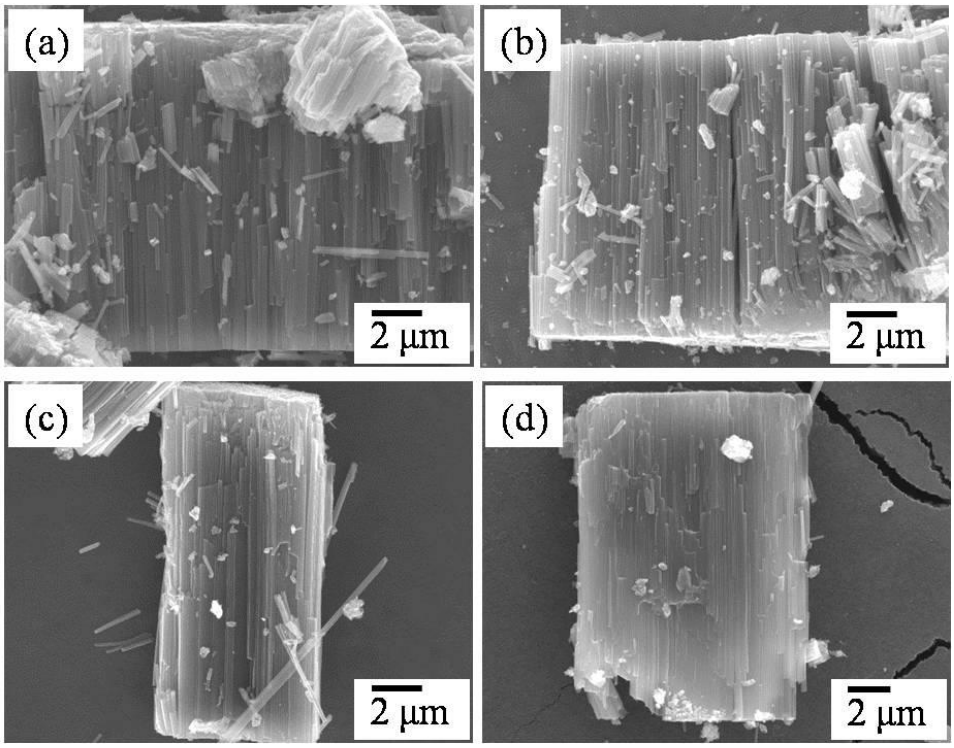

Fig. 2-14 Cross-sectional SEM images of oxide layers formed on ARB treated Ti substrates; (a) 0 cycle, (b) 2 cycles, (c) 4 cycles and (d) 6 cycles.

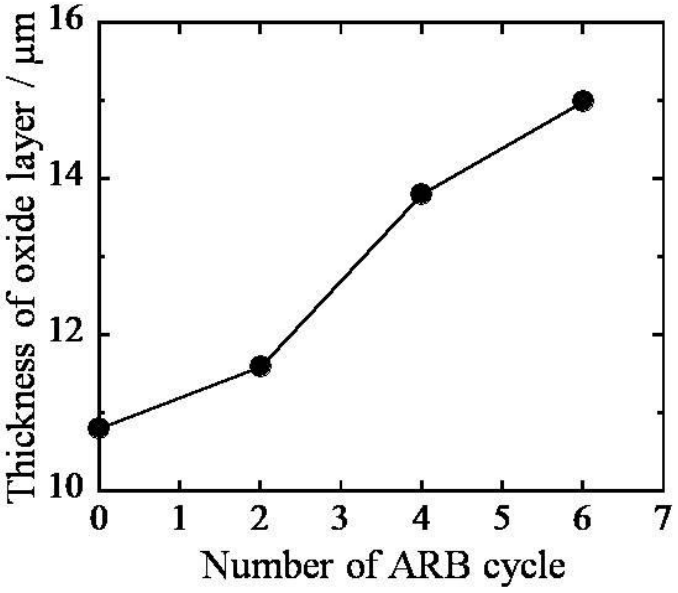

Fig. 2-15 Variation of oxide layer thickness obtained from Fig. 2-14.

2.3.3 Effect of defects on the growth of TiO_2 nanotubular oxide layer

In general, heat-treatment decreases defect in metallic substrates while cold work increases defect. Results presented in 2.3.1 and 2.3.2 indicate that heat-treatment decreases defects in Ti substrate, which leads to the decrease of current during anodization and the decreased thickness of resulting TiO_2 nanotubular layers. On the other hand, increased defects by cold work such as the ARB process enhance anodic current, resulting in the increased thickness of TiO_2 nanotubular layer.

In order to confirm the effect of defect on the growth of TiO_2 nanotubular layer, the following experiment was performed. In the experiment the amount of defect was varied on a single Ti substrate. First the growth of nanotubular oxide layer was examined on as-homogenized Ti substrate. Then in order to examine the effect of the decrease of defect in the substrate, the as-homogenized substrate was heat-treated in an Ar atmosphere at 500 ℃ for 12 hours. Prior to the heat-treatment the nanotubular oxide layer formed on the as-homogenized substrate was removed by polishing. After the heat-treatment, the Ti substrate was re-anodized to investigate the growth of nanotubular oxide layer. Finally the

heat-treated substrate was subjected to cold work with the reduction of 50% in order to see the effect of the increase of defect achieved by cold work. After the cold work the Ti substrate was anodized again. From the series of experiments, one can see the effect of defect in one single Ti substrate on the growth of nanotubular oxide layer. The result is presented in Fig. 2-16.

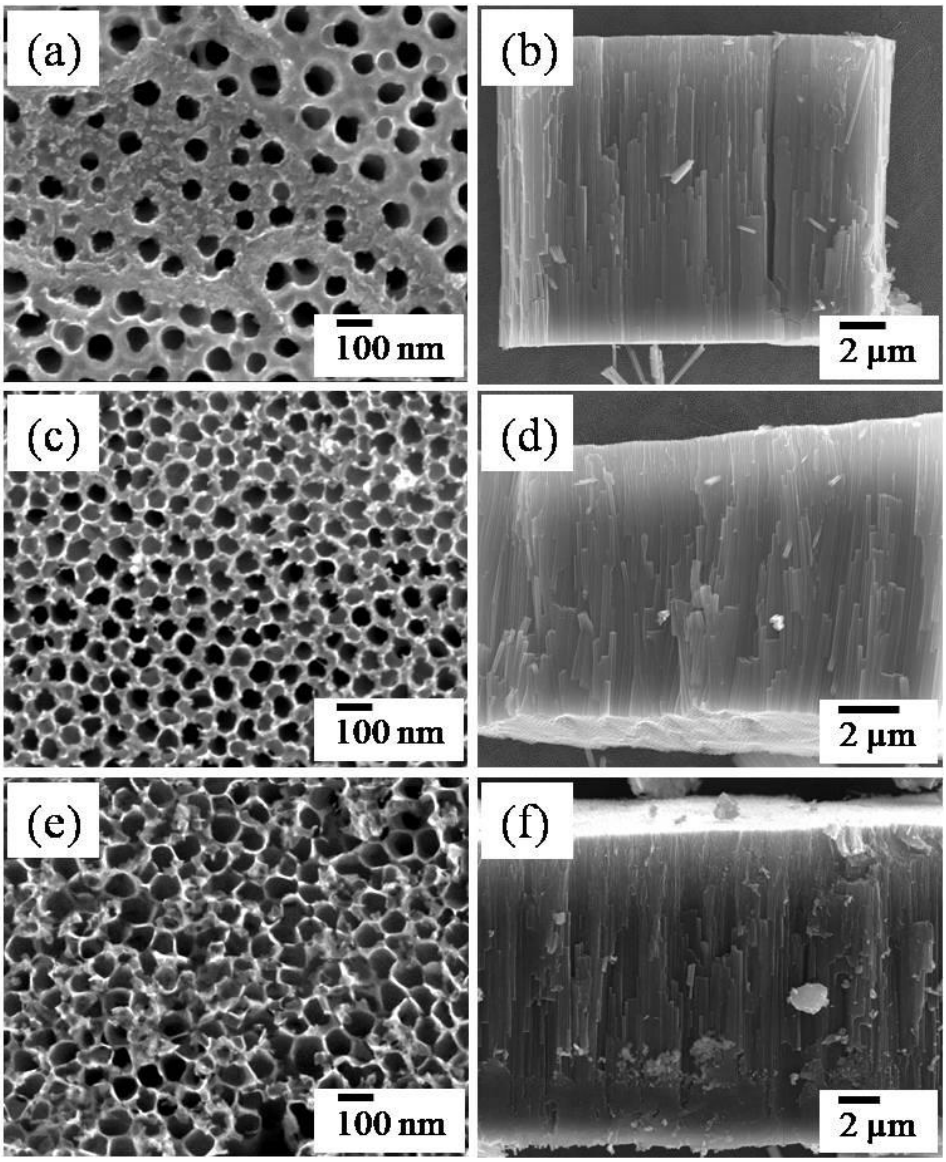

Fig. 2-16 Top-view and cross-sectional SEM images of oxide layers formed on Ti substrates with various conditions; (a, b) as-homogenized Ti sample at 500 ℃ for 12 h, (c, d) after homogenization, heat-treated at 500 ℃ for 12 h, (e, f) after homogenization and heat-treatment, cold-rolled with 50% reduction.

It is clear that the oxide layers exhibit nanotubular structure for all cases. Compared to the oxide layer on the as-homogenized substrate (Fig. 2-16(b)), apparently the layer thickness obtained for the heat-treated substrate is relatively thin. On the other hand, the cold work to the heat-treated substrate results in the increased thickness of tubular oxide layer from approximately 9.2 μm to 14.9 μm. This is also in accordance with the above-mentioned findings, that is, it can be concluded the defects that can be decreased by heat-treatment and increased by cold work strongly affect the growth of tubular oxide layer.

2.4 Conclusion

In the present chapter the author examined the growth of oxide layers on Ti substrates with different microstructures controlled by the ARB process and various heat-treatments. Nanotubular oxide layers were formed on the ARB-processed and heat-treated substrates by anodization. In the case of heat-treated substrates, however, the thickness of oxide layers was slightly decreased with increasing heat-treatment duration in all conditions (in air and Ar). On the other hand, the thickness of tubular oxide layer was significantly increased with the ARB process. Therefore, it is found that the oxide layer thickness can be decreased by heat-treatment and increased by cold work, which indicates that the substrate property strongly affects the growth of nanotubular oxide layer.

References :

1) F. Keller, M.S. Hunter, and D. L. Robinson, J. Electrochem.Soc., **100** (1953) 411.

2) H. Masuda, K. Fukuda, Science, **268** (1995) 1466.

3) M. Steinhart, J.H. Wendorff, A. Greiner, R.B. Wehrspohn, K. Nielsch, J. Schilling, J. Choi, U. Gösele, Science, **296** (2002) 1997.

4) G. Cao, D. Liu, Adv. Coll. Interface Sci., **136** (2008) 45.

5) M. Assefpour-Dezfuly, C. Vlachos, E.H. Andrews, J. Mater. Sci., **19** (1984) 3626.

6) V. Zwilling, M. Aucouturier, E. Darque-Ceretti, Electrochim. Acta, **45** (1999) 921.

7) V. Zwilling, E. Darque-Ceretti, A. Boutry-Forveille, D. David, M.Y. Perrin1, M. Aucouturier, Surf. Interface Anal., **27** (1999) 629.

8) H. Tsuchiya, J.M. Macak, A. Ghicov, L. Taveira, P. Schmuki, Corros. Sci., **47** (2005) 3324.

9) I. Sieber, B. Kannan, P. Schmuki, Electrochem. Solid-State Lett., **8** (2005) J10.

10) N.R. de Tacconi, C.R. Chenthamarakshan, G. Yogeeswaran, A. Watcharenwong, R.S. de Zoysa, N.A. Basit, K. Rajeshwar, J. Phys. Chem. B, **110** (2006) 25347.

11) W. Wei, J.M. Macak, P. Schmuki, Electrochem. Commun., **10** (2008) 428.

12) H. Tsuchiya, P. Schmuki, Electrochem. Commun., **7** (2005) 49.

13) C.Y. Lee, Z. Su, K. Lee, H. Tsuchiya, P. Schmuki, Chem. Commun., **50** (2014) 7067.

14) K. Yasuda, P. Schmuki, Adv. Mater., **19** (2007) 1757.

15) S.H. Jang, H.C. Choe, Y.M. Ko, W.A. Brantley, Thin Solid Films, **517** (2009) 5038.

16) Y.C. Nah, A. Ghicov, D. Kim, S. Berger, P. Schmuki, J. Am. Chem. Soc., **130** (2008) 16154.

17) H. Tsuchiya, T. Akaki, J. Nakata, D. Terada, N. Tsuji, Y. Koizumi, Y. Minamino, P. Schmuki, S. Fujimoto, Corros. Sci., **51** (2009) 1528.

18) Y.H. Jeong, K. Lee, H.C. Choe, Y.M. Ko, W.A. Brantley, Thin Solid Films, **517** (2009)

5365.

19) J.M. Macak, H. Hildebrand, U. Marten-Jahns, P. Schmuki, J. Electroanal.Chem., **621** (2008) 254.

20) C.P. Ferreira, M.C. Gonçalves, R. Caram, R. Bertazzoli, C.A. Rodrigues, Appl. Surf. Sci., **285** (2013) 226.

21) L. Zhang, Y. Han, Nanotechnology, **21** (2010) 055602.

22) Y. Saito, N. Tsuji, H. Utsunomiya, T. Sakai, R.G. Hong, Scripta Mater., **39** (1998) 1221.

23) P. Roy, S. Berger, P. Schmuki, Angew. Chem. Int. Ed., **50** (2011) 2904.

24) D. Terada, S. Inoue, N. Tsuji, J. Mater. Sci., **42** (2007) 1673.

Chapter 3 Morphology and growth of nanotubular oxide layers on Ti-Ni alloys with different Ni contents

3.1 Introduction

Assefpour-Dezfuly et al. and Zwilling et al.[1-3] firstly reported the formation of self-organized nanotubular oxide layers on Ti and Ti alloys by anodization in fluoride-containing electrolytes. On a variety of metals such as Zr[4], Nb[5], W[6], Ta[7], Hf[8] as well as several Ti alloys, since then, self-organized nanotubular and nanoporous oxide layers have been found[9-12]. In particular, owing to their various potential applications, in photocatalyst, dye-sensitized solar cells, gas sensors, electrochromic devices and surface coatings on biomedical Ti-based implants[13-17] self-organized nanotubular oxide layers on Ti and Ti alloys have attracted a great deal of attention.

In order to improve and enhance the properties relevant to the applications mentioned above, the morphology of the nanotubular oxide layers on Ti has been tailored by tuning anodization condition. It was reported that the thickness and tube diameter of nanotubular oxide layers increase with the increase of applied voltage[18]. Furthermore, the thickness of nanotubular oxide layers increased as anodization time proceeded, until equilibrium between oxide growth and oxide dissolution was established[19]. Extensive studies on the nanotube growth have revealed that the electrolyte composition also strongly affected the thickness of the oxide layer[20, 21]. Therefore, it is apparent that the anodization conditions clearly influence the morphology and growth of nanotubular oxide layers.

Recently, the effects of microstructure and alloy composition of substrate on the morphology and growth of nanotubular oxide layers have been also examined. For example, it was reported that the microstructures of Ti substrates varied by heat-treatment

or cold-work affect the growth rate of nanotubular oxide layers[22, 23] as also described in the chapter 2. The chemical composition of substrate also affects the anodic nanotubular oxide layer. So et al. demonstrated that the morphology of oxide layers formed by anodization of Ti-Ru alloy significantly changed depending on the Ru content of the alloy[24].

Ti-Ni alloy is one of the most investigated alloys due to its favorable mechanical properties, such as its superelasticity and shape memory effect[25, 26]. Therefore, anodization of Ti-Ni alloys has also been examined for the modification of their surfaces to fabricate functional materials[27-30]. These studies revealed that anodization conditions affect the morphology of oxide layers. It is well-known that the microstructures and mechanical properties of Ti-Ni alloys are strongly dependent on the Ni content of the alloys[31]. In the present chapter, the author presents the growth of anodic nanotubular oxide layers on Ti-Ni alloys with various Ni contents. Furthermore, the effect of the alloy crystal structure on the formation of anodic oxide layers is also described.

3.2 Experimental

Materials were various Ti-Ni alloys with different Ni contents. These alloys used were fabricated by melting Ti sheets (purity : 99.5%) and Ni sheets (purity : 99%) in an arc melting furnace. The alloys ingots obtained after the arc melting were homogenized at 1000 ℃ for 24 hours under a high vacuum condition and then cold-rolled with a reduction ratio of 20%. The chemical composition and crystal structure of the fabricated Ti-Ni alloys were examined using electron probe micro analyzer (EPMA, JEOL JXA-8800R) and X-ray diffraction (XRD, Philips PW3040/60 X'Pert Pro), respectively. The homogenized ingots were cut into sheets with dimensions of $15\times15\times2mm^3$. The samples were ground with SiC abrasive papers, and then mirror-finished. Prior to anodization, the mirror-finished samples were degreased by sonicating in acetone, ethanol, and methanol, successively, followed by

rinsing with deionized water. The electrochemical setup consisted of a two-electrode configuration with the fabricated Ti-Ni alloy as a working electrode and a platinum plate as a counter electrode. The electrochemical anodization was carried out in an ethylene glycol electrolyte containing 0.06 M NH_4F and 1.5 wt.% H_2O at different voltages for various anodization times using a high-voltage potentiostat (Hokuto Denko HA-3001A). After the anodization, the samples were rinsed with ethanol.

The morphology of anodic oxide layers was investigated using a field-emission scanning electron microscope (FE-SEM, JEOL JSM-7001FA). The cross-sectional views of the oxide layers were taken from mechanically scratched samples where oxide layers were lifted off. The compositions of the oxide layers and the substrate after anodization were examined by EPMA and energy dispersive X-ray analysis (EDX, NORAN model 500 analyzer) attached to a transmission electron microscope (TEM, Hitachi, HF-2000).

3.3 Results and discussion

3.3.1 Fabrication and characterization of Ti-Ni alloys

In the present work, the author prepared four Ti-Ni alloys with different Ni contents to investigate the effect of alloy composition on the growth of anodic oxide layer. The Ni content in the alloys was evaluated by EPMA. Although some small precipitates were observed as reported previously in literature[32, 33], the compositions of the four alloys were constant across the alloy surfaces, and the Ni content in the alloys was estimated as 49.0 at.% Ni, 51.1 at.% Ni, 52.2 at.% Ni and 52.5 at.% Ni. As reported previously, the crystal structure of Ti-Ni alloy depends on the Ni content[33]. Therefore, the crystal structures of the four Ti-Ni alloys were examined using XRD. Figure 3-1 presents XRD patterns of the Ti-Ni alloys. All diffraction peaks obtained on the Ti-49.0 at.% Ni alloy are ascribed to the B19’ martensitic phase whereas for the Ni-rich alloys of Ti-51.1 at.% Ni, Ti-52.2 at.% Ni

and Ti-52.5 at.% Ni, all peaks are attributed to the B2 austenitic phase. Therefore, the effect of crystal structure of the alloy substrates on the formation of anodic oxide layer is also investigated.

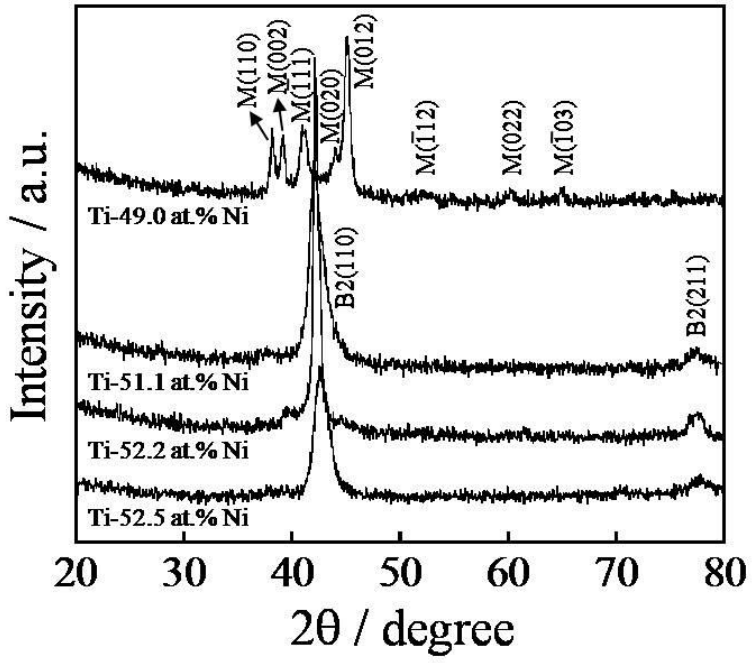

Fig. 3-1 XRD patterns of Ti-Ni alloys produced in the present study.

3.3.2 Anodization of Ti-49.0 at.% Ni at different applied voltages

Figure 3-2 shows the current-time curves obtained for the Ti-49.0 at.% Ni alloy during anodization at 20, 35 and 50 V for 5 min in the ethylene glycol based electrolyte containing 0.06 M NH_4F and 1.5 wt.% H_2O. At all applied voltages, similar current behavior is observed; the current density drastically decreases in the early stage of anodization, then increases, and finally decreases again to a steady state value. However, the current density is clearly different depending on the applied voltage, that is, higher currents are generated at higher applied voltages.

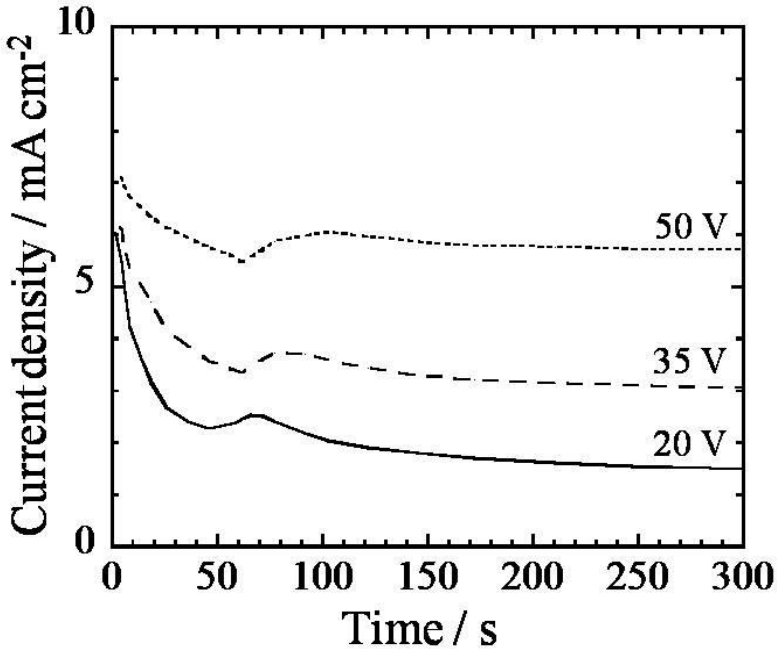

Fig. 3-2 Current-time curves of the Ti-49.0 at.% Ni alloy substrate recorded at various voltages for 5 min in the ethylene glycol electrolyte containing 0.06 M NH_4F and 1.5 wt.% H_2O.

The top-view and cross-sectional images of the oxide layers formed on the Ti-49.0 at.% Ni alloy at different applied voltages for 5 min are presented in Fig. 3-3. The top-views exhibit porous morphology, and the average pore diameter slightly increases with increasing applied voltage. However, it is apparent from the cross-sectional views that the oxide layer formed at 50 V shows distinct nanotubular structures, whereas at the other voltages of 20 V and 35 V the formation of such nanotubular structures is not recognized and instead irregular-shaped porous structures are visible.

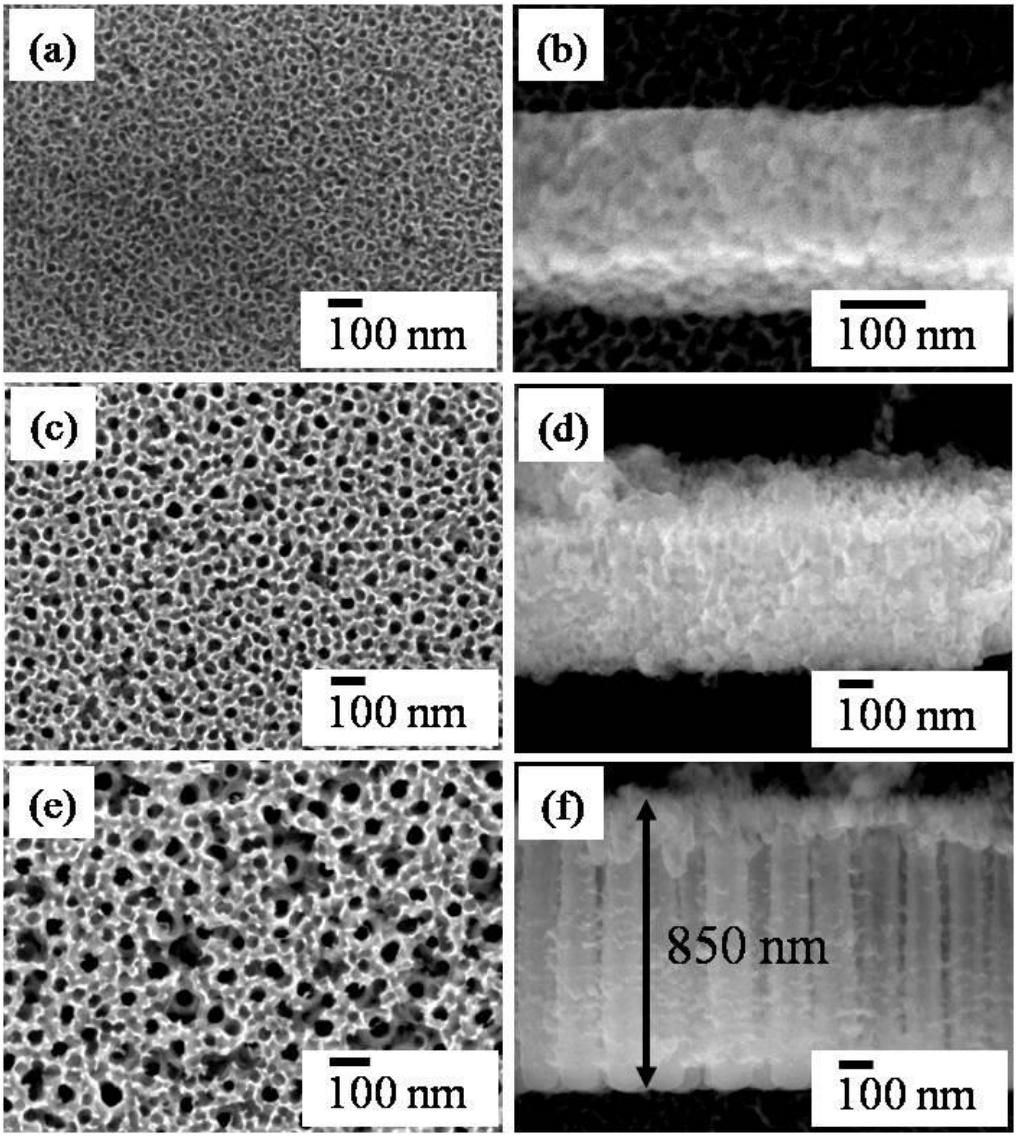

Fig. 3-3 Top-view and cross-sectional SEM images of oxide layers formed on the Ti-49.0 at.% Ni alloy at (a, b) 20 V, (c, d) 35 V and (e, f) 50 V for 5 min in the ethylene glycol electrolyte containing 0.06 M NH_4F and 1.5 wt.% H_2O.

Figure 3-4 shows SEM images of the oxide layers formed on pure Ti under the same conditions. It is clear that nanotubular structures are observed at all applied voltages. Therefore, one can find that a suitable voltage range for nanotube formation in the ethylene glycol based electrolyte is quite limited for Ti-Ni alloys, different from pure Ti. EPMA analysis on the oxide layers shown in Fig. 3-3 revealed that the oxide layers on the Ti-49.0

at.% Ni alloy at 20 V and 35 V exhibited similar cation ratios to the Ti-49.0 at.% Ni substrate, whereas the oxide layer at 50 V showed higher Ti content. This indicates that the selective oxidation of Ti occurred at 50 V. It was reported that self-organized nanoporous structures are formed on pure Ni under a very limited potential range[34]. For these reasons, nanotubular oxide layers could only be formed at 50 V on the present alloys. Therefore the following experiments were carried out at 50 V.

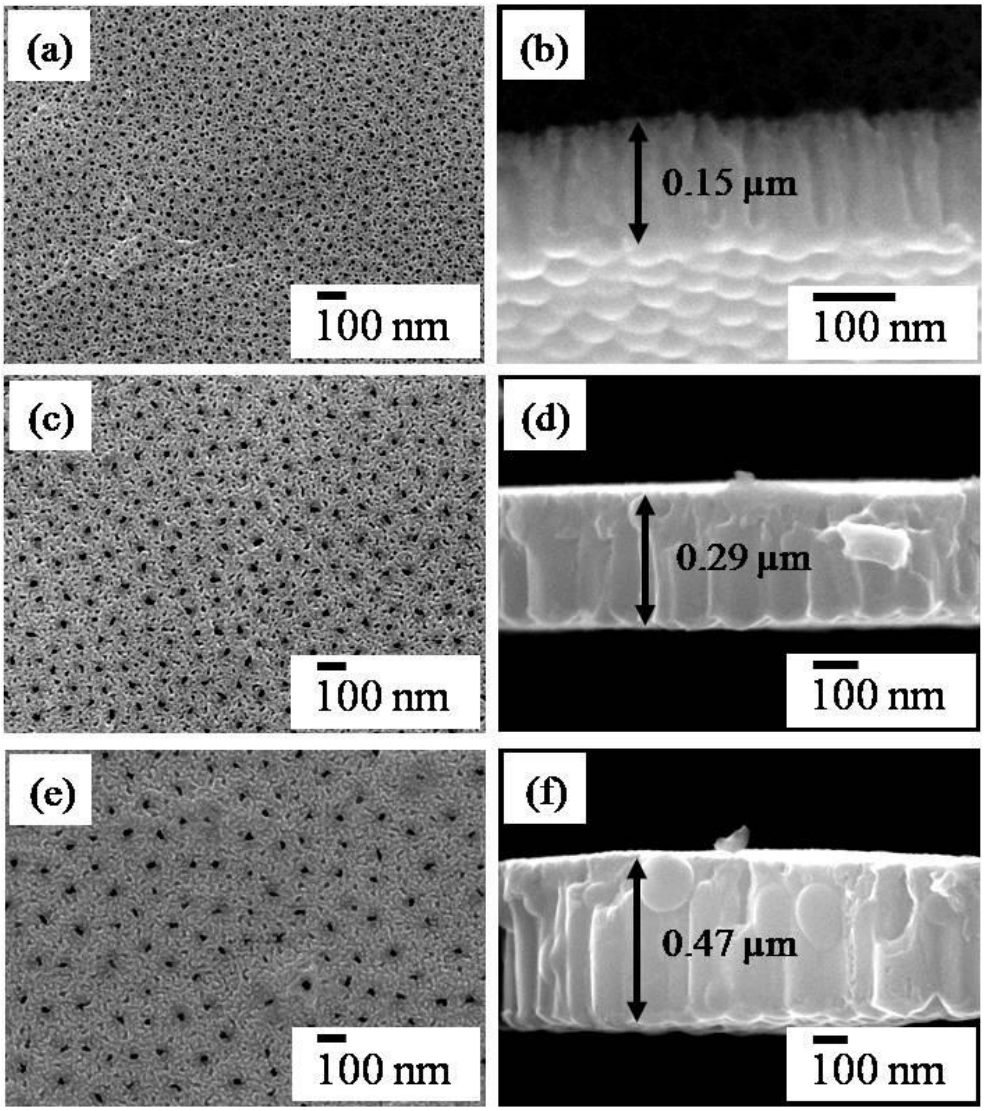

Fig. 3-4 Top-view and cross-sectional SEM images of oxide layers formed on pure Ti at (a, b) 20 V, (c, d) 35 V and (e, f) 50 V for 5 min in the ethylene glycol based electrolyte.

3.3.3 Effect of Ni concentration in Ti-Ni alloy and anodization time on the growth of nanotubular oxide layers

Figure 3-5 shows SEM images of the oxide layers on the Ni-rich Ti-Ni alloys at 50 V for 5 min. Self-organized nanotubular oxide layers are obviously formed on all Ni-rich Ti-Ni alloys examined, implying that the morphology of the oxide layers on the Ni-rich Ti-Ni alloys is similar to that of the Ti-rich Ti-49.0 at.% Ni alloy as shown in Figs. 3-3 (e) and (f).

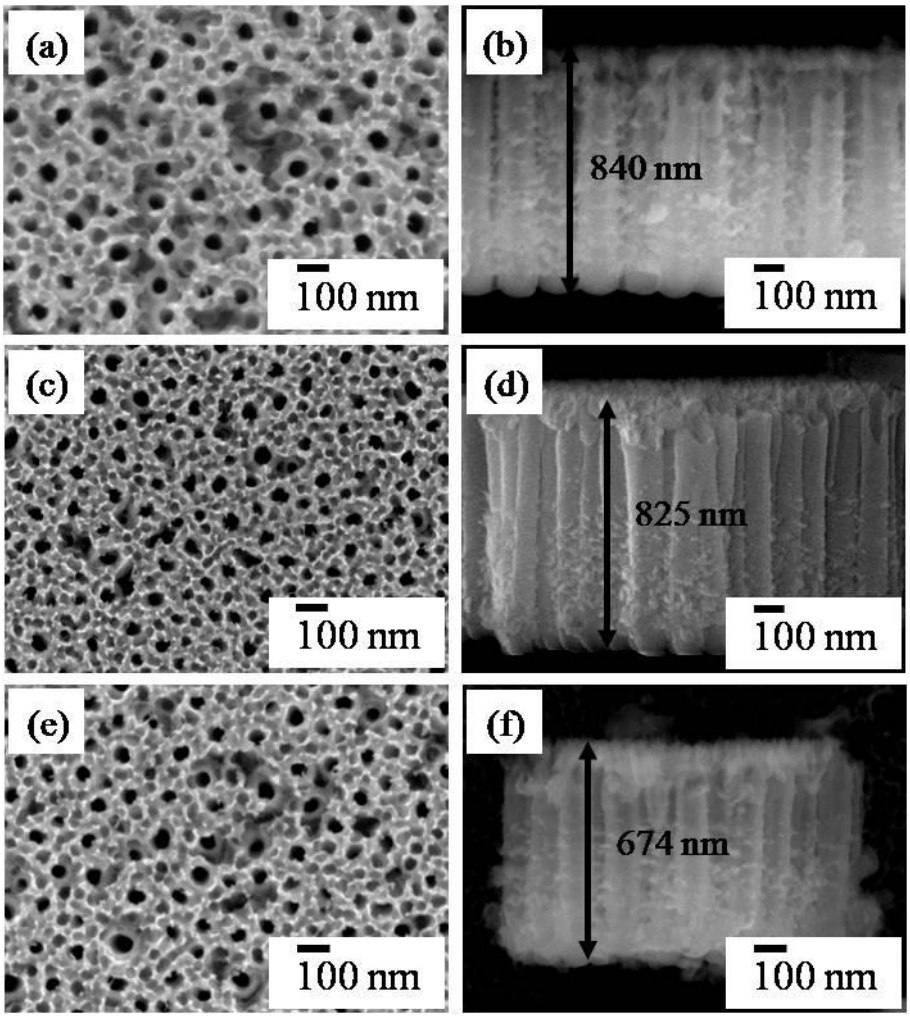

Fig. 3-5 Top-view and cross-sectional SEM images of oxide layers formed on (a, b) Ti-51.1 at.% Ni, (c, d) Ti-52.2 at.% Ni and (e, f) Ti-52.5 at.% Ni alloys at 50 V for 5 min in the ethylene glycol electrolyte containing 0.06 M NH_4F and 1.5 wt.% H_2O.

Extended anodization leads to the morphological change of the oxide layers on the Ti-Ni alloys. SEM images of the oxide layers formed on the Ti-Ni alloys for 20 min are shown in Fig. 3-6. It is clear that for Ti-49.0 at.% Ni, Ti-51.1 at.% Ni and Ti-52.2 at.% Ni alloys, the formation of a nanotubular oxide layer is recognized from the top-view images shown in Figs. 3-6 (a), (c) and (e). However, as displayed in the cross-sections in Figs. 3-6 (b), (d) and (f), an irregular-shaped porous oxide layer was grown underneath the nanotubular oxide layer. For Ti-52.5 at.% Ni alloy, on the other hand, the oxide layer exhibits only the irregular-shaped porous structure. After further anodization such as 60 min, the oxide layers on all Ti-Ni alloys were observed by SEM and the results are shown in Fig. 3-7. It is evident from top-view and cross-sectional images that an irregular-shaped porous oxide layer was formed regardless of the Ni concentration in alloy substrate.

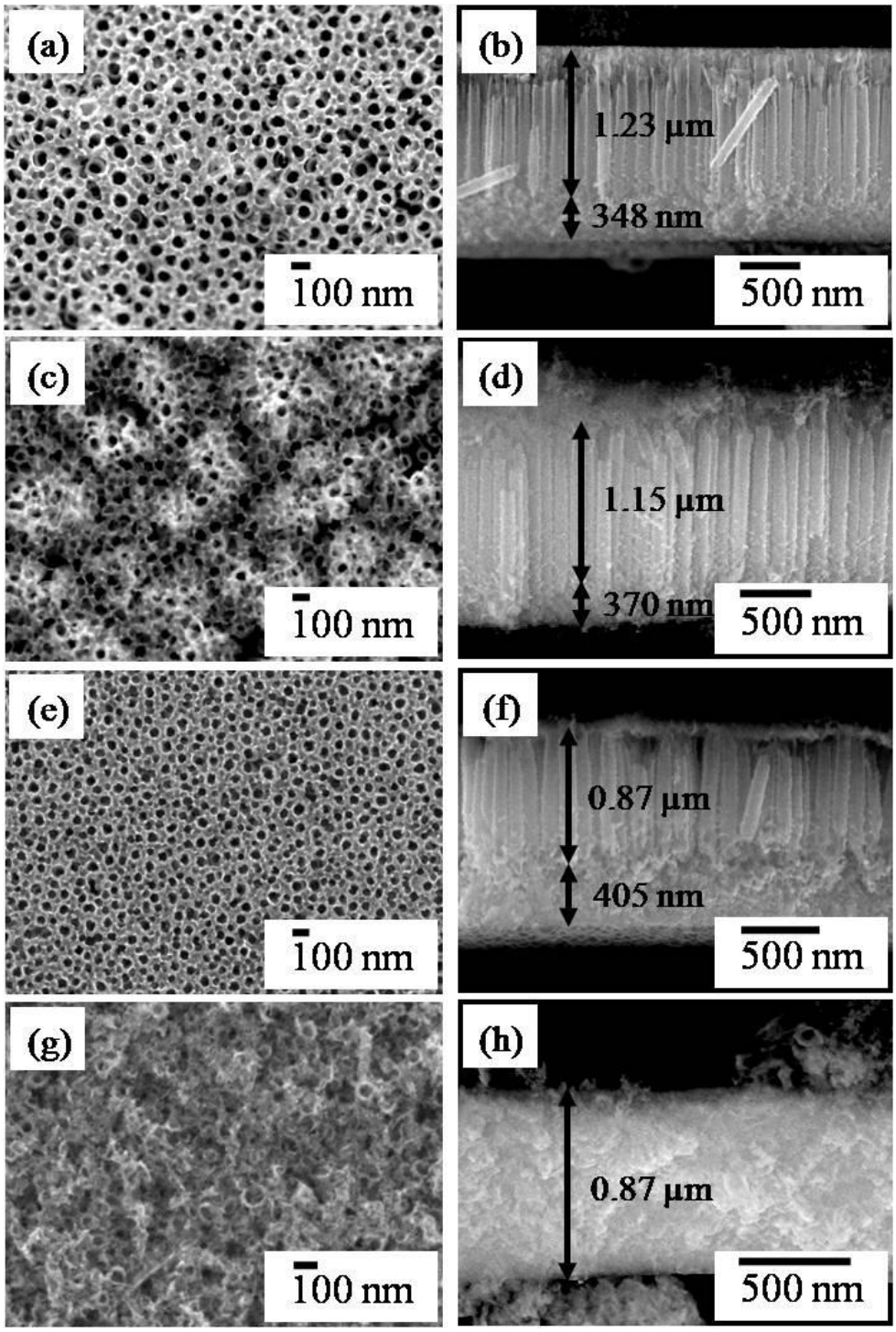

Fig. 3-6 Top-view and cross-sectional SEM images of oxide layers formed on (a, b) Ti-49.0 at.% Ni, (c, d) Ti-51.1 at.% Ni, (e, f) Ti-52.2 at.% Ni and (g, h) Ti-52.5 at.% Ni alloys at 50 V for 20 min in the ethylene glycol electrolyte containing 0.06 M NH_4F and 1.5 wt.% H_2O.

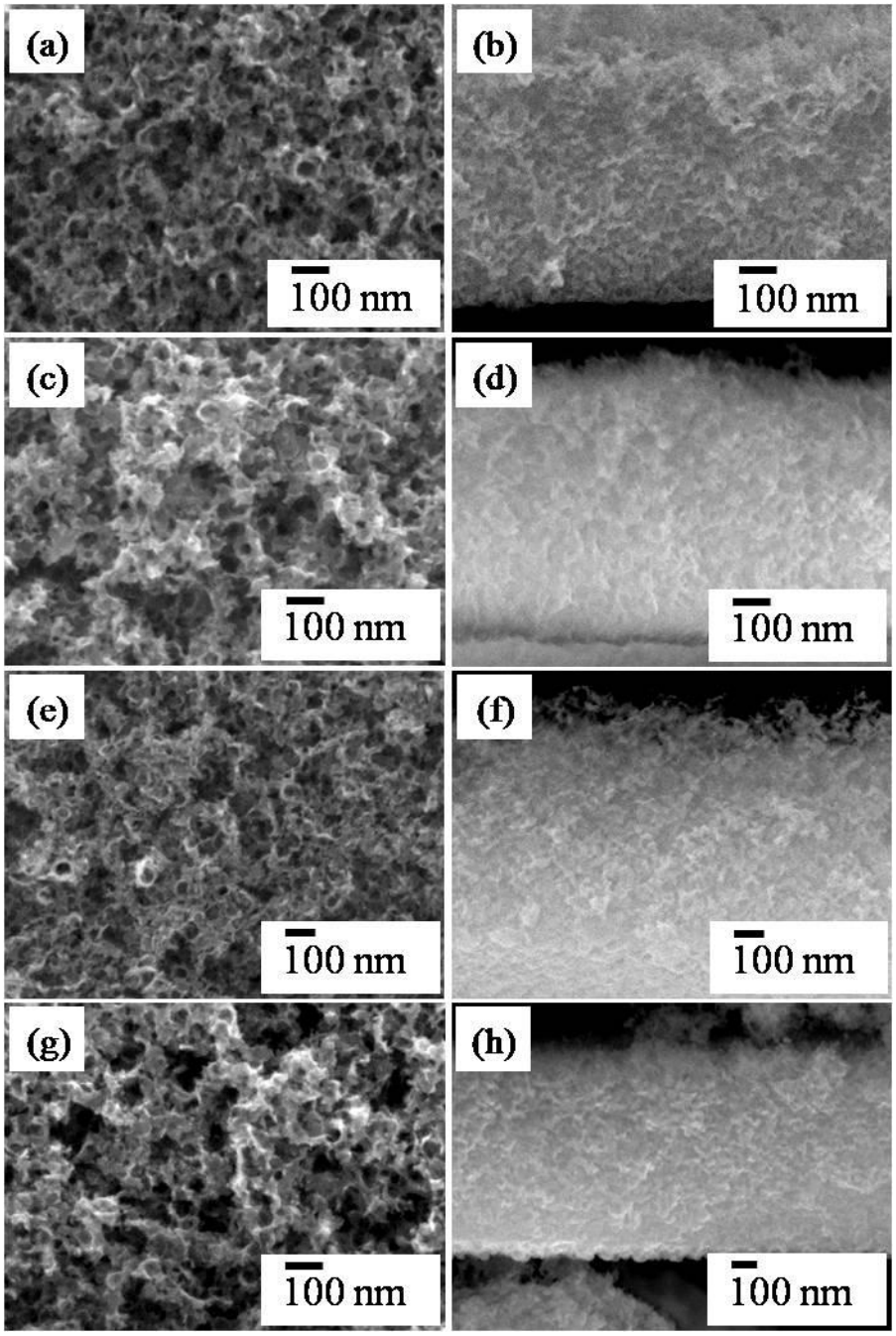

Fig. 3-7 Top-view and cross-sectional SEM images of oxide layers formed on (a, b) Ti-49.0 at.% Ni, (c, d) Ti-51.1 at.% Ni, (e, f) Ti-52.2 at.% Ni and (g, h) Ti-52.5 at.% Ni alloys at 50 V for 60 min in the ethylene glycol electrolyte containing 0.06 M NH_4F and 1.5 wt.% H_2O.

Figures 3-8 (a) and (b) exhibit the bottom-view images of the oxide layers formed on the Ti-49.0 at.% Ni alloy at 50 V for 5 min and 20 min, respectively. It is clear that the

morphology of the bottom-view of the oxide layer significantly changes from distinctly ordered circular to irregular-shaped porous structures as the anodization time is increased. Similar bottom structures were obtained also for the Ti-51.1 at.% Ni and Ti-52.2 at.% Ni alloys after anodization for 20 min. These observations indicate that the oxide layers formed on the Ti-49.0 at.% Ni, Ti-51.1 at.% Ni and Ti-52.2 at.% Ni alloys for 20 min, are composed of layered structure, outer tubular structures and inner irregular-shaped porous structures. On the other hand, for the Ti-52.5 at.% Ni alloy, the oxide layer formed after 20 min shows only the irregular-shaped porous structures. Further anodization for 60 min results in irregular-shaped porous structure on all Ti-Ni alloys examined in the present work.

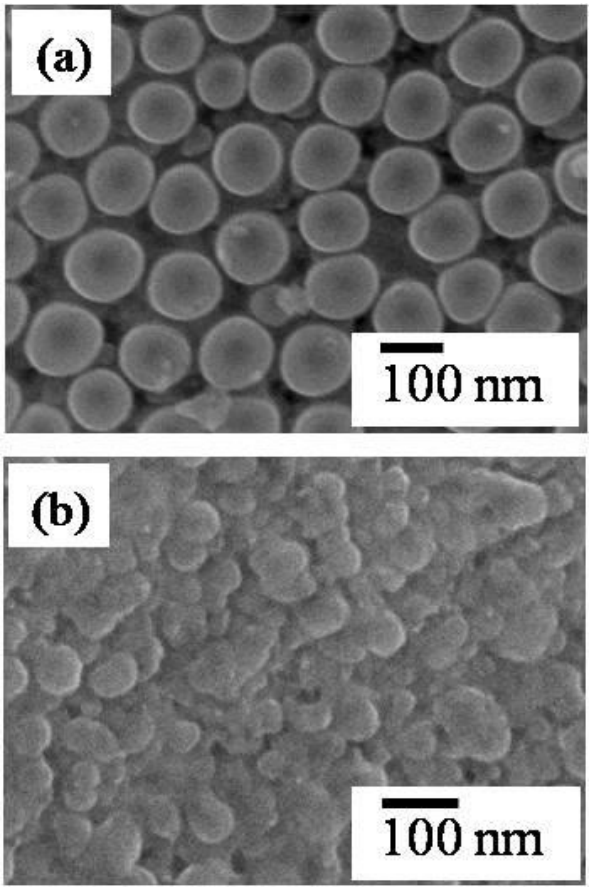

Fig. 3-8 Bottom-view SEM images of oxide layers formed on a Ti-49.0 at.% Ni alloy at 50 V for (a) 5 min and (b) 20 min.

3.3.4 Morphological transition from nanotubular to irregular-shaped porous structures

The results presented in 3.3.2 and 3.3.3 indicate that the morphology of formed oxide layers is affected by the chemical composition of the Ti-Ni alloy rather than the crystal structure of the substrate, and that the morphological transition of oxide layers from tubular to irregular-shaped porous structure proceeds as anodization time is increased. Although nanotubular oxide layers on the Ti-50.8 at.% Ni alloy was reported by several groups, this morphological transition has not been recognized[28-30]. As presented in Fig. 3-6, even when nanotubular oxide layers are confirmed from top-view images, irregular-shaped porous oxide layers are grown underneath the nanotubular layers. Thus, the detailed cross-sectional observations carried out in the present work reveal the morphological transition of anodic oxide layers on Ti-Ni alloy.

As mentioned above, the nanotubular oxide layers on the Ti-Ni alloys at 50 V are Ti-rich, which is in accordance with previously published observations[30]. The preferential anodization of Ti can lead to changes in chemical composition of the alloy substrates adjacent to the oxide layer, which can be considered to be related to the morphological transition. Therefore, the chemical composition of the alloy substrate was measured using EDX for the samples where the layered structures of nanotubular and irregular-shaped porous oxides were formed.

Figure 3-9 shows the depth distribution of Ni content in the Ti-49.0 at.% Ni alloy from the interface between the alloy substrate and the oxide layer formed by anodization at 50 V for 20 min. It is clear that Ni content away from the interface (more than 10 nm) is equivalent to that of the bulk level (49.0 at.%), while Ni content in the vicinity of the interface (less than 10 nm) drastically increases upto 58.8 at.% at 2 nm from the interface. This demonstrates that Ni accumulation occurred during anodization due to the preferential

anodization of Ti. The accumulation of alloying elements at the interface between substrate and oxide layer was also reported for Al-W alloys that formed compact oxide layers[35].

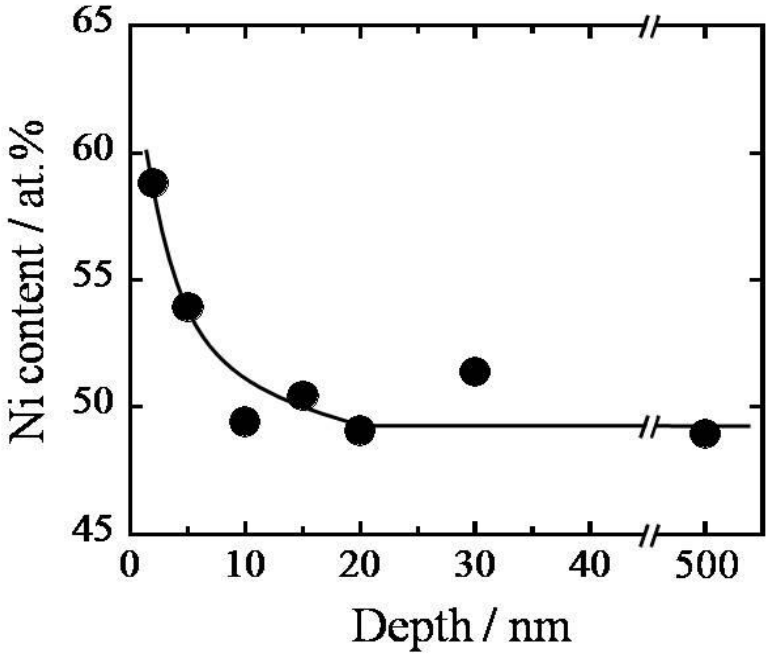

Fig. 3-9 Depth distribution of Ni content in the Ti-49.0 at.% Ni alloy substrate from the interface between the alloy substrate and the anodic oxide layer.

As shown in Fig. 3-6, the higher the Ni concentration of the alloy substrate, the more rapid the formation of irregular-shaped porous oxide layers. One can conclude from these findings, that once the Ni concentration in the vicinity of the interface reaches a threshold amount due to the preferential anodization of Ti, nanotubular oxide layers cannot be grown, and irregular-shaped porous oxide layers are instead formed underneath the nanotubular layers. Furthermore, after long-term anodization (60 min), the irregular-shaped porous oxide layers are visible from a top-view, as the nanotubular oxide layers on the top are completely dissolved.

3.4 Conclusion

In the present chapter the author examined the growth of anodic oxide layers on four Ti-Ni alloys with different Ni contents in the ethylene glycol containing 0.06 M NH_4F and 1.5 wt.% H_2O. The morphology of resulting oxide layers was not influenced by the crystal structure of the alloy substrates, but clearly affected by Ni content in the substrates and anodization time. Anodization of all Ti-Ni alloys for a short time resulted in the formation of nanotubular oxide layers. Extended anodization formed irregular-shaped porous layers underneath the nanotubular layers. After further longer anodization, only the irregular-shaped porous layers remained due to the dissolution of the nanotubular layers. This morphological transition occurred faster for higher Ni content alloy. The morphological transition was attributed to Ni enrichment in the vicinity of the interface between the alloy substrates and formed oxide layers due to the preferential anodization of Ti.

References :

1) M. Assefpour-Dezfuly, C. Vlachos, E. H. Andrews, J. Mater. Sci., **19** (1984) 3626.

2) V. Zwilling, E. Darque-Ceretti, A. Boutry-Forveille, D. David, M. Y. Perrin1, M. Aucouturier, Surf. Interface Anal., **27** (1999) 629.

3) V. Zwilling M. Aucouturier, E. Darque-Ceretti, Electrochim. Acta, **45** (1999) 921.

4) W.J. Lee, W.H. Smyrl, Electrochem. Solid State Lett., **8** (2005) B7.

5) I. Sieber, H. Hildebrand, A. Friedrich, P. Schmuki, Electrochem. Commun., **7** (2005) 97.

6) N.R. de Tacconi, C.R. Chenthamarakshan, G. Yogeeswaran, A. Watcharenwong, R.S. de Zoysa, N.A. Basit, K. Rajeshwar, J. Phys. Chem. B, **110** (2006) 25347.

7) I. Sieber, B. Kannan, P. Schmuki, Electrochem. Solid-State Lett., **8** (2005) J10.

8) H. Tsuchiya, P. Schmuki, Electrochem. Commun., **7** (2005) 49.

9) S.H. Jang, H.C. Choe, Y.M. Ko, W.A. Brantley, Thin Solid Films, **517** (2009) 5038.

10) D. Ding, C. Ning, L. Huang, F. Jin, Y. Hao, S. Bai, Y. Li, M. Li, D. Mao, Nanotechnol., **20** (2009) 305103.

11) H. Tsuchiya, T. Akaki, Y. Koizumi, Y. Minamino, S. Fujimoto, Electrochem. Commun., **26** (2013) 117.

12) J. Zhao, X. Wang, Y. Kang, X. Xu, Y. Li, Photonics Technol. Lett., IEEE, **20** (2008) 1213.

13) J.G. Yu, G.P. Dai, B. Cheng, J. Phys. Chem. C, **114** (2010) 19378.

14) G.K. Mor, K. Shankar, M. Paulose, O.K. Varghese and C.A. Grimes, Nano Lett., **6** (2006) 215.

15) H.F. Lu, F. Li, G. Liu, Z. Chen, D. Wang, H. Fang, G. Lu, Z. Jiang, H. Cheng, Nanotechnology, **19** (2008) 405504.

16) S. Berger, A. Ghicov, Y.C. Nah, P. Schmuki, Langmuir, **25** (2009) 4841.

17) K. Das, S. Bose, A. Bandyopadhyay, J. Biomed. Mater. Res. A, **90** (2009) 225.

18) Y. Lai, L. Sun, Y. Chen, H. Zhuang, Ch. Lin, J.W. Chin, J. Electrochem. Soc., **153** (2006) D123.

19) J.M. Macak, P. Schmuki, Electrochim. Acta, **52** (2006) 1258.

20) J.M. Macak, L.V. Taveira, H. Tsuchiya, K. Sirotna, P. Schmuki, J. Electroceram., **16** (2006) 29.

21) J.M. Macak, H. Tsuchiya, L. Taveira, S. Aldabergerova, P. Schmuki, Angew. Chem. Int. Ed., **44** (2005) 7463.

22) C.P. Ferreira, M. C. Goncalves, R. Caram, R. Bertazzoli, C.A. Rodrigues, Appl. Surf. Sci., **285** (2013) 226.

23) M.S. Kim, S. Yamamoto, H. Tsuchiya, S. Fujimoto, ECS Trans., **66** (2015) 135.

24) S. So, K. Lee, P. Schmuki, Phys. Stat. Sol. RRL, **6** (2012) 169.

25) S. Miyazaki, K. Otsuka, C.M. Wayman, Acta Metall, **7** (1989) 1885.

26) Y. Liu, P.G. McCormick, Acta Metall Mater, **7** (1990) 1321.

27) Z. Li, D. Ding, Q. Liu, C. Ning, Sensors, **13** (2013) 8393.

28) R. Hang, X. Huang, L. Tian, Z. He, B. Tang, Electrochim. Acta, **70** (2012) 382.

29) J.H. Kim, K. Zhu, Y.F. Yan, C.L. Perkins, A. Frank, Nano Lett., **10** (2010) 4099.

30) R. Qin, D.Y. Ding, C.Q. Ning, H.G. Liu, B.S. Zhu, M. Li, D.L. Mao, Appl. Surf. Sci., **257** (2011) 6308.

31) B. Strnadel, S. Ohashi, H. Ohtsuka, S. Miyazaki, T. Ishihara, Mater. Sci. Eng. A, **203** (1995) 187.

32) J. Frenzel, E.P. George, A. Dlouhy, Ch. Somsen, M.F.-X. Wagner, G. Eggeler, Acta Mater., **58** (2010) 3444.

33) H. Moon, S. Chun, Y. Liu, H. Yang, Y. Kim, T. Nam, J. Alloys Comp., **577S** (2013) S259.

34) N.K. Shrestha, M. Yang, P. Schmuki, Electrochem. Solid-State Lett., **13** (2010) C2.

35) H. Habazaki, K. Shimizu, P. Skeldon, G.E. Thompson, G.C. Wood, J. Electrochem. Soc., **143** (1996) 2465.

Chapter 4 Formation of anodic nano-structured oxide layers on Ti-Fe alloys

4.1 Introduction

The formation of self-organized nano-structures and nano-patterns has attracted much attention due to not only the scientific interests to self-organizing phenomena but also the technological impacts for the production of functional devices. Therefore, a variety of synthesis routes have been proposed and demonstrated. Electrochemical anodization is one of the highly promising routes to form self-organized nano-structures. A well-established example achieved by anodization is highly ordered nanoporous oxide layers on Al substrate[1, 2]. It has been reported that the morphology of nanoporous aluminum oxide layers can be varied by controlling anodization parameters and many applications of the ordered structures have been proposed, such as photonic crystal and a template for the secondary material depositions[3-7].

In the last decades, on the other hand, the formation of self-organized nanoporous or nanotubular oxide layers has been reported on the other metals than Al; Ti[8-13], Zr[14, 15], Hf[16], Nb[17, 18], Ta[19, 20] and W[21]. In particular extensive researches have been carried out for TiO_2 nanotubular layer due to a wide range of applications of TiO_2. TiO_2 nanotubular layer was firstly reported by Assefpour-Dezfuly et al. and Zwilling et al. in electrolytes containing a small amount of fluoride species[8, 9]. In the electrolytes the thickness of TiO_2 nanotubolar layers was reported to be several hundred nanometers. TiO_2 nanotubular oxide layers are grown further by tailoring electrolyte composition – in neutral electrolytes the thickness reached a few micrometers[11] and furthermore in organic electrolytes TiO_2 nanotubular oxide layers with the thickness of several micrometers were reported[12].

Recently the thickness reached a few hundred micrometers by optimizing electrolyte composition[13].

TiO_2 nanotubular layers have been applied for various applications such as photocatalyst[22-24], dye-sensitized solar cell[25, 26], other functional and biomedical devices[27-29]. Among the applications photocatalyst is one of the most examined applications of TiO_2 nanotubular layer. To enhance and improve photocatalytic efficiency of TiO_2 nanotubular oxide layers, in addition to the increased surface area by controlling the morphology, several surface modifications have been proposed, for examples, the decoration of metal or other semiconductor particles by different methods such as photoreduction, sputter deposition and wet chemical precipitation[30-32]. Other unique route to modify TiO_2 nanotubular layer is alloy anodization. Paramasivam et al. reported that TiO_2 nanotubular layers containing WO_3 prepared by anodization of Ti-W alloys exhibited higher photocatalytic activity compared to bare TiO_2 nanotubular layers[33], indicating that the photocatalytic activity of TiO_2 nanotubular layer can be tuned by alloy anodization. Therefore, other elements that can improve the photocatalytic activity of TiO_2 are expected to be examined. Fe is the one of the candidates as it has been reported that porous oxide layers are formed on Fe surface by anodization and furthermore its oxides exhibit photocatalytic activity in visible light region, different from TiO_2[34, 35].

The present chapter reports the formation of nano-structured oxide layers by anodization of Ti-Fe alloy with a wide range of Fe content and especially addresses how substrate composition and anodization conditions affect the morphology of anodic oxide layers.

4.2 Experimental

Materials were Ti-x at.% Fe alloys (x = 10, 50 and 70). The Ti-Fe alloys were

fabricated by melting high purity Ti and Fe sheets in an arc melting furnace. Specimens were cut into sheets with a dimension of 15×15×3 mm^3 from the alloy ingots by spark machining. Some of the specimens were homogenized at 1000 ℃ for 24 hours and then water-quenched. The crystal structure of the Ti-Fe alloys was examined using X-ray diffraction (XRD, Philips PW3040/60 X'Pert Pro). Prior to anodization all specimens were mirror-finished, followed by sonicating successively in aceton, methanol and deionized water. The electrochemical cell consisted of a two-electrode configuration with a platinum plate as a counter electrode. The sheet specimens were pressed against an O-ring on the electrochemical cell, leaving the surface area of 0.785 cm^2 exposed to an electrolyte. The electrolyte used in the present work was an ethylene glycol containing 0.05 M NH_4F and 2 vol.% H_2O. For anodization applied voltage increased from 0 V to a desired voltage with the ramp rate of 1 Vs^{-1} and then was kept at the voltage for various anodization times. After the anodization the specimens were rinsed with ethanol and then dried with N_2 stream. Morphological characterization of resulting oxide layers was carried out using a field-emission scanning electron microscope (FE-SEM, JEOL JSM-7001FA). Cross-sectional SEM images were taken from mechanically scratched samples, where a partial lift-off of oxide layers occurred.

4.3 Results and discussion

4.3.1 Fabrication and characterization of Ti-Fe alloys

Figures 4-1 (a)-(c) shows XRD patterns of as-cast Ti-Fe alloys that were prepared by the arc melting. It is clear from the figures that peaks detected from as-cast Ti-50 at.% Fe and Ti-70 at.% Fe alloys are ascribed to peaks originated from TiFe and $TiFe_2$, respectively. On the other hand, peaks obtained for as-cast Ti-10 at.% Fe alloy are assigned to those from α-Ti or β-Ti, indicating that Ti-10 at.% Fe alloy consisted of the binary phases. It was

reported that anodization of the binary phase alloys such as Ti6Al4V and Ti6Al7Nb resulted in the growth of inhomogeneous oxide layers due to the selective dissolution of less stable phase and different reaction rates depending on phases whereas homogenous surface structures were obtained on single phase alloys[36, 37]. This result indicates that single phase alloy is required to form homogeneous oxide layers by anodization. Therefore, in the present work, the heat-treatment was carried out for Ti-10 at.% Fe alloy. XRD pattern of the heat-treated Ti-10 at.% Fe alloy is presented in Fig. 4-1 (d). All peaks are assigned to those for β-Ti, meaning that a single phase alloy was obtained after the heat-treatment. These single phase alloys were subjected to anodization experiments.

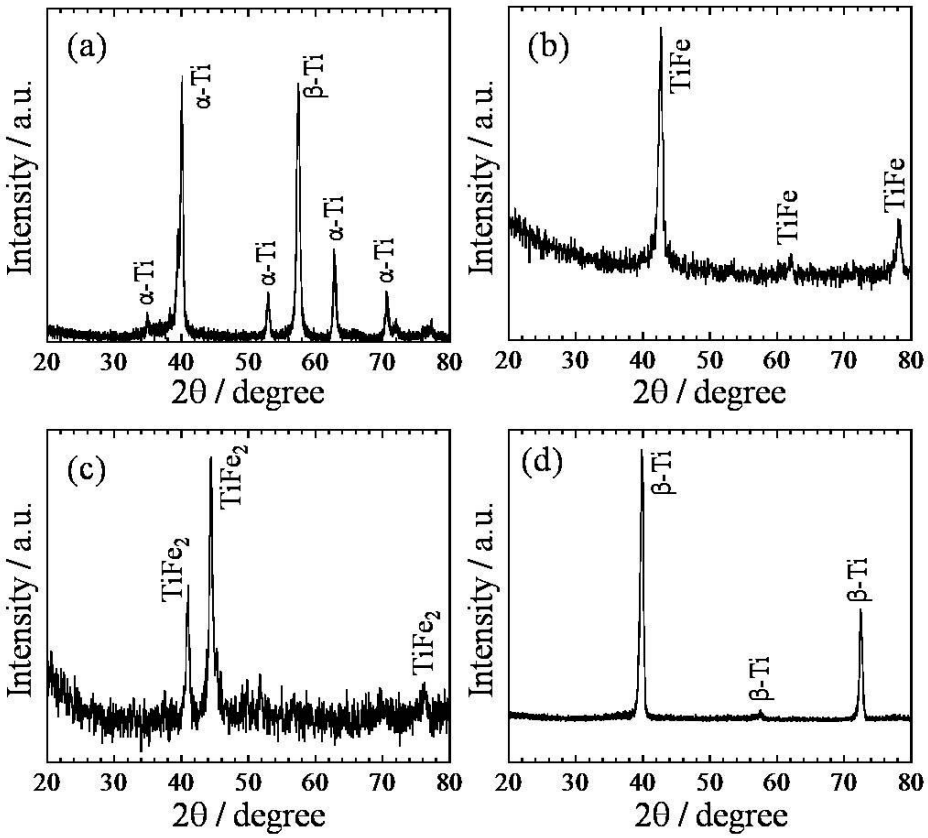

Fig. 4-1 XRD patterns of Ti-Fe alloys; (a) as-cast Ti-10 at.% Fe, (b) as-cast Ti-50 at.% Fe, (c) as-cast Ti-70 at.% Fe alloy and (d) heat-treated Ti-10 at.% Fe alloy.

4.3.2 Growth of anodic oxide layers formed on Ti-Fe alloys

From a set of preliminary anodization experiments, an ethylene glycol containing 0.05 M NH_4F and 2 vol.% H_2O was determined as anodization electrolyte for the Ti-Fe alloys. Figure 4-2 shows current-voltage curves from 0 V to 30 V and subsequent current-time curves at 30 V obtained on the Ti-Fe alloys for 3 hours in the electrolyte. The one obtained for pure Ti was also included as comparison. For pure Ti and Ti-10 at.% Fe alloy, the current density steeply increases until the applied voltage reaches 10 V and then exhibits gradual increase with increasing applied voltage. On the other hand, the current density obtained on Ti-50 at.% Fe and Ti-70 at.% Fe alloys significantly increases upto the anodization voltage of 30 V. After switching to the constant voltage of 30 V, the current-time curves of all substrates exhibit drastic decrease in the very early stage, then slight increase once and finally gradual decrease to a steady state value. The steady state currents for the Ti-10 at.% Fe and Ti-50 at.% Fe alloys are found to be similar to that for pure Ti. However, the current obtained for the Ti-70 at.% Fe alloy is clearly much higher compared to those for pure Ti and the Ti-Fe alloys with lower Fe content.

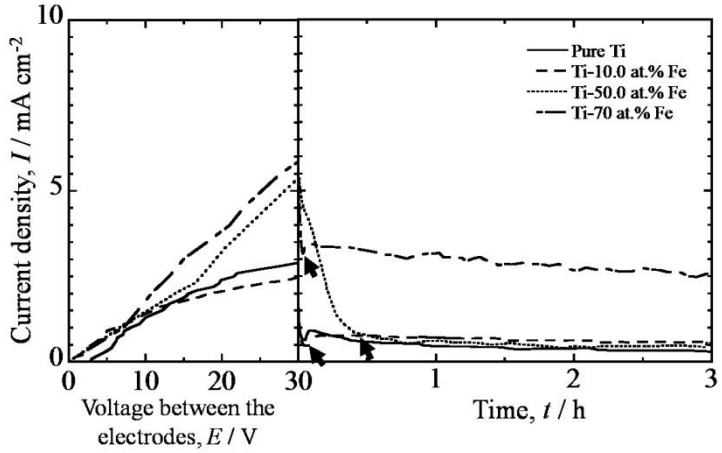

Fig. 4-2 Current transients during the anodization of pure Ti, Ti-10 at.% Fe, Ti-50 at.% Fe and Ti-70 at.% Fe alloys at 30 V in the ethylene glycol containing 0.05 M NH_4F and 2 vol.% H_2O. The arrows indicate the current density defined as the initial current.

Figures 4-3 and 4-4 show top-view and cross-sectional images of resulting oxide layers, respectively. Nanotubular oxide layers were grown of pure Ti, Ti-10 at.% Fe and Ti-70 at.% Fe alloy although the initiation layers[38] still remain even after anodization for 3 hours. On the other hand, it is obvious from Figs. 4-3 (c) and 4-4 (c) that totally different morphology is observed for the oxide layer formed on the Ti-50 at.% Fe alloy – an irregular-shaped porous oxide layer is formed on the alloy. Furthermore the thickness of the oxide layer on the Ti-50 at.% Fe alloy is quite thinner compared to those for pure Ti, the Ti-10 at.% Fe and Ti-70 at.% Fe alloy.

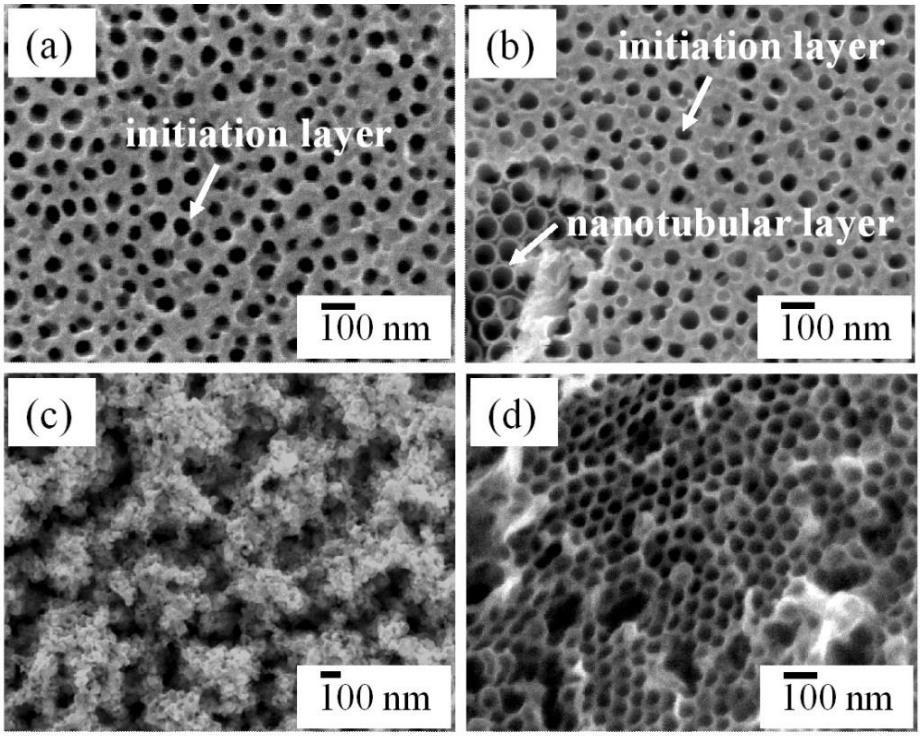

Fig. 4-3 Top-view SEM images of anodic oxide layers formed on (a) pure Ti, (b) Ti-10 at.% Fe, (c) Ti-50 at.% Fe and (d) Ti-70 at.% Fe alloys at 30 V for 3 h in the ethylene glycol containing 0.05 M NH_4F and 2 vol.% H_2O.

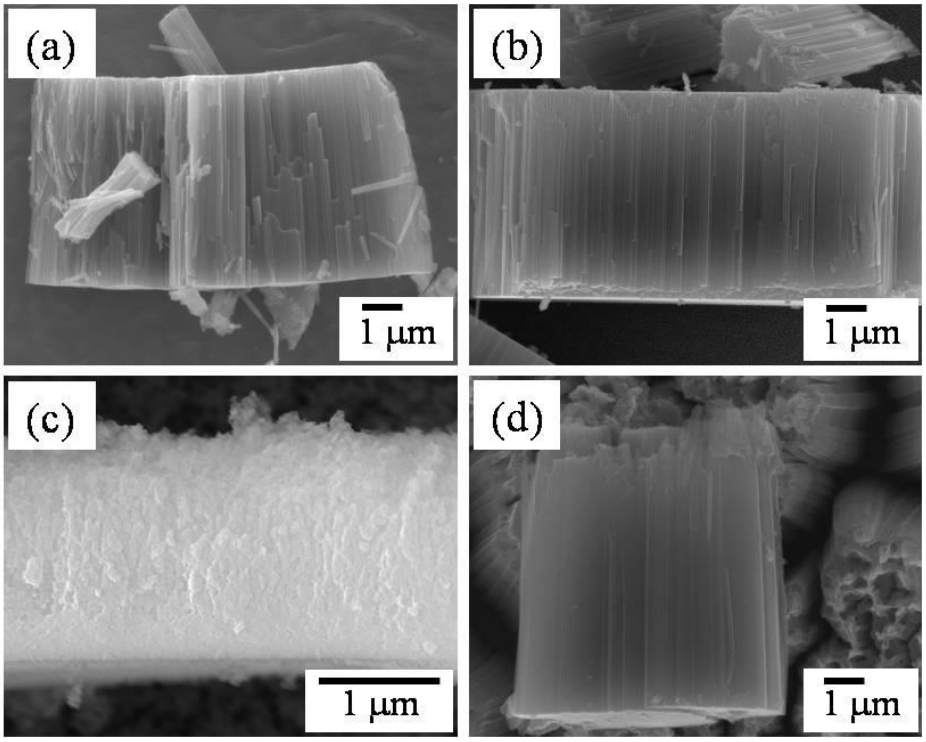

Fig. 4-4 Cross-sectional SEM images of anodic oxide layers formed on (a) pure Ti, (b) Ti-10 at.% Fe, (c) Ti-50 at.% Fe and (d) Ti-70 at.% Fe alloys at 30 V for 3 h in the ethylene glycol containing 0.05 M NH_4F and 2 vol.% H_2O.

4.3.3 Effect of applied voltage on the growth of anodic oxide layers on Ti-Fe alloys

As presented in Figs. 4-3 and 4-4, the morphology of anodic oxide layer clearly depends on the chemical composition of substrate when anodized at 30 V. The effect of applied voltage on the morphology of anodic oxide layer was examined and SEM images of anodic oxide layers formed on pure Ti and the Ti-Fe alloys at 50 V are shown in Fig. 4-5. As apparent from the images, nanotubular oxide layers were formed on pure Ti and the Ti-10 at.% Fe alloy at 50 V as similar to 30 V, whereas on Ti-50 at.% Fe and Ti-70 at.% Fe irregular-shaped porous oxide layers were grown. However, the effect of applied voltage on the oxide morphology observed for the specimens anodized at 10 V is strongly different compared to those presented at the higher applied voltages. Figure 4-6 shows SEM images of anodic oxide layers formed on the Ti-Fe alloys with different Fe contents at 10 V. It is clear that the anodic oxide layers exhibit nanotubular structure on all substrates at this

voltage.

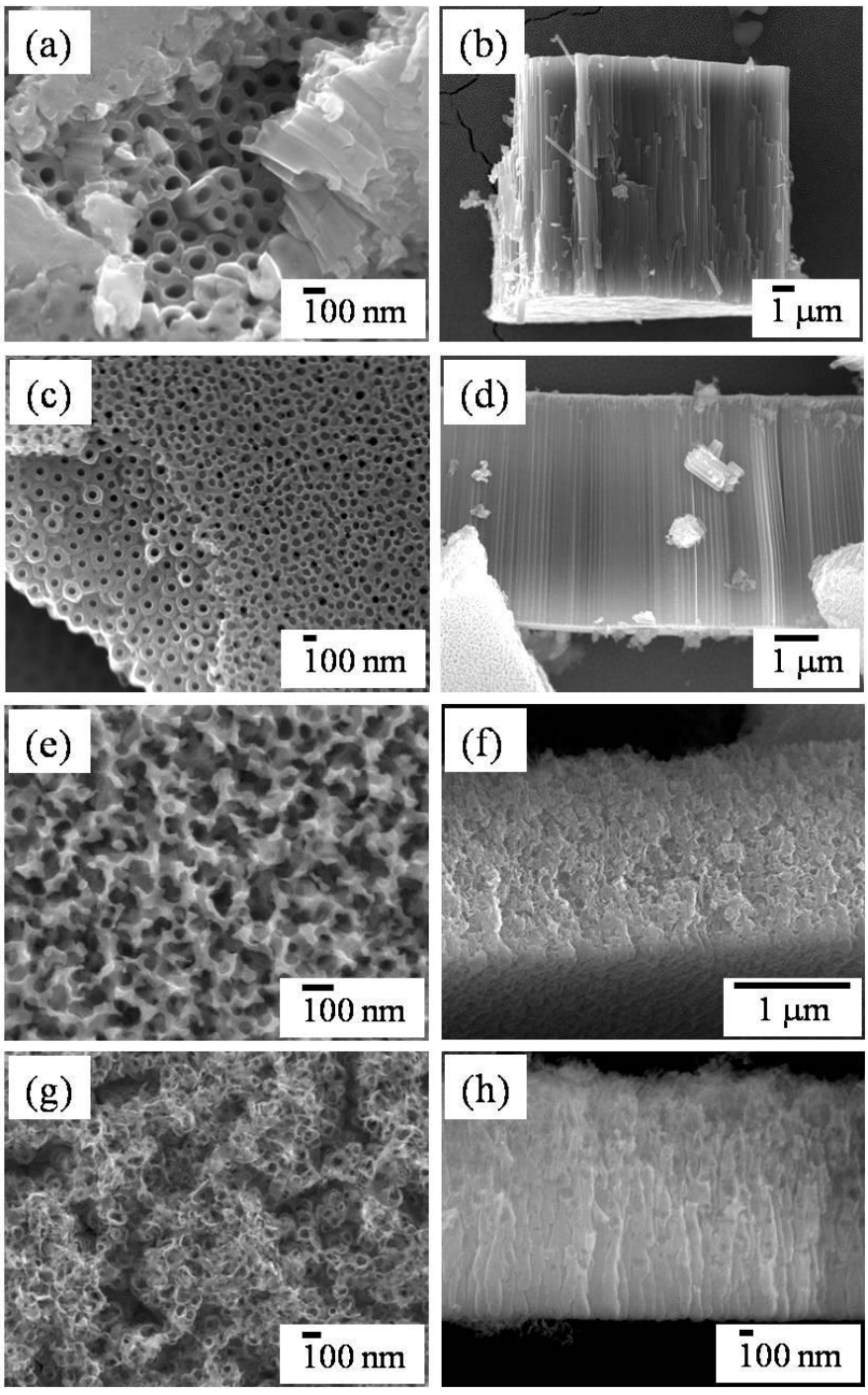

Fig. 4-5 Top-view and cross-sectional SEM images of anodic oxide layers formed on pure Ti ((a) and (b)), Ti-10 at.% Fe ((c) and (d)), Ti-50 at.% Fe ((e) and (f)) and Ti-70 at.% Fe ((g) and (h)) at 50 V for 3 h in the ethylene glycol containing 0.05 M NH_4F and 2 vol.% H_2O; (a), (c), (e) and (g) top-view image, (b), (d), (f) and (h) cross-sectional image.

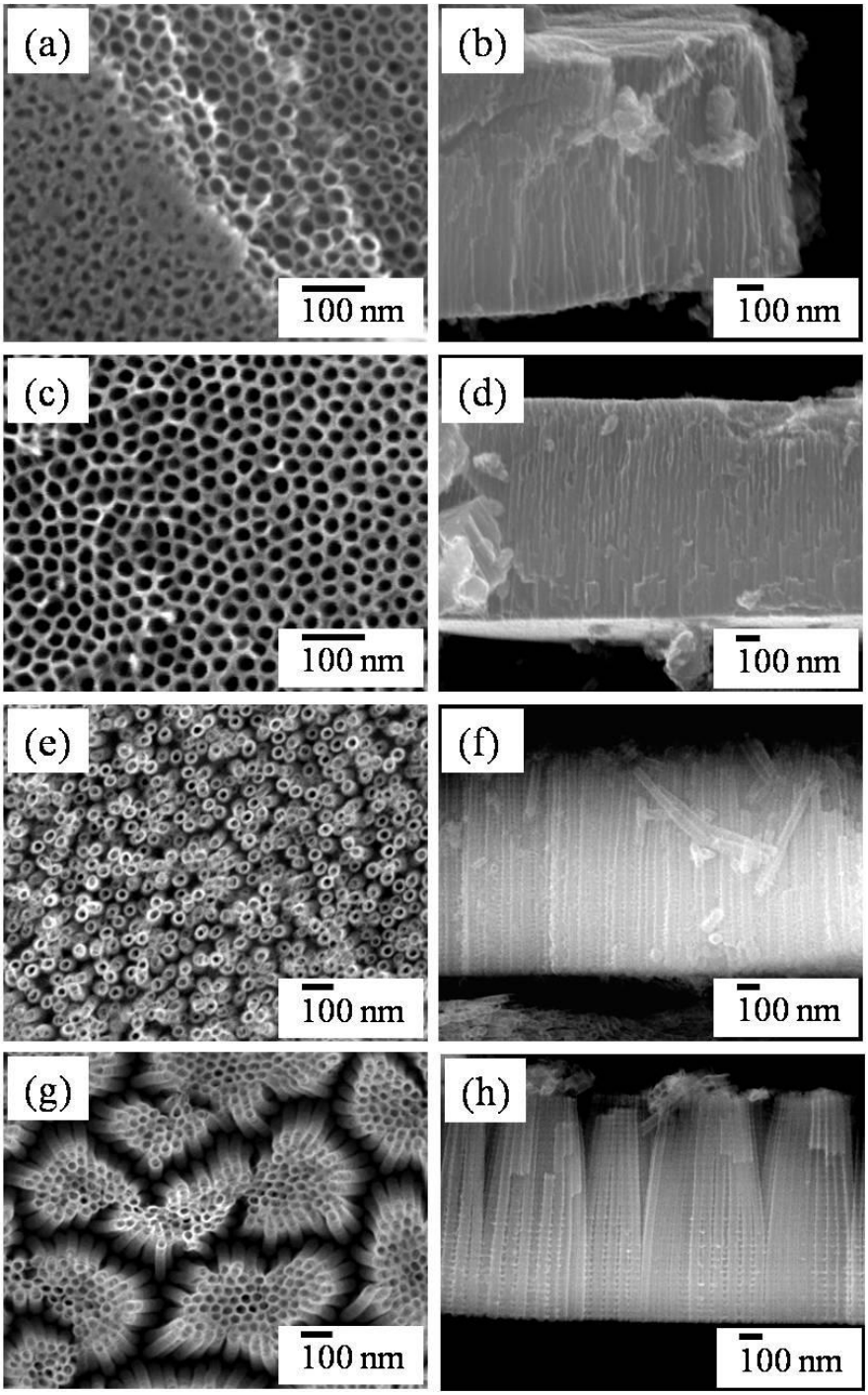

Fig. 4-6 Top-view and cross-sectional SEM images of anodic oxide layers formed on pure Ti ((a) and (b)), Ti-10 at.% Fe ((c) and (d)), Ti-50 at.% Fe ((e) and (f)) and Ti-70 at.% Fe ((g) and (h)) at 10 V for 3 h in the ethylene glycol containing 0.05 M NH_4F and 2 vol.% H_2O; (a), (c), (e) and (g) top-view image, (b), (d), (f) and (h) cross-sectional image.

Therefore it was found that nanotubular oxide layers were formed on pure Ti and the Ti-10 at.% Fe alloy at various applied voltages ranged from 10 V to 50 V. For the Ti-50 at.% Fe and Ti-70 at.% Fe alloy, on the other hand, significant changes in the oxide morphology were recognized, that is, the morphological transition from nanotubular structure to an irregular-shaped porous structure occurred although the threshold applied voltage for the transition was different according to Fe content in the alloys.

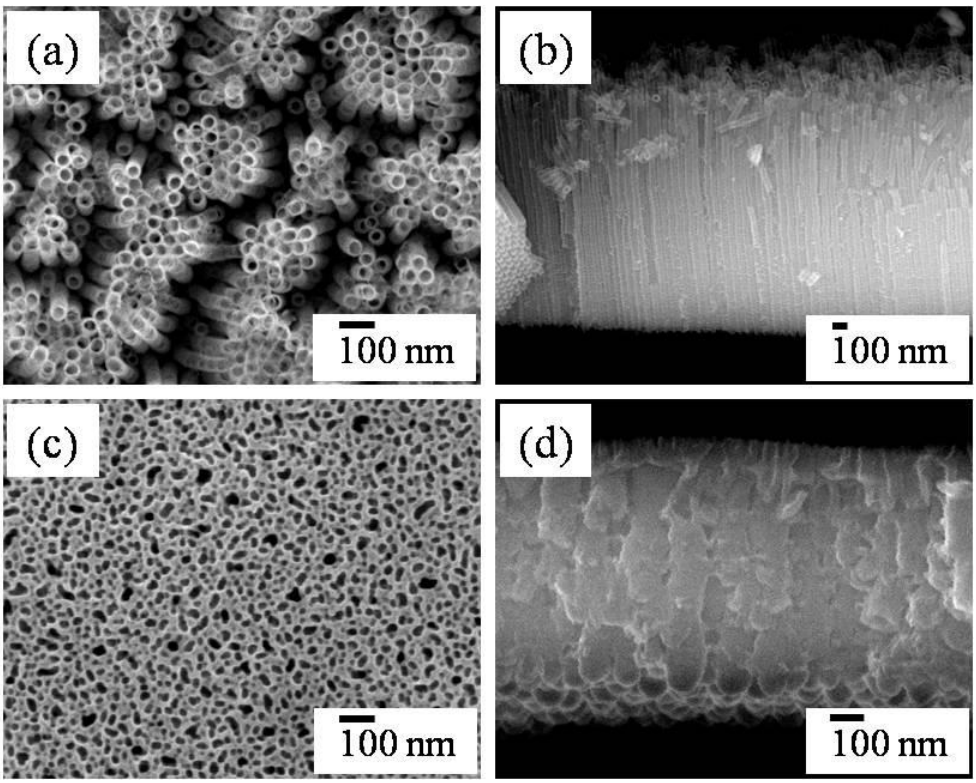

Fig. 4-7 Top-view and cross-sectional SEM images of anodic oxide layers formed on Ti-50 at.% Fe alloy at 10 V for 18 h ((a) and (b)) and at 30 V for 1 h ((c) and (d)) in the ethylene glycol containing 0.05 M NH_4F and 2 vol.% H_2O; (a) and (c) top-view image, (b) and (d) cross-sectional image.

As mentioned above the anodic oxide layers on the Ti-50 at.% Fe and Ti-70 at.% Fe alloys exhibit different morphologies – nanotubular or irregular-shaped porous structures – depending on applied voltage. Similar morphological transition was observed on Ti-Ni

alloys where the transition in the oxide morphology form nanotubular to irregular-shaped porous structures occurred as the anodization time was increased as described in chapter 3[39]. Therefore, it may be considered that the anodization time of 3 hours is long enough to reach the situation where irregular-shaped porous oxide layers are grown on the Ti-50 at.% Fe at 30 V whereas at 10 V longer anodization time than 3 hours may be required to grow irregular-shaped porous structures. In order to get this point clear, anodization experiments were carried out for different anodization times. Figures 4-7 (a)-(b) and (c)-(d) shows SEM images of oxide layers formed on the Ti-50 at.% Fe at 10 V for 18 hours and at 30 V for 1 hour, respectively. A nanotubular oxide layer is clearly formed on the alloy after anodization at 10 V for 18 hours. On the other hand, the morphology of the anodic oxide layer after anodized at 30 V for 1 hour exhibits irregular-shaped porous structure. Therefore, it is found that the morphological transition is not affected by anodization time for the Ti-Fe alloy.

4.3.4 Effect of anodic reaction rate on the morphology of anodic oxide layers

The results presented in 4.3.2 and 4.3.3 were obtained by potentiostatic anodization where anodic oxide layers were grown on the Ti-Fe alloys at constant voltage. In order to examine the effect of anodic reaction rate on the morphology of anodic oxide layers galvanostatic anodization of the Ti-Fe alloys was also preformed, that is, constant current was applied. Figure 4-8 shows SEM images of anodic oxide layers formed on the Ti-50 at.% Fe at different constant current densities for 3 hours.

It is clear that the anodic oxide layers formed at the smaller current densities such as 0.12 mA cm^{-2} and 0.35 mA cm^{-2} exhibit nanotubular structures while irregular-shaped porous structure is obtained for the oxide layer formed at the larger current density as 0.63 mA cm^{-2} as shown in Fig. 4-8 (f). This indicates that the current density can be responsible

for the formation of the irregular-shaped porous oxide layers. Therefore, the morphology of anodic oxide layers is discussed in terms of current density. As presented in Fig. 4-2, the amplitude of current density obtained during anodization varied depending on alloy composition. On the other hand, the current transient is almost similar for all substrates, that is, the current density generated at constant voltage significantly decrease in the early stage, slightly increases and then gradually decreases to a steady state value. In the present work, hereafter, the current density after the initial decay as pointed by the arrows in Fig. 4-2 and the current density obtained just before the termination of anodization are defined as the initial current and the final current, respectively. Figure 4-9 (a) summarizes the morphology of anodic oxide layers formed on the Ti-50 at.% Fe alloy using the initial current and the final current. It is note that for the galvanostatic anodization the initial current is equivalent to the final current. It is clear from the figure that the morphology of anodic oxide layers on the Ti-50 at.% Fe alloy is found to be determined by the initial current rather than the final current. Similar explanation can be adopted for the Ti-10 at.% Fe and Ti-70 at.% Fe as shown in Figs. 4-9 (b) and (c), respectively. Therefore, one can deduce that the initial current strongly affects the morphology of anodic oxide layers, that is, lower initial current is required for the formation of nanotubular oxide layers whereas irregular-shaped porous oxide layers are formed when higher initial current is generated or applied although the threshold from nanotubular to irregular-shaped porous structures strongly differs depending on the alloy composition. In order to demonstrate that the initial current strongly affects the nanotube formation, two-step galvanostatic anodization was performed on Ti-50 at.% Fe alloy. In this experiment the anodization was divided into successive two processes. For one specimen a lower current than the threshold current for the Ti-50 at.% Fe alloy was applied for 1 hour as the first step and then a larger current than the threshold was applied for the same period as the second step. For the other, the

constant current was applied in the reverse procedure, that is, the larger current was applied first, then switched to the lower current. SEM images of the resulting oxide layers are presented in Fig. 4-10. For the experiment the constant current density of 0.35 mA cm^{-2} and 0.63 mA cm^{-2} were selected as a smaller current and a larger current than the threshold current density.

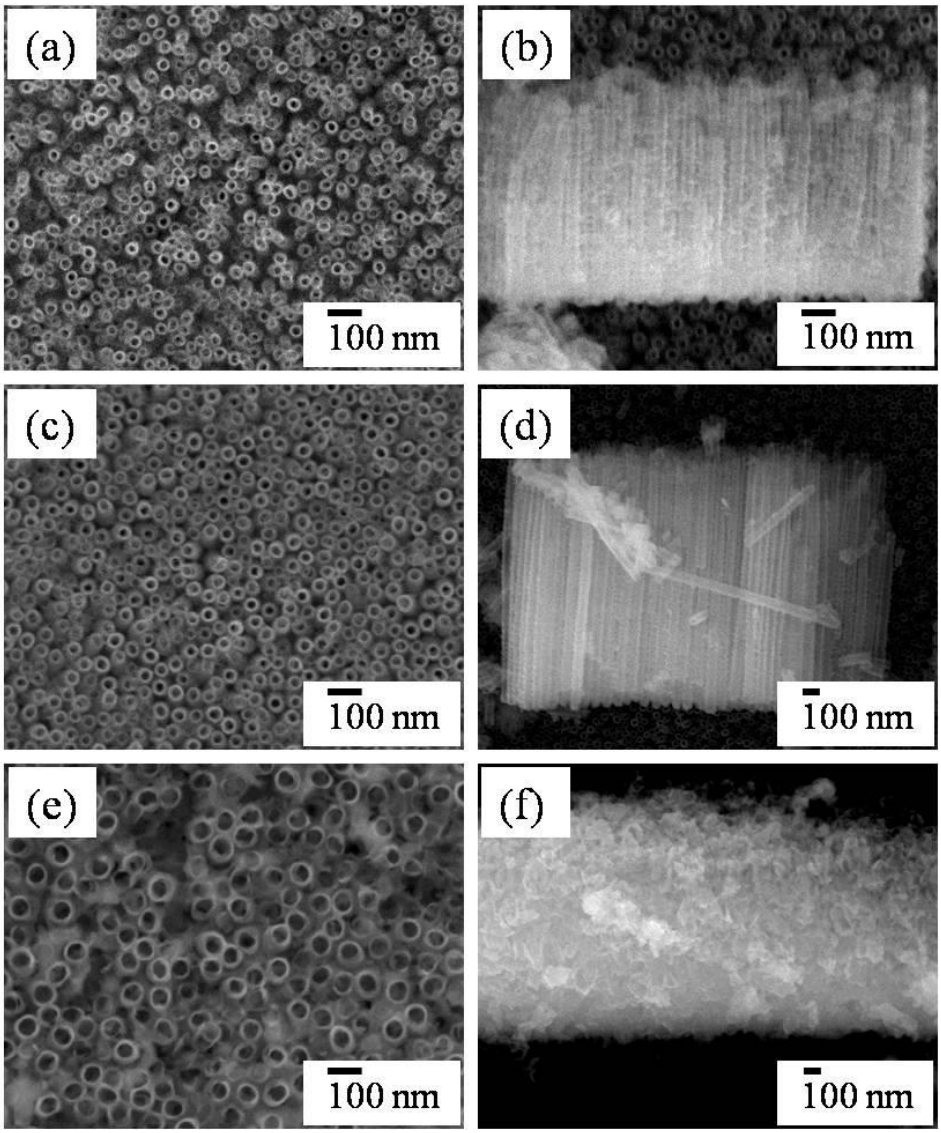

Fig. 4-8 Top-view and cross-sectional SEM images of anodic oxide layers formed on Ti-50 at.% Fe alloy at at 0.12 mA cm^{-2} ((a) and (b)), 0.35 mA cm^{-2} ((c) and (d)) and 0.63 mA cm^{-2} ((e) and (f)) for 3 h in the ethylene glycol containing 0.05 M NH_4F and 2 vol.% H_2O; (a,) (c) and (e) top-view image, (b), (d) and (f) cross-sectional image.

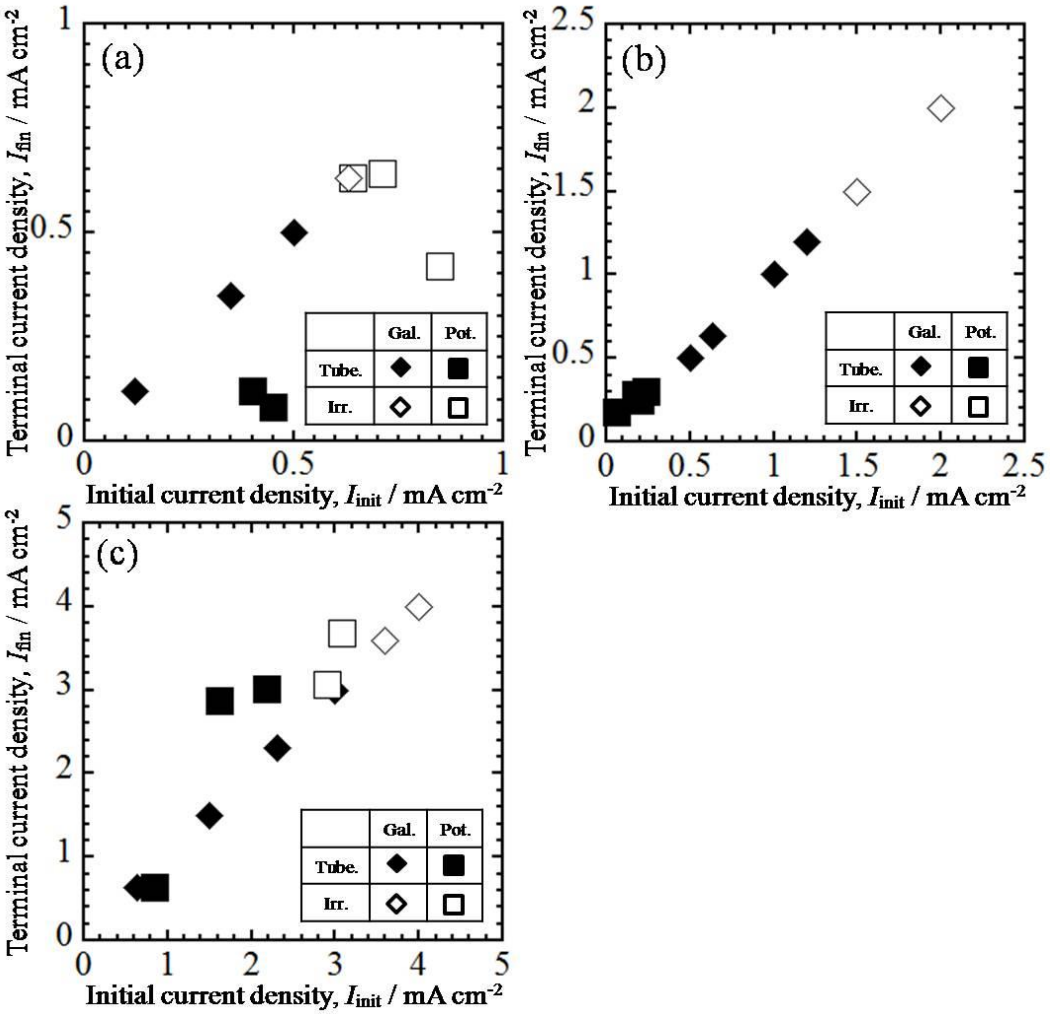

Fig. 4-9 Relationship between the initial current density, the final current density and the morphology of resulting oxide layers formed on (a) Ti-50 at.% Fe alloy, (b) Ti-10 at.% Fe and (c) Ti-70 at.% Fe alloy in the ethylene glycol containing 0.05 M NH_4F and 2 vol.% H_2O under various anodization conditions. "Gal." and "Pot."in the inset table indicate anodization was carried out galvanostatically and potentiostatically, respectively. "Irr." and "Tube" mean that irregular-shaped porous layer and nanotubular layer were formed after anodization, respectively.

Figure 4-10 (a) shows the cross-section of the oxide layer formed on the Ti-50 at.% Fe alloy by a two-step galvanostatic anodization where the larger current density first and then the smaller current density were applied. It is clear that the anodic oxide layer exhibits irregular-shaped porous structure. On the other hand, when the constant currents were applied in the reverse procedure, the formation of nanotubes was confirmed as shown in

Fig. 4-10 (b). From these results one can deduce that the formation of the irregular-shaped porous oxide layers at higher voltage is attributed to the generation of large current in the initial stage of anodization, in other words, it can be required to suppress initial current density during anodization in order to form nanotubular oxide layers on the Ti-Fe alloys.

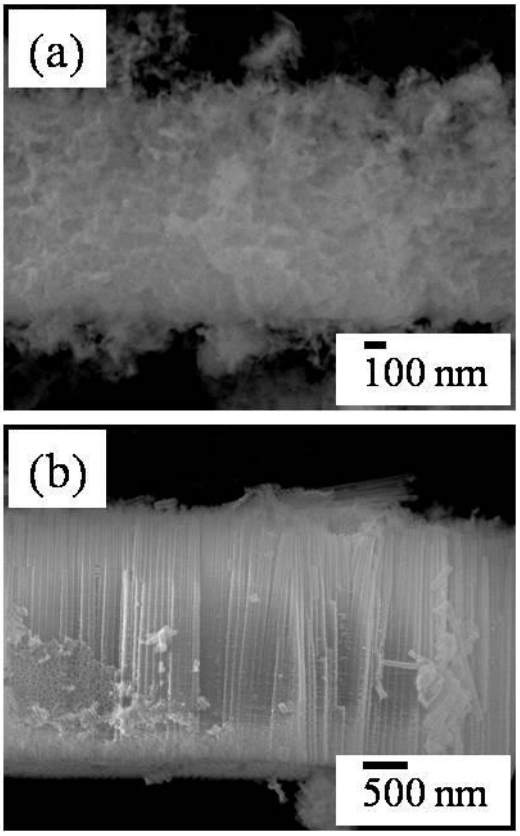

Fig. 4-10 Cross-sectional SEM images of anodic oxide layers formed on Ti-50 at.% Fe alloy by the two-step galvanostatic anodization in the ethylene glycol containing 0.05 M NH_4F and 2 vol.% H_2O; (a) the larger current (0.63 mA cm^{-2}) in the 1st step and the smaller current (0.35 mA cm^{-2}) in the 2nd step were applied successively, (b) the two different currents were applied in the reverse procedure.

4.4 Conclusion

In the present work the author examined the morphology of anodic oxide layers on the Ti-Fe alloys at various applied voltages in the ethylene glycol containing 0.05 M NH_4F and

2 vol.% H_2O. The morphology of anodic oxide layers was affected by substrate composition as well as applied voltage. On pure Ti and Ti-10 at.% Fe alloy, nanotubular oxide layers were formed at all applied voltages examined. In the case of Ti-50 at.% Fe, a nanotubular oxide layer was grown only at 10 V. At the higher voltages as 30 V and 50 V, on the other hand, irregular-shaped porous structures were obtained; the morphological transition from nanotubular to irregular-shaped porous structures was observed on the Ti-50 at.% Fe alloy. Similar transition occurred also on the Ti-70 at.% Fe, but the threshold voltage was higher compared to the Ti-50 at.% Fe alloy. It was found that the current density generated in the early stage of anodization strongly affected the morphology of anodic oxide layer on the Ti-Fe alloys, that is, lower initial current density could be required to form nanotubular oxide layers on the Ti-Fe alloys.

References :

1) H. Masuda and K. Fukuda, Science, **268** (1995) 1466.

2) A.P. Li, F. Müller, A. Birner, K. Nielsch, U. Gösele, J. Appl. Phys., **84** (1998) 6023.

3) S. Ono, M. Saito, H. Asoh, Electrochim. Acta, **51** (2005) 827.

4) W. Lee, R. Ji, U. Gösele, K. Nielsch, Nat. Mater., **5** (2006) 741.

5) R.B. Wehrspohn, J. Schilling, MRS Bull., **26** (2001) 623.

6) M. Steinhart, J.H. Wendorff, A. Greiner, R.B. Wehrspohn, K. Nielsch, J. Schilling, J. Choi, U. Gosele, Science, **296** (2002) 1997.

7) S.Z. Chu, K. Wada, S. Inoue, S. Todoroki, Chem. Mater., **14** (2002) 266.

8) M. Assefpour-Dezfuly, C. Vlachos, E.H. Andrews, J. Mater. Sci., **19** (1984) 3626.

9) V. Zwilling, E. Darque-Ceretti, A. Boutry-Forveille, D. David, M.Y. Perrin1, M. Aucouturier, Surf. Interface Anal., **27** (1999) 629.

10) R. Beranek, H. Hildebrand, P. Schmuki, Electrochem. Solid-State Lett., **6** (2003) B12.

11) J.M. Macak, H. Tsuchiya, P. Schmuki, Angew. Chem., Int. Ed., **44** (2005) 2100.

12) J.M. Macak, H. Tsuchiya, L. Taveira, S. Aldabergerova, P. Schmuki, Angew. Chem., Int. Ed., **44** (2005) 7463.

13) S.P. Albu, A. Ghicov, J.M. Macak, P. Schmuki, Phys. Stat. Sol. RRL, **1** (2007) R65.

14) H. Tsuchiya, J.M. Macak, L.V. Taveira, P. Schmuki, Chem. Phys. Lett., **410** (2005) 188.

15) W.J. Lee, W.H. Smyrl, Electrochem. Solid-State Lett., **8** (2005) B7.

16) H. Tsuchiya, P. Schmuki, Electrochem. Commun., **7** (2005) 49.

17) I. Sieber, H. Hildebrand, A. Friedrich, P. Schmuki, Electrochem Commun, **7** (2005) 97.

18) V. Galstyan, E. Comini, G. Faglia and G. Sberveglieri, CrystEngComm, **16** (2014) 10273.

19) I. Sieber, B. Kannan, P. Schmuki, Electrochem. Solid-State Lett., **8** (2005) J10.

20) N.K. Allam, X.J. Feng, C.A. Grimes, Chem. Mater., **20** (2008) 6477.

21) H. Tsuchiya, J.M. Macak, I. Sieber, L. Taveira, A. Ghicov, K. Sirotna, P. Schmuki, Electrochem. Commun., **7** (2005) 295.

22) H.J. Oh, J.H. Lee, Y.J. Kim, S.J. Suh, J.H. Lee, C.S. Chi, Appl. Catal. B: Environ., **84** (2008) 142.

23) Y. Liao, W. Que, J. Alloys Compd., **505** (2010) 243.

24) J.W. Ng, X.W. Zhang, T. Zhang, J.H. Pan, J-H.A. Du, D.D. Sun, J. Chem. Technol. Biotechnol., **85** (2010) 1061.

25) D. Kuang, J. Brillet, P. Chen, M. Takata, S. Uchida, H. Miura, K. Sumioka, S.M. Zakeeruddin, M. Grätzel, ACS Nano, **2** (2008) 1113.

26) J.R. Jennings, A. Ghicov, L.M. Peter, P. Schmuki, A.B. Walker, J. Am. Chem. Soc., **130** (2008) 13364.

27) S. Liu, A. Chen, Langmuir, **21** (2005) 8409.

28) J. Park, S. Bauer, K. von der Mark, P. Schmuki, Nano Lett, **7** (2007) 1686.

29) S. Oh, Ch. Daraio, L.H. Chen, T.R. Pisanic, R.R. Fiñones, S. Jim, J. Biomed. Mater. Res., **78A** (2006) 97.

30) I. Paramasivam, J.M. Macak, P. Schmuki, Electrochem. Commun., **10** (2008) 71.

31) Y.Q. Liang, Z.D. Cui, S.L. Zhu, X.J. Yang, Electrochim. Acta, **55** (2010) 5245.

32) J.G. Yu, G.P. Dai, B.B. Huang, J. Phys. Chem. C, **113** (2009) 16394.

33) I. Paramasivam, Y.C. Nah, C. Das, N.K. Shrestha, P. Schmuki, Chem. Eur. J., **16** (2010) 8993.

34) S.K. Mohapatra, S.E. John, S. Banerjee, Chemistry of Materials, **21** (2009) 3048.

35) Z. Zhang, M.F. Hossain, T. Takahashi, Mater. Lett., **64** (2010) 435.

36) J.M. Macak, H. Tsuchiya, L. Taveira, A. Ghicov, P. Schmuki, J. Biomed. Mater. Res., **75A** (2005) 928.

37) H. Tsuchiya, J.M. Macak, A. Ghicov, P. Schmuki, Small, **2** (2006) 888.

38) L.V. Taveira, J.M. Macak, H. Tsuchiya, L.F.P. Dick, P. Schmuki, J. Electrochem. Soc., **152** (2005) B405.

39) M.S. Kim, H. Tsuchiya, S. Fujimoto, Appl. Surf. Sci., (in press).

Chapter 5 Growth of anodic oxide layers on Ti-based alloys with different alloying elements

5.1 Introduction

The fabrication of TiO_2 nanotubular layers by the electrochemical anodization process has been studied extensively over the last decades. The electrochemical parameters such as applied voltage, anodization time and electrolyte are tuned to control the tube diameter, thickness, and morphology[1-3]. Furthermore, the doping of other elements into TiO_2 nanotubular layer or the decoration of TiO_2 nanotubular layers with other metal oxide has attracted much attention for improving the various characteristics of TiO_2 nanotubular layers. For example, TiO_2 nanotubular layers with a minor amount of V_2O_5 formed by anodization of Ti-V alloy exhibit significantly enhanced capacitive properties compared with bare TiO_2 nanotubular layers. These characteristic can be ascribed to the V^{4+}/V^{5+} redox reaction of the V_2O_5 phase[4]. Roy et al. reported that a strong and stable enhancement of the photoelectrochemical water splitting activity for RuO_2-decorated TiO_2 nanotubular layers formed on the Ti-Ru alloys[5].

In chapters 3 and 4, the author reported the morphology and growth of anodic oxide layer on Ti-Ni alloy and Ti-Fe alloys that consist of Ti and transition metal. The results clearly indicate that the morphology and growth of the layers are strongly affected by the species and amount of the alloying element in the Ti alloys. In the present chapter, the author examined the effect of other transition metal, Co, on the morphology of anodic oxide layers and compared results obtained for Ti-Co alloy with those for Ti-Ni and Ti-Fe alloys.

5.2 Experimental

Materials examined were Ti-50 at.% Fe, Ti-49.5 at.% Co and Ti-49 at.% Ni alloy. These alloys were fabricated by melting in an arc melting furnace. Some of alloys ingots were homogenized at 1000 ℃ for 24 hours in a high vacuum. The crystal structure of the alloys was examined using X-ray diffraction (XRD, Philips PW3040/60 X'Pert Pro). The ingots were cut into sheet substrates with dimensions of $15\times15\times2mm^3$. The samples were ground with SiC abrasive papers, and then mirror-finished with diamond paste and colloidal silica suspension. Prior to anodization, the samples were cleaned by successively sonication in acetone, ethanol, and methanol, followed by rinsing with deionized water. The electrochemical setup consisted of a two-electrode configuration with the alloys as the working electrode and a platinum plate as the counter electrode. The electrochemical anodization was carried out in an ethylene glycol electrolyte containing 0.06 M NH_4F and 1.5 wt.% H_2O at different voltages for various times using a high-voltage potentiostat (Hokuto Denko HA-3001A). After the anodization, the samples were rinsed with ethanol.

The morphology of oxide layers formed by anodization was investigated using a field-emission scanning electron microscope (FE-SEM, JEOL JSM-7001FA). The cross-sections of the oxide layers were observed from mechanically scratched samples. The chemical compositions of the oxide layers and the substrate were evaluated by EPMA. After the anodization, the concentration of dissolved cations into the electrolyte was measured by atomic absorption spectroscopy (AAS, SHIMADZU AA-6600G).

5.3 Results and discussion

In the chapters 3 and 4, the author reported the growth of nanotubular oxide layers on Ti-Ni and Ti-Fe alloys. The results revealed that the morphology and growth of anodic oxide layers was affected by the amount of alloying element in the substrates and

anodization parameters such as applied voltage and anodization time. Furthermore the author found that the morphological transition from nanotubular structures to irregular-shaped porous structures occurs on Ti-Ni and Ti-Fe alloys.

In the present chapter, the effect of cobalt in Ti-Co alloy on the morphology and growth of anodic oxide layers is examined and the results obtained for the Ti-Co alloy are compared with those for Ti-Ni and Ti-Fe.

5.3.1 Crystal structure and microstructure of Ti-based alloys

In the present chapter, three Ti-based alloys with different alloying elements such as Fe, Co and Ni were prepared in order to examine the effect of alloying element on the growth of anodic oxide layers. Figure 5-1 shows XRD patterns obtained for the Ti-Fe, Ti-Co and Ti-Ni alloys. It is clear that the diffraction peaks detected from (a) Ti-50 at.% Fe alloy and (b) Ti-49.5 at.% Co alloy are attributed to the TiFe and TiCo phase, respectively. As already mentioned in chapter 3, all diffraction peaks detected for (c) Ti-49 at.% Ni alloy correspond to peaks originated from the B19’ martensitic phase. Figure 5-2 shows backscattered electron micrographs of the each alloy. Although peaks assigned to precipitates are not detected by XRD, relatively small precipitates still remain. EPMA revealed that the chemical composition of the alloys on the rest of the surface is almost constant independent of location.

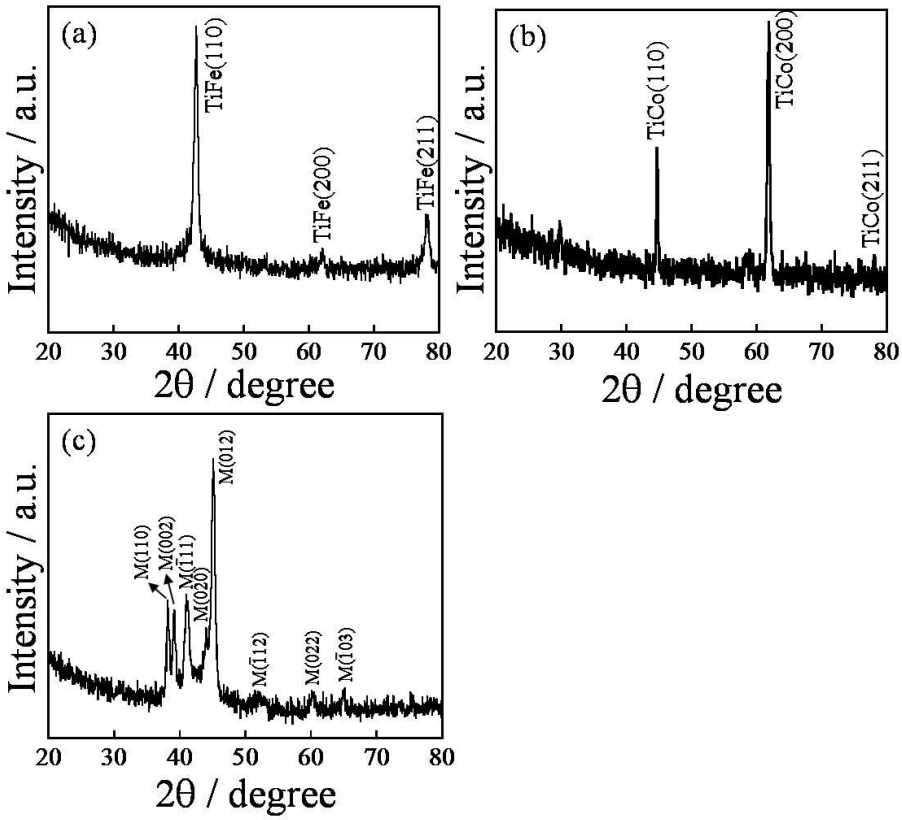

Fig. 5-1 XRD patterns of Ti-based alloys; (a) Ti-50 at.% Fe, (b) Ti-49.5 at.% Co and (c) Ti-49 at.% Ni alloy.

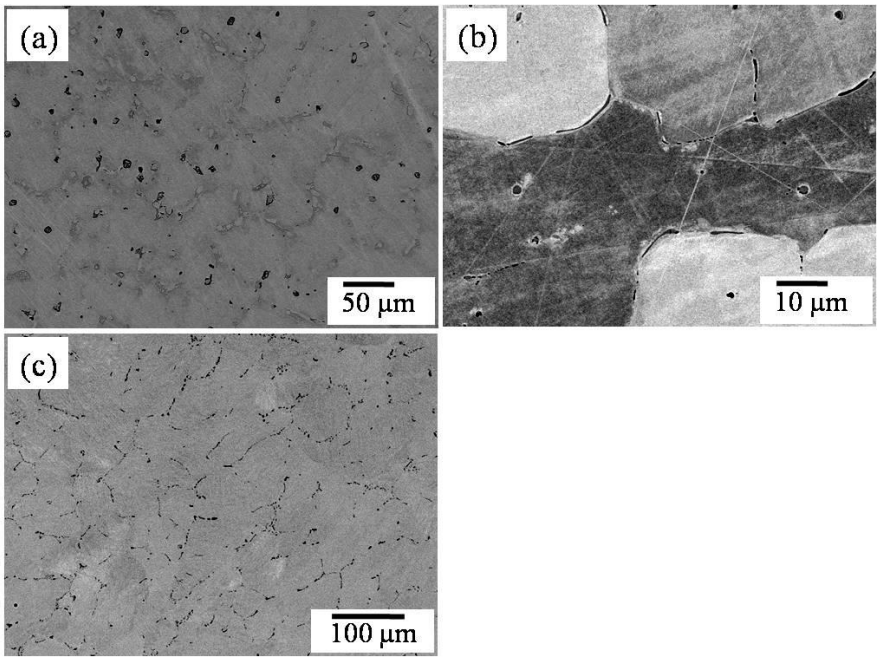

Fig. 5-2 Back scattered images of (a) Ti-50 at.% Fe, (b) Ti-49.5 Co alloy and (c) Ti-49 at.% Ni alloy.

5.3.2 Growth of anodic oxide layers on Ti-49 at.% Ni and Ti-50 at.% Fe

In the present chapter, all anodization experiments were performed in an ethylene glycol containing 0.06 M NH_4F and 1.5 wt.% H_2O. Figure 5-3 shows SEM images of anodic oxide layers formed on Ti-49 at.% Ni at 50 V for various anodization time in the electrolyte. As described in chapter 3, the morphology of anodic oxide layer changes from nanotubular to irregular-shaped porous structures. This morphological transition is explained by the selective anodization of Ti and resulting Ni accumulation. In the chapter 4, anodization of Ti-50 at.% Fe was already examined in details. However, the electrolyte used in the present work is slightly different from that used in the previous chapter 4. Figure 5-4 shows current-time curves obtained for the Ti-50 at.% Fe in the ethylene glycol containing 0.06 M NH_4F and 1.5 wt.% H_2O at different applied voltages. It is clear that the current transients are quite similar to those shown in chapter 4; the current drastically decreases in the early stage of anodization, once increases at a certain time and then decreases to steady-state values. As discussed in chapter 4, the initial current strongly affects the morphology of anodic oxide layers (the definition of the initial current can be referred in chapter 4). The initial current slightly increases with increasing the applied voltage, indicating that irregular-shaped porous oxide layers will be formed at higher applied voltage.

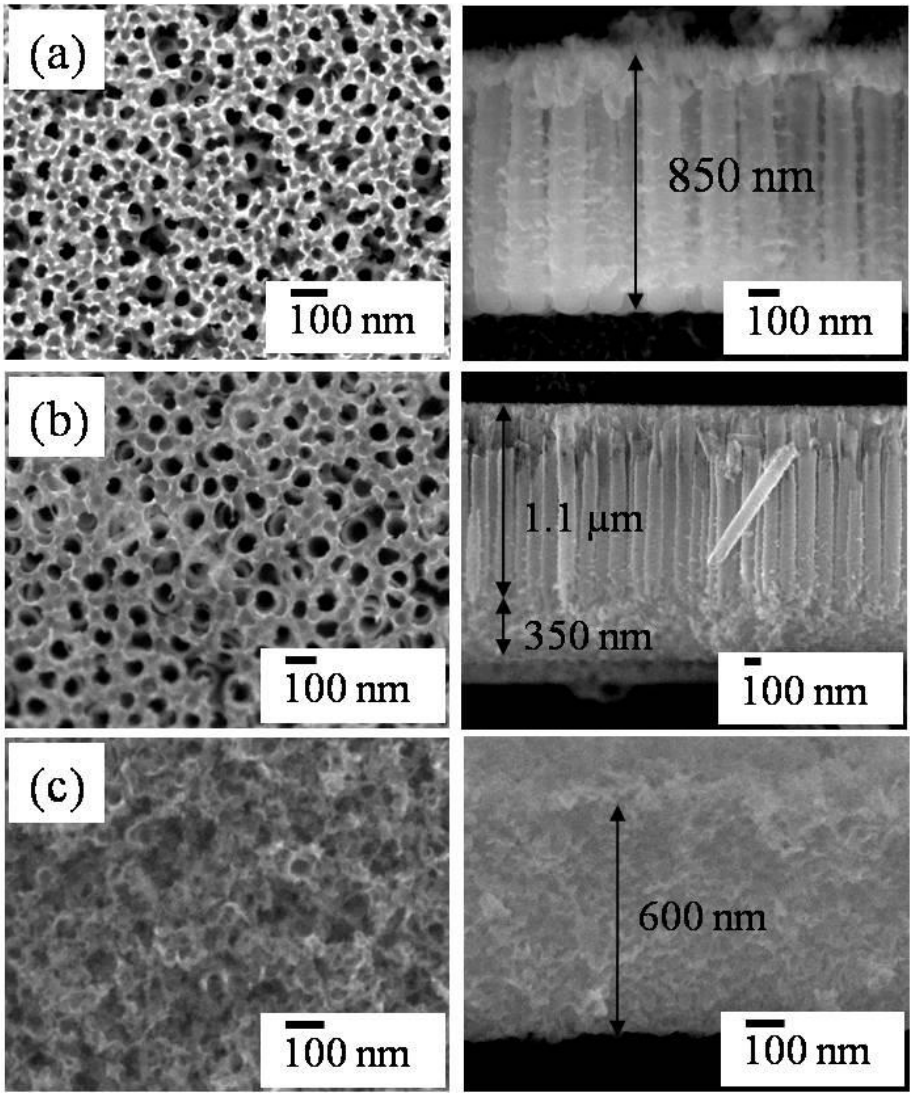

Fig. 5-3 Top-view and cross-sectional SEM images of oxide layers formed on Ti-49 at.% Ni alloy at 50 V for (a) 5 min, (b) 20 min and (c) 60 min in the ethylene glycol containing 0.06 M NH_4F and 1.5 wt.% H_2O.

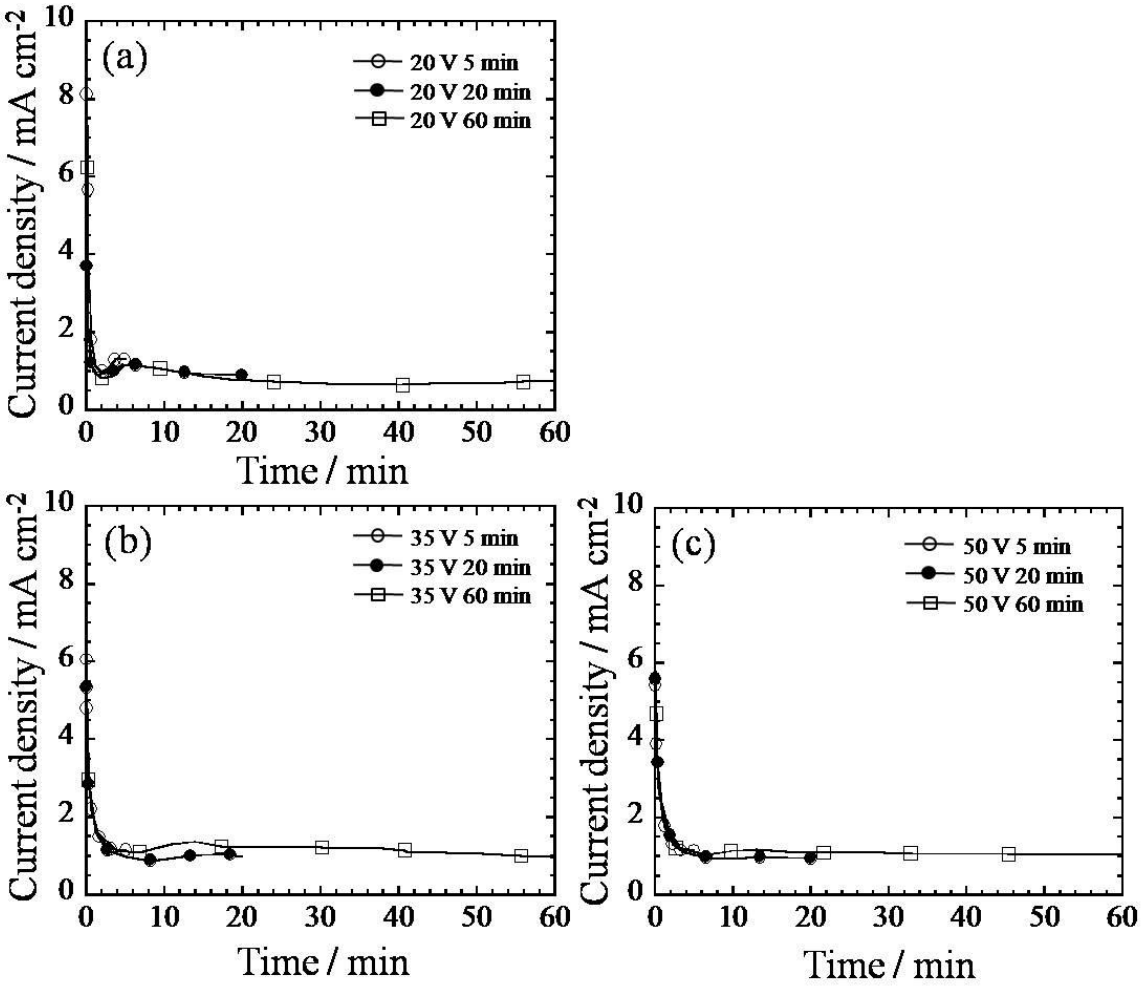

Fig. 5-4 Current-time curves recorded at various voltages and times in the ethylene glycol containing 0.06 M NH_4F and 1.5 wt.% H_2O on Ti-50 at.% Fe alloy.

Top-view and cross-sectional SEM images of resulting anodic oxide layers are presented in Figs. 5-5 and 5-6, respectively. It is clear that after some period at 20 V nanotubular oxide layers were formed on the alloy surface. At the higher applied voltages such as 35 V and 50 V, however, irregular-shaped porous oxide layers were grown as expected from the current behavior. That is, the morphological transition occurs also in this electrolyte when the initial current becomes beyond a threshold. The threshold current is slightly difference from that reported in chapter 4 due to the different electrolyte condition.

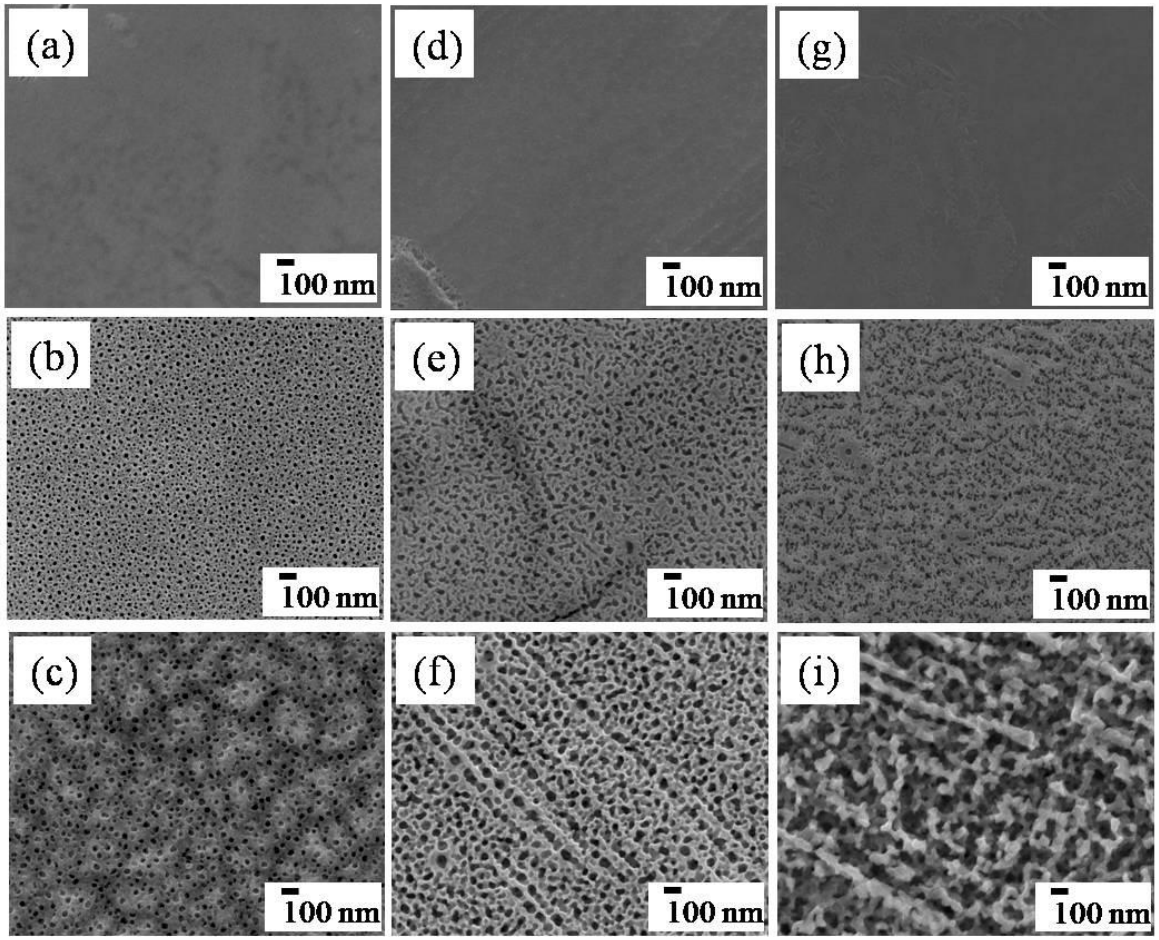

Fig. 5-5 Top-view SEM images of anodic oxide layers on Ti-50 at.% Fe alloy at (a, b, c) 20 V for 5, 20, 60 min, (d, e, f) 35 V for 5, 20, 60 min and (g, h, i) 50 V for 5, 20, 60 min in the ethylene glycol containing 0.06 M NH_4F and 1.5 wt.% H_2O.

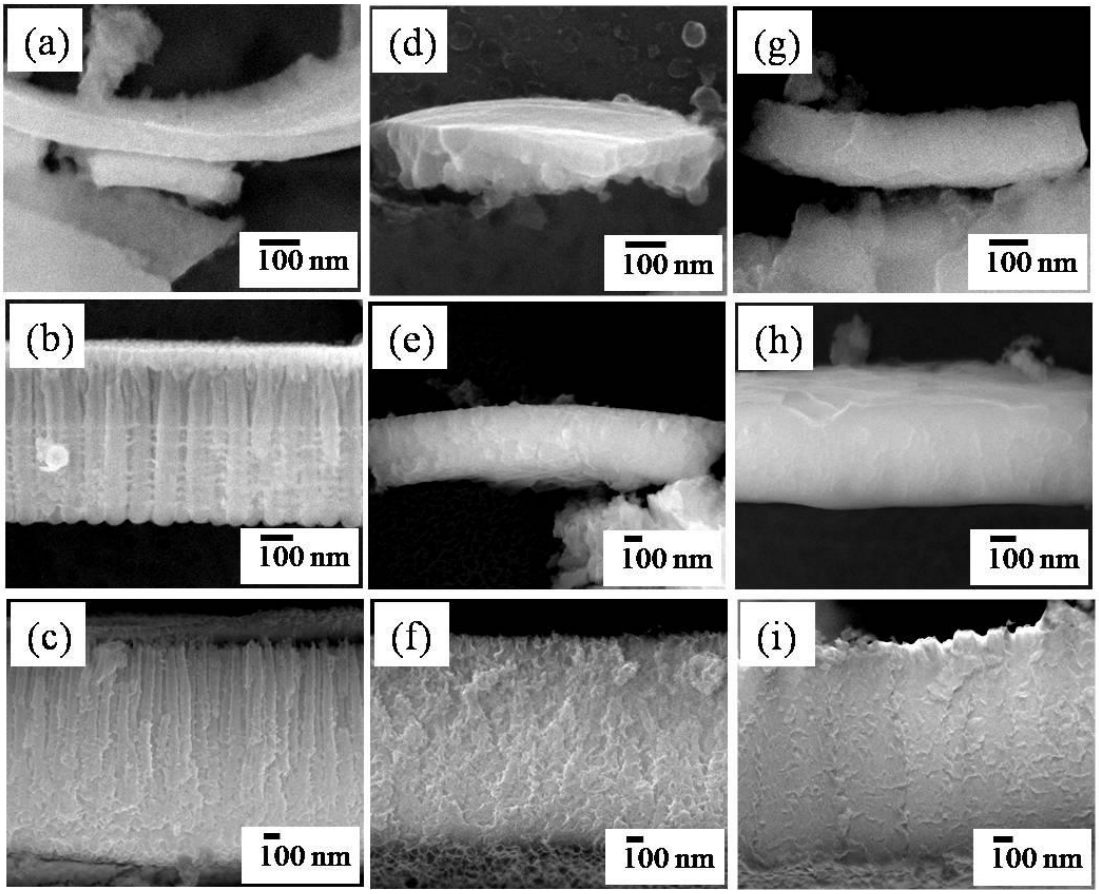

Fig. 5-6 Cross-sectional SEM images of anodic oxide layers on Ti-50 at.% Fe alloy at (a, b, c) 20 V for 5, 20, 60 min, (d, e, f) 35 V for 5, 20, 60 min and (g, h, i) 50 V for 5, 20, 60 min in the ethylene glycol containing 0.06 M NH_4F and 1.5 wt.% H_2O.

5.3.3 Effect of cobalt in Ti-Co alloy on the morphology of anodic oxide layer

Figure 5-7 shows current-time curves obtained during the anodization of Ti-49.5 at.% Co in the ethylene glycol containing 0.06 M NH_4F and 1.5 wt.% H_2O. It is clear that the current behavior exhibits the typical sequence for the nanotube formation, that is, the current significantly decreases in the early stage of the process, then increases once and finally decreases to a steady state current. As apparent, higher steady state current is observed at higher applied voltage on Ti-49.5 at.% Co and furthermore, the steady state current is relatively higher for the Ti-49.5 at.% Co compared to those obtained for the Ti-49 at.% Ni and Ti-50 at.% Fe.

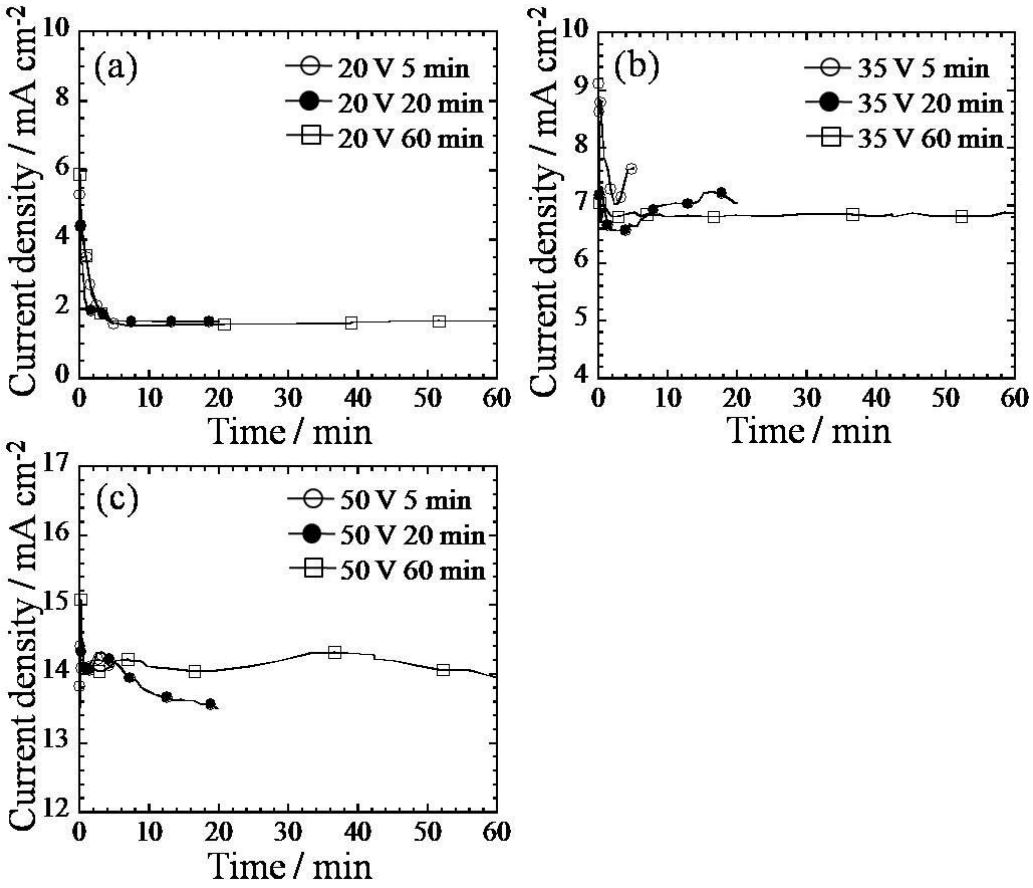

Fig. 5-7 Current-time curves recorded at various voltages and times in the ethylene glycol containing 0.06 M NH_4F and 1.5 wt.% H_2O on Ti-49.5 at.% Co alloy.

Morphology of resulting oxide layers is summarized in Fig. 5-8 for top-views and in Fig. 5-9 for cross-sections. Obviously nanotubular oxide layers formed on the Ti-Co alloy under all anodization conditions, that is, the completely different behavior in the case of the Ti-Co alloy from the cases of the Ti-Ni and the Ti-Fe is observed. Nanotube diameter and layer thickness of nanotubular oxide layer on the Ti-Co alloy slightly increase with increasing applied voltage as similar to pure Ti. However, detailed observation on the oxide layers reveals that the nanotubular structures become disordered as anodization time proceeds although the framework of the nanotubular structures still remains. Furthermore despite relatively high anodic current on the Ti-Co alloy compared to those on the other

alloys, the thickness of nanotubular oxide layers on the Co-containing Ti alloy is not so different from those for Ti-Fe and Ti-Ni alloy.

EPMA analysis revealed that the nanotubular oxide layers formed on the Ti-Co alloy consists of a mixture of titanium oxide and cobalt oxide. It is known that cobalt oxides are electrocatalytically active. Therefore, it is found that some part of the anodic current shown in Fig. 5-7 may contribute for water oxidation. The oxygen evolution due to the water oxidation reaction may be related to the disordering of nanotubular structure with anodization time. In the present work the dissolution of cation into electrolyte during anodization was examined with AAS. Figure 5-10 presents dissolved cation into the electrolyte during anodization of the Ti-Co alloy at 50 V for different anodization times. It is evident that the total amount of dissolved cations with increasing anodization time, in particular the dissolution of Co significantly increases with anodization time. This rapid dissolution can be related to the disordering of nanotubular structure with time. Therefore, it is concluded that the reactivity of constituent oxide in anodic oxide layers also affects the morphology of the layers.

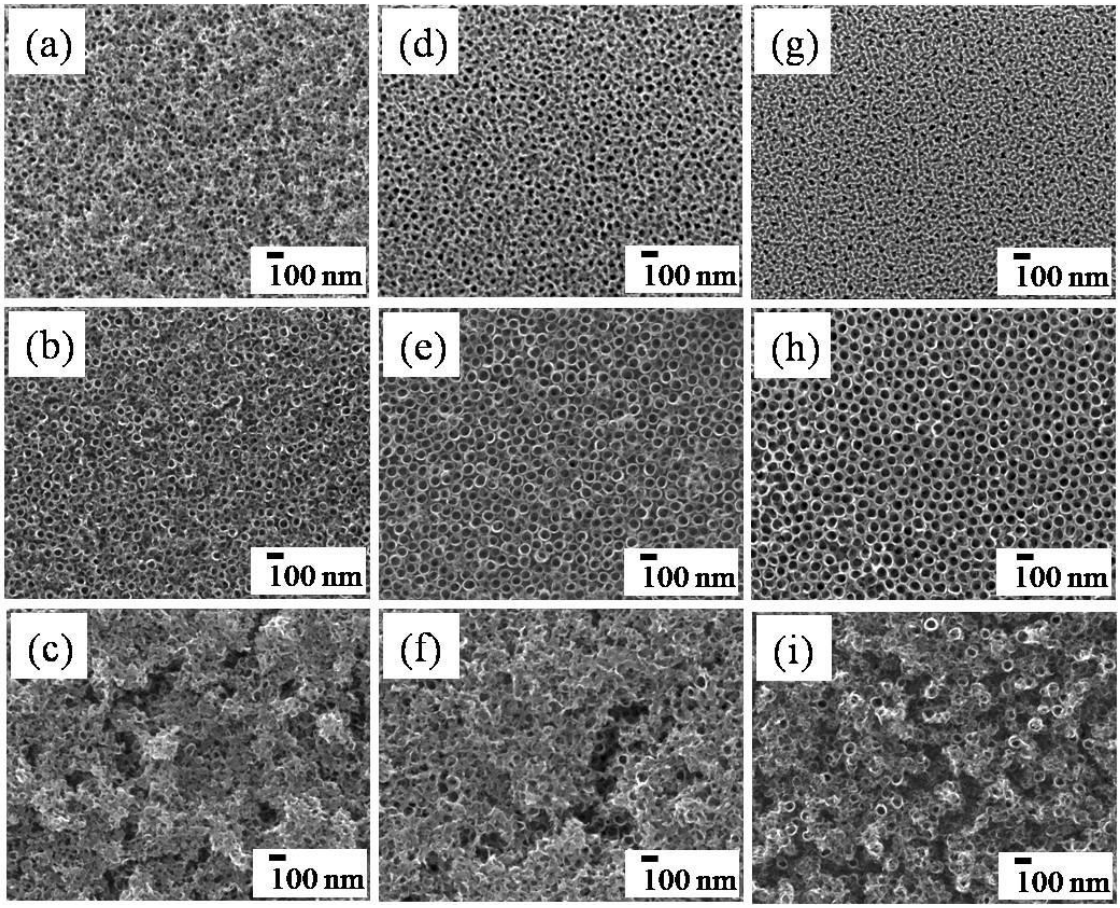

Fig. 5-8 Top-view SEM images of anodic oxide layers on Ti-49.5 at.% Co alloy at (a, b, c) 20 V for 5, 20, 60 min, (d, e, f) 35 V for 5, 20, 60 min and (g, h, i) 50 V for 5, 20, 60 min in the ethylene glycol containing 0.06 M NH_4F and 1.5 wt.% H_2O.

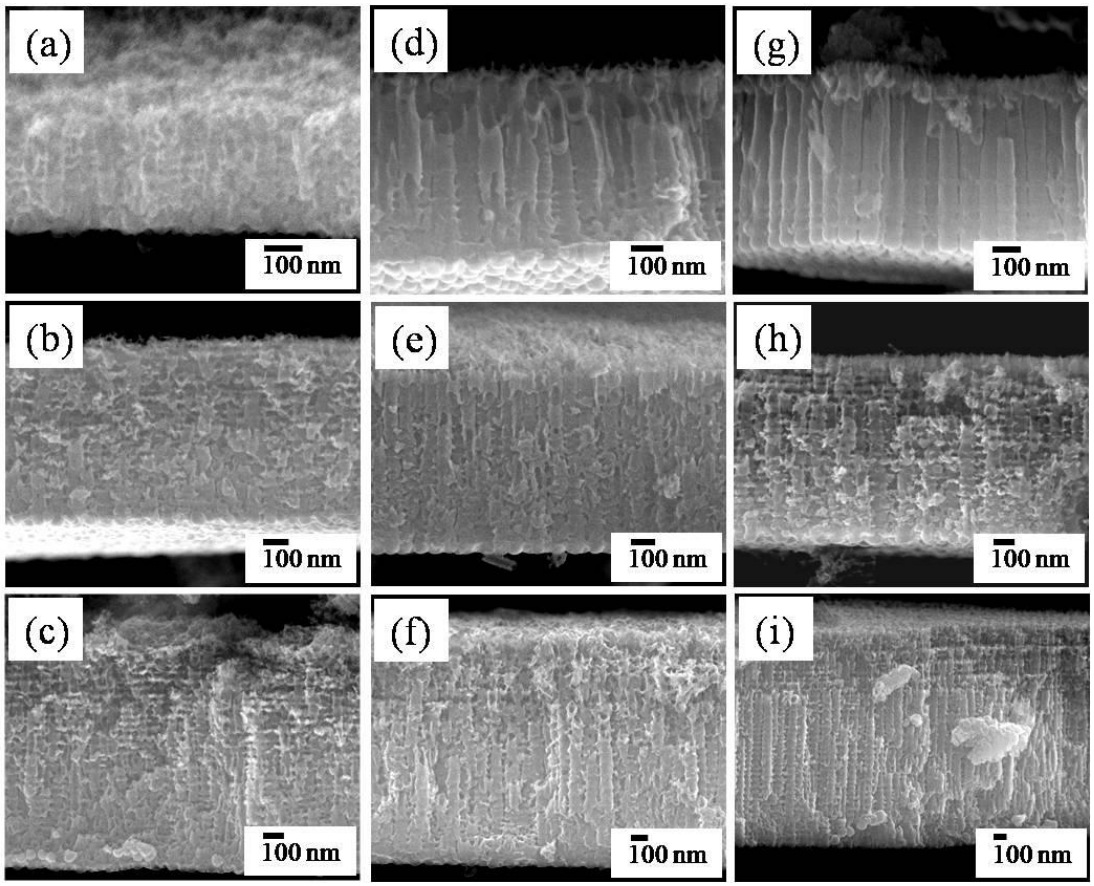

Fig. 5-9 Cross-sectional SEM images of anodic oxide layers on Ti-49.5 at.% Co alloy at (a, b, c) 20 V for 5, 20, 60 min, (d, e, f) 35 V for 5, 20, 60 min and (g, h, i) 50 V for 5, 20, 60 min in the ethylene glycol containing 0.06 M NH_4F and 1.5 wt.% H_2O.

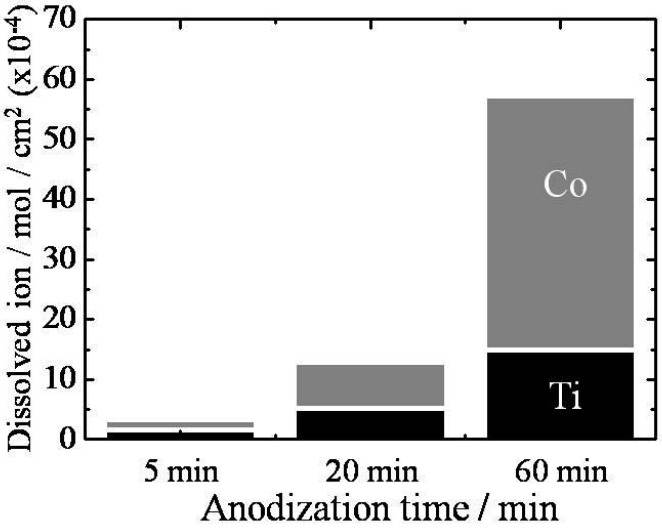

Fig. 5-10 The total amount of dissolved cations during the anodization of the Ti-49.5 at.% Co alloy at 50 V for various time.

5.4 Conclusion

In the present chapter, the author examined the morphology and growth of anodic oxide layers formed on the Ti-based alloys containing different transition metals by anodization in the ethylene glycol containing 0.06 M NH_4F and 1.5 wt.% H_2O. The morphology of anodic oxide layer on Ti-Ni and Ti-Fe alloy is changed from nanotubular structures to irregular-shaped porous structures. This is attributed to the selective anotization of Ti in Ti-Ni substrate and initial current density during the anotization of Ti-Fe (as discussed in chapters 3 and 4). In the case of Ti-Co alloy, on the other hand, the morphology of nanotubular structures also changed to disordered-shaped structures although the framework of nanotubular structures still remains. This transition is attributed to the preferential dissolution of cobalt oxide in the nanotubular oxide layers formed on Ti-Co alloy. Therefore, it is concluded that the reactivity of constituent alloying element in Ti-based alloys strongly affects the morphology of the anodic oxide layers.

References :

1) S. Kaneco, Y.S. Chen, P. Westerhoff, J.C. Crittenden, Scr. Mater., **56** (2007) 373.

2) A. Watcharenwong, W. Chanmanee, N.R. de Tacconi, C.R. Chenthamarakshan, P. Kajitvichyanukul, K. Rajeshwar, J. Mater. Res., **22** (2007) 3186.

3) S. Yoriya, M. Paulose, O.K. Varghese, G.K. Mor, C.A. Grimes, J. Phys. Chem. C, **111** (2007) 13770.

4) Y. Yang, D. Kim, M. Yang, P. Schmuki, Chem. Commun., **47** (2011) 7746.

5) P. Roy, C. Das, K. Lee, R. Hahn, T. Ruff, M. Moll, P. Schmuki, J. Am. Chem. Soc., **133** (2011) 5629.

Chapter 6 Effect of microstructure on the growth of anodic oxide layers on Ti-Ni alloy

6.1 Introduction

Ti-Ni shape memory alloys (SMA) exhibit two unique properties; a shape memory effect and superelasticity[1, 2]. Owing to these properties, Ti-Ni alloys have been extensively studied for various applications in actuators, sensor and in biomedical devices[3-5]. Amongst them, eager demand comes from medical applications. However, the Ni ion release from Ti-Ni alloy induced by corrosion would induce allergenic reaction and toxic responses if its concentration in the human body exceeds a certain limit[6]. In order to circumvent the problem, anodization was examined to form protective compact oxide layers on the alloy surface[7, 8]. More recently, a different morphology of anodic oxide layer has been reported for a Ti-Ni alloy, so-called nanotubular oxide layers. The formation of nanotubular oxide layer was firstly realized by Assefpour-Dezfuly et al and Zwilling et al for Ti and its alloy and then have been formed for a wide range of metals and alloys[9-19]. Numerous researches have targeted not only practical applications of nanotubular oxide layer but also fundamental studies on nanotube formation. So far various electrochemical parameters for anodization as well as metallurgical factors have been examined mainly for pure Ti. The effect of electrochemical parameters on the morphology and growth of nanotubular oxide layer on a Ti-Ni alloy were also studied. However, metallurgical factors on the growth of nanotubular oxide layer on Ti-Ni alloy have not been clear yet. Therefore, the author examined the effect of Ni content in Ti-Ni alloy on the morphology and growth of anodic oxide layer and found peculiar growth behavior, that is, morphological transition from nanotubular structures to irregular-shaped porous structures occurs as described in chapter

3. The present chapter reports the growth of anodic oxide layers on Ti-Ni alloys with different microstructures.

6.2 Experimental

Ti-xNi alloys (x = 49.0 and 52.2 at.% Ni) used in the present study were fabricated in an arc melting furnace from Ti sheets of 99.5% purity and Ni sheets of 99% purity. The alloy samples fabricated were subjected to homogenization at 1000 ℃ for 24 hours under a high vacuum atmosphere. After the homogenization, samples were cold-worked with a reduction rate of 20% and some of the samples were subsequently heat-treated at 500 ℃ for 1 hour. Prior to anodization, all samples were ground with SiC abrasive papers, then mirror-finished with diamond paste and colloidal silica, finally followed by ultra-sonication in acetone, ethanol, and methanol, successively, and rinsing with deionized water. The electrochemical setup consisted of a two-electrode configuration. A platinum plate was used as the counter electrode. The samples were pressed against an O-ring on the electrochemical cell, leaving the area of 0.785 cm^2 to an electrolyte. The electrolyte used for anodization was an ethylene glycol electrolyte containing 0.06 M NH_4F and 1.5 wt.% H_2O. The anodization was carried out at 50 V for different anodization times using a high-voltage potentiostat (Hokuto Denko HA-3001A). After the anodization, the anodized samples were rinsed with ethanol. Top-view and cross-sectional images of oxide layers formed on the samples were investigated using a field-emission scanning electron microscope (FE-SEM, JEOL JSM-7001FA). The crystal structure and chemical composition of as-rolled and heat-treated Ti-Ni alloys were characterized by X-ray diffraction (XRD, Philips PW3040/60 X'Pert Pro) and electron probe micro analyzer (EPMA, JEOL JXA-8800R), respectively.

6.3 Results and discussion

In the chapter 3, the author reported the growth of nanotubular oxide layers on various Ti-Ni alloys. The results revealed that the morphology and growth of anodic oxide layers were affected by Ni content in the substrates and anodization time rather than the crystal structure of the substrate. Furthermore the author found that the morphological transition from the nanotubular structures to the irregular-shaped porous structures occurs on Ti-Ni alloys due to the selective anodization of Ti and resulting Ni accumulation at the interface between the alloy substrate and the formed oxide layer.

In chapter 2, on the other hand, the author clearly demonstrated that the microstructure of Ti substrate strongly changes the growth of TiO_2 nanotubular layer. In the present chapter, the effect of microstructure on the morphology and growth of anodic oxide layers on Ti-Ni alloy is examined and discussed.

6.3.1 Characterization of as-rolled and heat-treated Ti-Ni alloys

Figure 6-1 shows XRD patterns of as-rolled and heat-treated Ti-49.0 at.% Ni and Ti-52.2 at.% Ni alloy. As described in 6.2 the as-rolled samples were prepared by the homogenization at 1000 ℃ for 24 hours, and subsequent cold-work with the reduction ratio of 20 %. On the other hand, the heat-treated samples were additionally subjected to the heat-treatment at 500 ℃ for 1 hour after the cold-work. From Fig. 6-1 (a), it is evident that the all diffraction peaks obtained from the Ti-49.0 at.% Ni are attributed to the B19’ martensitic phase whereas the Ni-rich alloy (Fig. 6-1(b)) of the Ti-52.2 at.% Ni exhibits peaks ascribed to the B2 austenitic phase, indicating that the crystal structure of the Ti-Ni alloys is not influenced by heat-treatment of substrate.

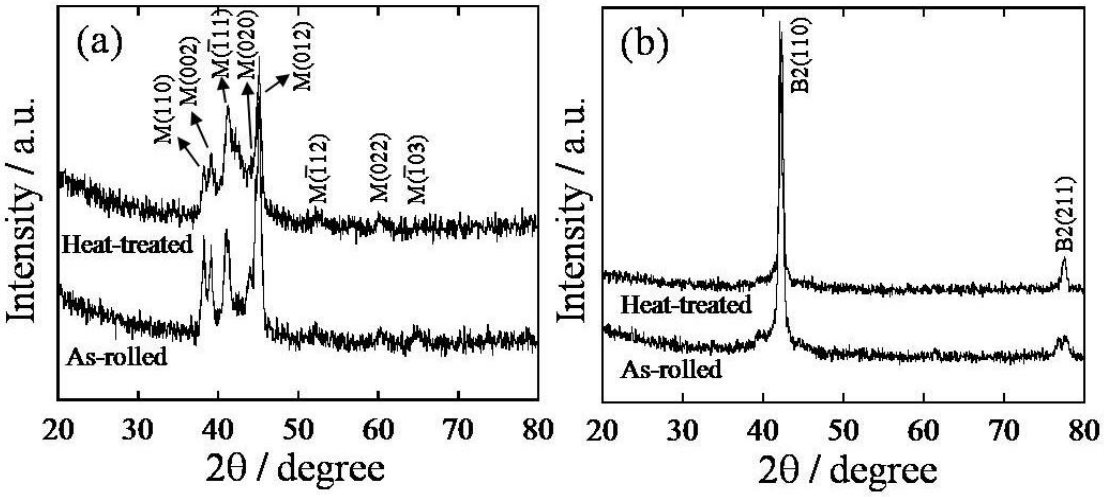

Fig. 6-1 XRD patterns of as-rolled and heat-treated (500 ℃ 1h) Ti-Ni alloys; (a) Ti-49.0 at.% Ni alloy and (b) Ti-52.2 at.% Ni alloy.

Figure 6-2 shows backscattered electron micrographs of the Ti-49 at.% Ni and Ti-52.2 at.% Ni alloys. From Fig. 6-2, two distinct areas are observed in the micrographs. It was revealed from EPMA analysis that the dark areas are found to be Ti_2Ni precipitates and the bright areas are Ti-Ni matrix. No peaks assigned to the Ti_2Ni were observed in the XRD patterns as shown in Fig. 6-1 due to the small volume fraction of the precipitates. The volume fraction and average size of precipitate in the Ti-49.0 at.% Ni increase from 0.96% and 1.8 μm to 4.80% and 5.6 μm after heat-treatment at 500 ℃ for 1 hour, respectively. Those of the Ti-52.2 at.% Ni alloy also increased from 0.54% and 1.5 μm to 1.0% and 1.6 μm. That is, the volume fraction and size of precipitate increase after the heat-treatment. The microstructure of as-rolled and heat-treated samples is presented in Fig. 6-3. The average grain sizes observed in Fig. 6-3 (a)-(d) were estimated at 11.2, 7.1, 8.2 and 5.1 μm, respectively. It is clear that the grain size of the as-rolled samples is larger than that of the heat-treated samples, in order words, the heat-treatment decreased the grain size.

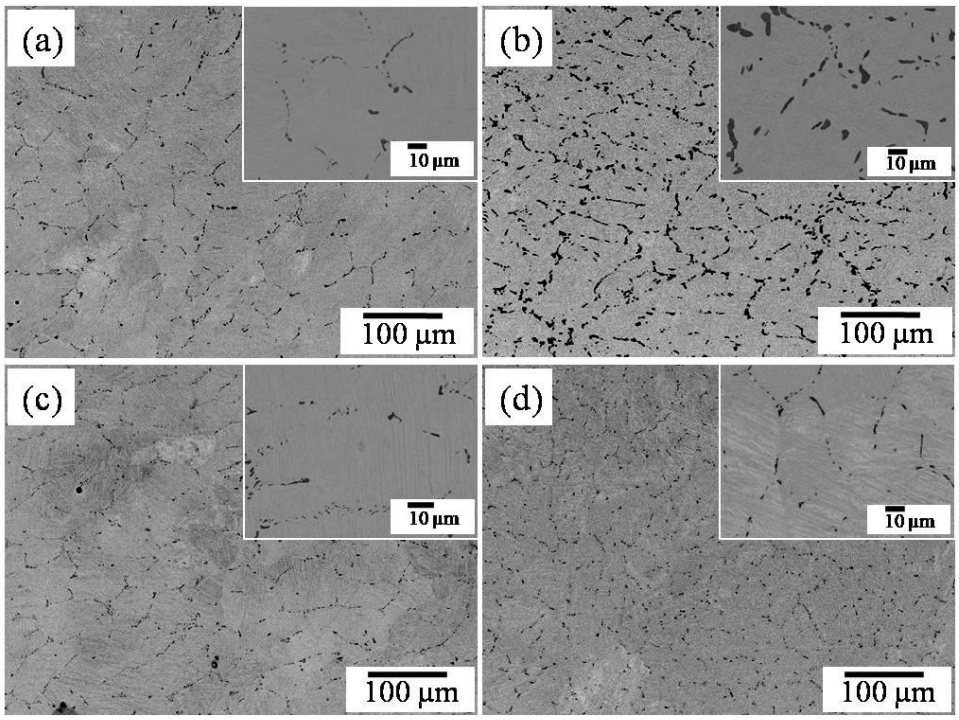

Fig. 6-2 Back scattered images of (a) as-rolled and (b) heat-treated (500 ℃, 1h) Ti-49.0 at.% Ni and (c) as-rolled and (d) heat-treated (500 ℃, 1h) Ti-52.2 at.% Ni alloy.

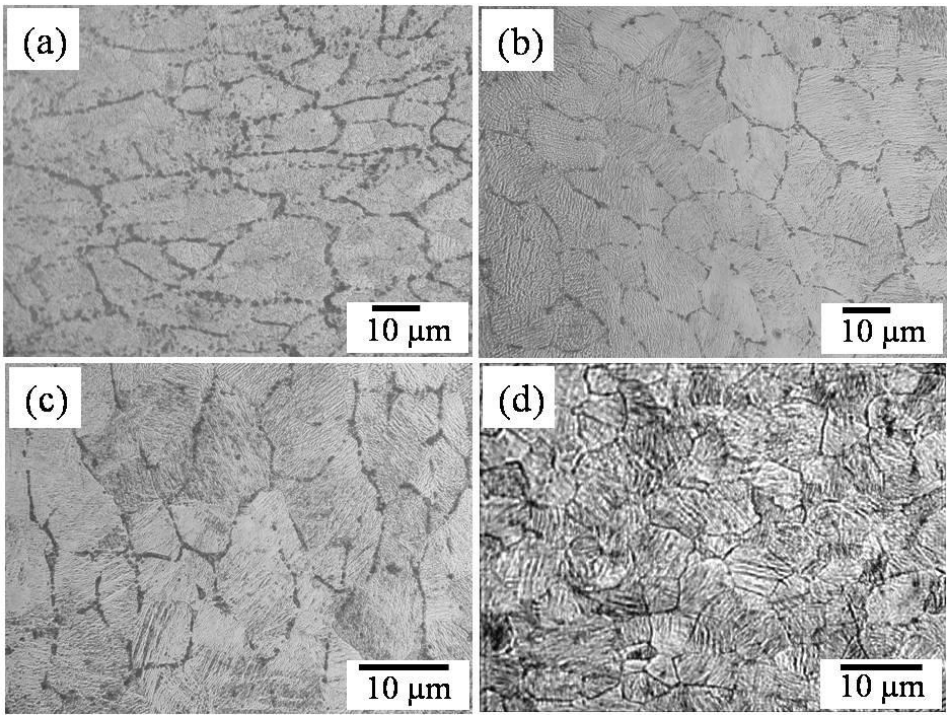

Fig. 6-3 Microstructures of (a) as-rolled and (b) heat-treated (500 ℃, 1h) Ti-49.0 at.% Ni and (c) as-rolled and (d) heat-treated (500 ℃, 1h) Ti-52.2 at.% Ni alloy.

6.3.2 Growth of nanotubular oxide layers on Ti-Ni alloys with different microstructures

Figure 6-4 shows the current-time curves recorded for the as-rolled and heat-treated Ti-Ni alloys at 50 V for 20 min in the ethylene glycol containing 0.06 M NH_4F and 1.5 wt.% H_2O.

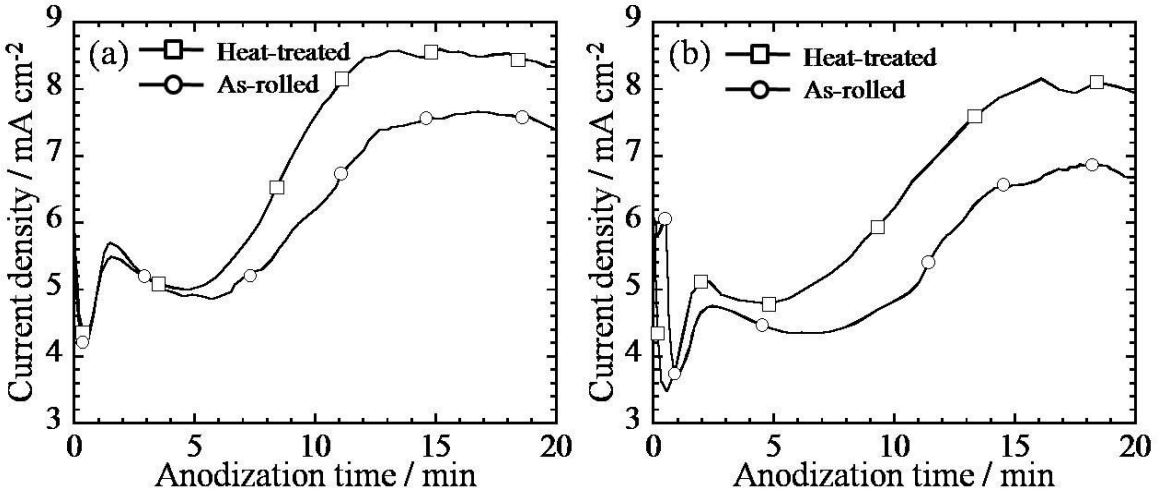

Fig. 6-4 Current-time curves recorded at 50 V for 20 min in the ethylene glycol electrolyte containing 0.06 M NH_4F and 1.5 wt.% H_2O on (a) as-rolled and heat-treated Ti-49.0 at.% Ni and (b) as-rolled and heat-treated Ti-52.2 at.% Ni alloy.

As apparent from Fig. 6-4, similar current behavior is observed for as-rolled and heat-treated Ti-Ni alloys. In addition, the current density of heat-treated Ti-Ni alloys is larger than that of the as-rolled Ti-Ni alloys. Top-view and cross-sectional SEM images of the oxide layers formed on the Ti-49.0 at.% Ni and Ti-52.2 at.% Ni alloys at 50 V for 5 min in the ethylene glycol electrolyte containing 0.06 M NH_4F and 1.5 wt.% H_2O are presented in Fig. 6-5. It is obvious from the cross-sectional images that the oxide layers exhibit tubular structure, although such tubular structure is not observed from the top-views due to the remaining initiation layer. The thickness of nanotubular oxide layers formed on the heat-treated Ti-Ni alloy substrates is slightly larger compared to that for the cold-worked

samples. This is clearly attributed to larger electric charge generated during the anodization of the heat-treated alloys for 5 min.

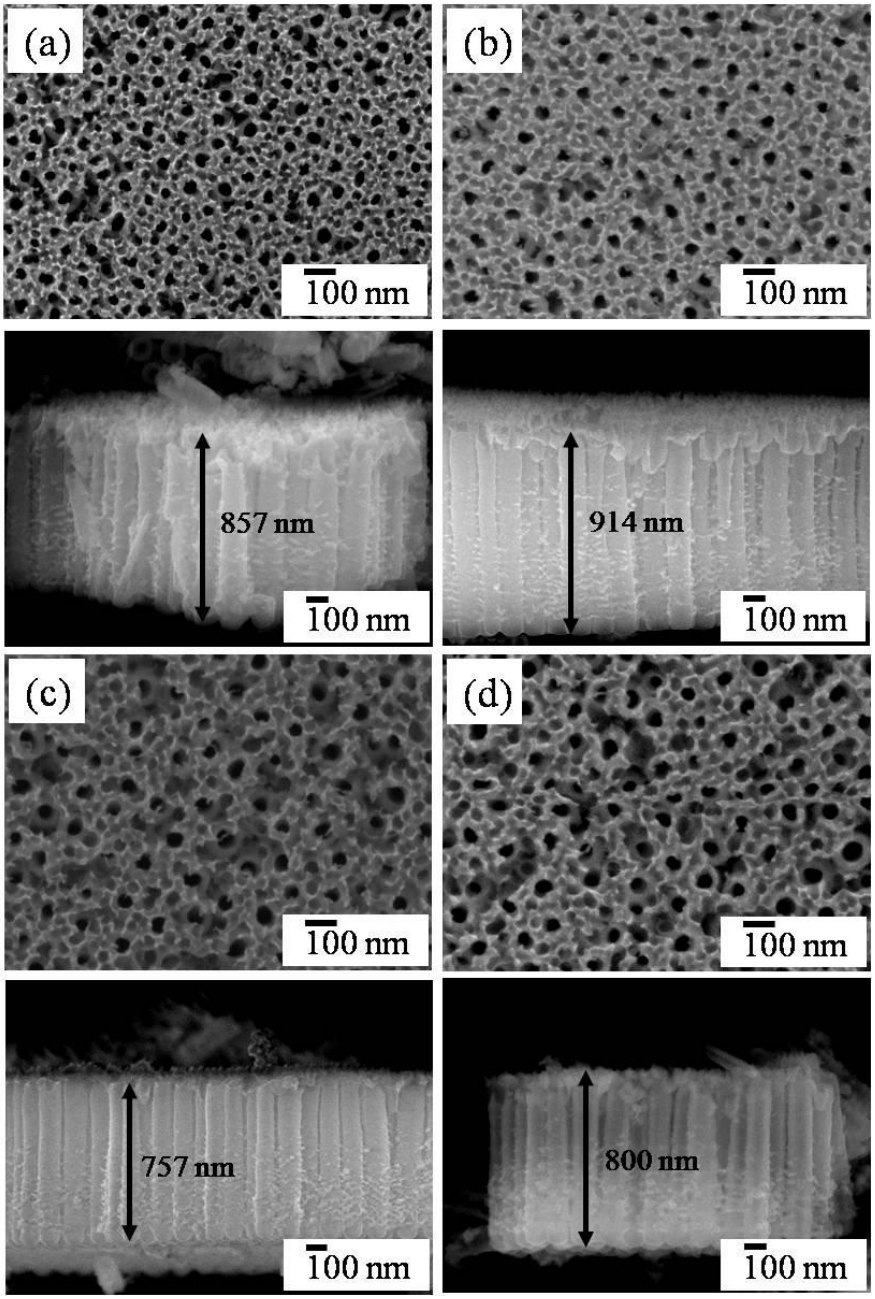

Fig. 6-5 Top-view and cross-sectional SEM images of oxide layers formed on (a) as-rolled and (b) heat-treated Ti-49.0 at.% Ni and (c) as-rolled and (d) heat-treated Ti-52.2 at.% Ni alloy at 50 V for 5 min in the ethylene glycol containing 0.06 M NH_4F and 1.5 wt.% H_2O.

Furthermore, the morphology of nanotubular oxide layers on the Ti-Ni alloys has changed with increasing anodization time. Figure 6-6 presents SEM images of anodic oxide layers on the alloys after 20 min. It is found that all samples exhibited the formation of irregular-shaped porous oxide layers underneath the nanotubular oxide layers.

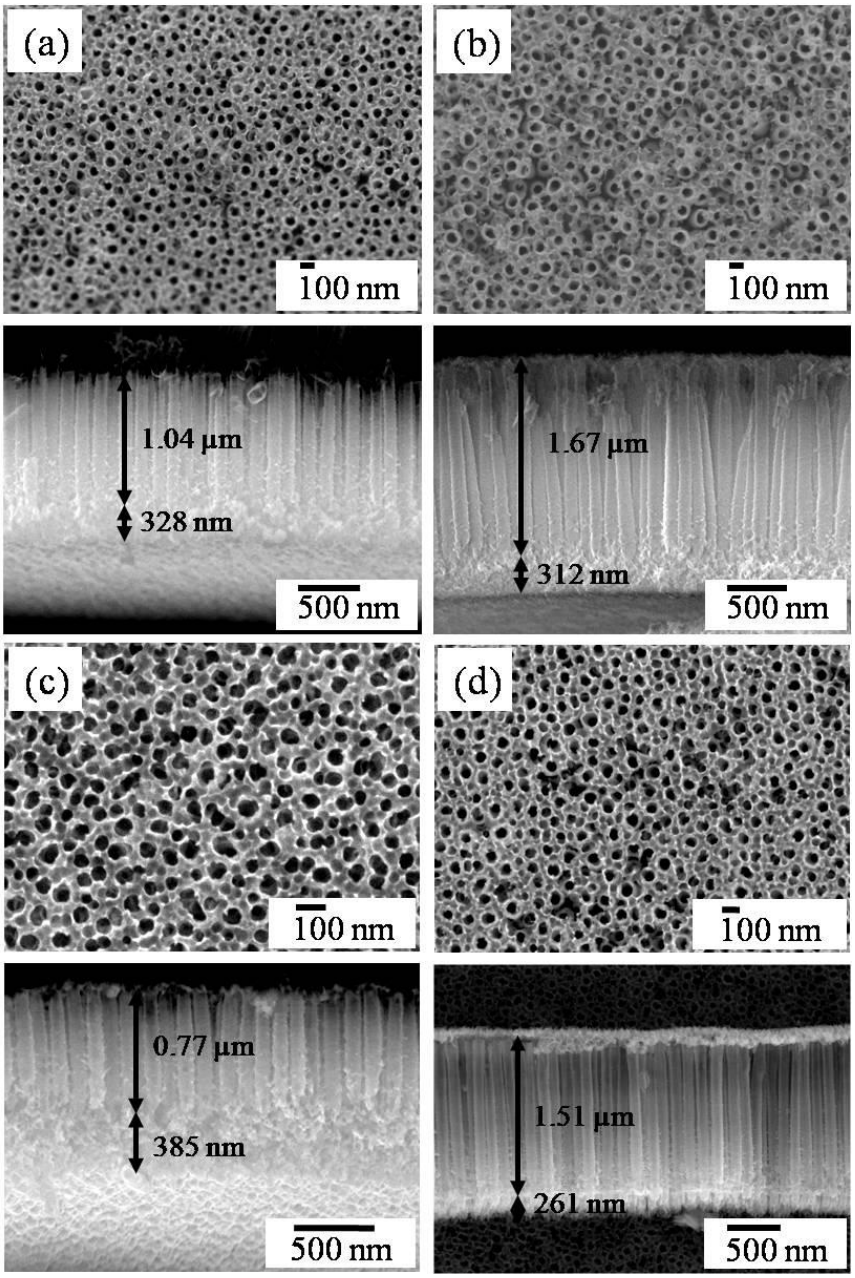

Fig. 6-6 SEM images of oxide layers formed on (a) as-rolled and (b) heat-treated Ti-49.0 at.% Ni and (c) as-rolled and (d) heat-treated Ti-52.2 at.% Ni alloy at 50 V for 20 min in the ethylene glycol containing 0.06 M NH_4F and 1.5 wt.% H_2O.

Although after the heat-treatment the thickness of irregular-shaped porous oxide layers formed on the heat-treated Ti-Ni alloys is similar to that on the as-rolled Ti-Ni alloys, the thickness of nanotubular oxide layers is significantly higher for the heat-treated alloys than that for the as-rolled alloys. That is, the heat-treatment of substrate accelerated the growth of nanotubular layers, which are related to the generated current density during anodization. As mentioned above, higher current was generated for the heat-treated alloys compared to for the as-rolled alloys, leading to the enhanced growth of nanotubular oxide layer observed for the heat-treated alloys. In addition, precipitate size and volume fraction of precipitate increased after the heat-treatment. From the result it might be deduced that the migration of defects might be inhibited during the heat-treatment by precipitate, which implies that defects could be stacked near precipitates. Therefore, it is found that stacked defects in Ti-Ni alloys may contribute to the higher current for the heat-treated alloys, leading to the enhanced growth of nanotubular oxide layer. Further experiments are required to clarify this point.

6.4 Conclusion

In the present chapter the author examined the effect of microstructure on the growth of anodic oxide layers formed on Ti-Ni alloys by anodization in the ethylene glycol containing 0.06 M NH_4F and 1.5 wt.% H_2O. The microstructure of alloys was controlled by heat-treatment. The volume fraction and size of precipitate in the Ti-Ni alloys increased after the heat-treatment. The increased size and fraction of precipitate may cause the accumulation of defect near precipitate, which will contribute the higher current generated for the heat-treated alloys. As a result, the enhanced growth of nanotubular oxide layer would be achieved on the alloys.

References :

1) S. Miyazaki, C.M. Wayman, Acta Metall., **36** (1988) 188.

2) K. Otsuka, C.M. Wayman, K. Nakai, H. Sakamoto, K. Shimizu, Acta Mater., **40** (1999) 7.

3) D. Favier, H. Louche, P. Schlosser, L. Orgeas, P. Vacher, L. Debove, Acta Mater., **55** (2007) 5310.

4) W. Predki, A. Knopik, B. Bauer, Mater. Sci. Eng. A, **481–482** (2008) 598.

5) C. Chu, C.Y. Chung, P.H. Lin, S.D. Wang, Mater. Sci. Eng. A, **366** (2004) 114.

6) R. Hang, X. Huang, L. Tian, Z. He, B. Tang, Electrochim. Acta, **70** (2012) 382.

7) P. Shi, F.T. Cheng, H.C. Man, Mater. Lett., **61** (2007) 2385.

8) F.T. Cheng, P. Shi, G.K.H. Pang, M.H. Wong, H.C. Man, J. Alloys Compd., **438** (2007) 238.

9) M. Assefpour-Dezfuly, C. Vlachos, E.H. Andrews, J. Mater. Sci., **19** (1984) 3626.

10) V. Zwilling, E. Darque-Ceretti, A. Boutry-Forveille, D. David, M.Y. Perrin1, M. Aucouturier, Surf. Interface Anal., **27** (1999) 629.

11) V. Zwilling, M. Aucouturier, E. Darque-Ceretti, Electrochim. Acta, **45** (1999) 921.

12) L. Guo, J. Zhao, X. Wang, X. Xu, H. Liu, Y. Li, Int. J. Appl. Ceram. Technol., **6** (2009) 636.

13) J. Choi, J.H. Lim, J. Lee, K.J. Kim, Nanotechnology, **18** (2007) 055603.

14) N.R. de Tacconi, C.R. Chenthamarakshan, G. Yogeeswaran, A. Watcharenwong, R.S. de Zoysa, N.A. Basit, K. Rajeshwar, J. Phys Chem. B, **110** (2006) 25347.

15) N.K. Allam, X.J. Feng, C.A. Grimes, Chem. Mater., **20** (2008) 6477.

16) S. Berger, F. Jakubka, P. Schmuki, Electrochem. Sol. State Lett., **12** (2009) K45.

17) S. Grigorescu, C. Ungureanu, R. Kirchgeorg, P. Schmuki, I. Demetrescu, Appl. Surf. Sci., **270** (2013) 190.

18) B. Luo, H. Yang, S. Liu, W. Fu, P. Sun, M. Yuan, Y. Zhang, Z. Liu, Mater. Lett., **62** (2008) 4512.

19) V.S. Saji, H.C. Choe, W.A. Brantley, Acta Biomaterialia, **5** (2009) 2303.

Chapter 7 Conclusions

In the present study, the author has investigated the effect of substrate microstructure and composition on the morphology and growth of anodic oxide layers on the pure Ti and its alloys. As a result, the following conclusions have been derived.

Chapter 1

The author has introduced the overview of the growth of anodic oxide layers, particularly focusing on the effect of various anodization parameters such as applied voltage, pH of electrolyte, anodization time, the chemical composition and microstructure of substrate, followed by the purpose of the present thesis.

Chapter 2

The chapter 2 reports the growth of anodic oxide layers formed on pure Ti with different microstructures. The microstructure of Ti substrate was changed by the heat-treatment in different atmosphere (in air or Ar) and the ARB process. Nanotubular oxide layers were formed on all Ti substrates regardless of the microstructure. In the case of heat-treated specimens, the thickness of nanotubular oxide layers decreased with increasing the heat-treatment duration and temperature in both atmospheres (Air and Ar). The atmosphere also affected the growth of TiO_2 nanotubular layer, that is, the nanotubular layer formed on the air heat-treated substrates was thicker compared to that on the Ar heat-treated substrates. On the other hand, in the case of ARB treated substrates, the thickness of nanotubular oxide layers increased with increasing ARB cycle. These indicate that the growth of nanotubular oxide layer is affected by the microstructure of substrate, that is, the increased defect in Ti substrate results in the enhanced growth of nanotubular

oxide layer whereas the growth of the layer becomes slower when the defect in the substrate is decreased by heat-treatment.

Chapter 3

In the chapter 3, the effect of Ni content in Ti-Ni alloy on the growth of anodic oxide layers is investigated using Ti-Ni alloys containing different Ni contents. The Ti-49.0 at.% Ni alloy is in the martensitic phase whereas Ti-51.1 at.% Ni, Ti-52.2 at.% Ni and Ti-52.5 at.% Ni alloys are in the austenitic phase. Nanotubular oxide layers are formed on all Ti-Ni alloys for a short time (5 min). However, for further anodization (20 min), the irregular-shaped porous oxide layers are grown underneath the nanotubular oxide layers. After 60 min, only the irregular-shaped porous oxide layers remain due to the dissolution of the nanotubular layers. This morphological transition is observed on all Ti-Ni alloys examined and occurs faster for higher Ni content alloy. These results indicate that the morphology of anodic oxide layer on the Ti-Ni alloys is affected by the chemical composition of substrate rather than the crystal structure.

Chapter 4

The chapter 4 reports the growth of anodic oxide layers on the Ti-Fe alloys with different Fe content. Anodization of pure Ti, the Ti-10 at.% Fe and Ti-70 at.% Fe alloys at 30 V for 3 hours results in the formation of nanotubular oxide layers, whereas on the Ti-50 at.% Fe alloy an irregular-shaped porous oxide layer is formed under the same anodization condition. On the Ti-50 at.% Fe alloy, nanotubular oxide layer is formed at the lower voltage of 10 V and furthermore irregular-shaped porous oxide layer is grown on the Ti-50 at.% Fe alloy at the higher voltage of 50 V, indicating that the morphology of anodic oxide layers depends on applied voltage. These morphological transitions are related to the initial

current during the anodization, that is, nanotubular oxide layers are formed at low initial current whereas irregular-shaped porous oxide layers are formed when higher initial current is applied or generated. Therefore, it can be required to suppress initial current density during anodization in order to form nanotubular oxide layers on the Ti-Fe alloys.

Chapter 5

The chapter 5 the author examines the effect of alloying elements on the growth of anodic oxide layers formed on Ti-based alloys, especially the effect of Co is focused. The morphological transition from nanotubular structures to irregular-shaped porous structures is observed on the anodic oxide layers on Ti-Ni and Ti-Fe alloys, which is attributed to the preferential oxidation of Ti in the Ti-Ni alloy substrate and the generated initial current during the anodization, respectively. On the other hand, the morphology of anodic oxide layer on Ti-Co alloy exhibits the different transition – from ordered nanotubular to disordered nanotubular structure – although the framework of nanotubular structures still remains even after extended anodization of 60 min. This morphology transition is explained based on the preferential dissolution of cobalt oxide from the nanotubular oxide layer. Therefore, it is concluded that the reactivity of constituent element in Ti-based alloys strongly affects the morphology of the anodic oxide layers.

Chapter 6

In the chapter 6, the growth of anodic oxide layers formed on the Ti-Ni alloys with different microstructure is investigated. The microstructure of the alloys is changed by the heat-treatment of as-rolled substrates at 500 ℃ for 1 hour. After the heat-treatment, the size and volume of precipitate in the alloys are slightly increased. The change of microstructure affects current behavior during anodization. Higher current is generated for the heat-treated

alloys compared to as-rolled alloy. The increased size and fraction of precipitate may cause the accumulation of defect near precipitate, which would contribute to generate the higher current for the heat-treated alloys. As a result, the growth of nanotubular oxide layer is found to be enhanced on the heat-treated alloys.

Additionally, the author hopes that the knowledge on the effect of substrate microstructure and composition on the growth of anodic oxide layers obtained in this study will be useful for the alloy design for functional electrodes based on TiO_2 nanotubular oxide layers

List of Publications

Publications related to this thesis

1. Min Su Kim, Shota Yamamoto, Hiroaki Tsuchiya, Shinji Fujimoto
   Growth of TiO_2 nanotube layers on Ti substrates with different microstructure
   ECS Transactions, **66** (2015)135-145.

2. Hiroaki Tsuchiya, Min-Su Kim, Yuki Otani, Yasutomo Shimizu, Shinji Fujimoto
   Fabrication of TiO_2 Nanotube Arrays by Self-Organizing Anodization; Influence of Electrolyte Composition
   Proceedings of 24th International Symposium on Processing and Fabrication of Advanced Materials (2015) 722-730.

3. Min-Su Kim, Hiroaki Tsuchiya, Shinji Fujimoto
   Growth of nanotubular oxide layer on Ti-Ni alloys with different Ni contents
   Applied Surface Science (in press).

4. Min-Su Kim, Hiroaki Tsuchiya, Toshiaki Erami, Shinji Fujimoto
   Formation of nano-structured oxide layers formed on Ti-Fe alloys by anodization
   Materials Transactions (accepted).

Other Publication

1. Min-su Kim, Yong-Hee Lee, Jung-Pil Noh, Tae-Hyun Nam, Yeon-Wook Kim, Shuichi Miyazaki.
   Crystallization behavior of cold worked Ti-30Ni-20Cu (at%) alloy ribbons Intermetallics, **18** (2010) 1913.

2. Min-su Kim, Gyu-bong Cho, Jung-Pil Noh, Young-Min Jeon, Yeon-Wook Kim, Shuichi Miyazaki and Tae-Hyun Nam.
   Grain refinement of a rapidly solidified Ti-30Ni-20Cu alloy by two-step annealing Scripta Materialia, **63** (2010) 1001.

3. Min-su Kim, Young-Min Jeon, Yeon-Min Im, Yong-Hee Lee, Min-Gyun Kim, Tae-Hyun Nam.
   Crystallization Behavior of Ti-(50-x)Ni-xCu(at%)(x=20-30) Alloy Ribbons Transactions on electrical and electronic materials, **12** (2011) 20

4. Min-su Kim, Jung-Pil Noh, Gyu-bong Cho, Yeon-Wook Kim, Yinong Liu, Hong Yang, Tae-Hyun Nam.
   Crystallization and grain refinement of Ti-30Ni-20Cu(at%) alloy ribbons prepared by melt spinning
   Journal of Alloys and Compounds, **577S** (2013) S179.

5. Jae-hyun Kim, Hui-jin Choi, Min-suKim, Shuichi Miyazaki, Yeon-wook Kim, Byong Sun Chun, Tae-hyun Nam.
   Crystallization and martensitic transformation behavior of Ti-Ni-Sn alloy ribbons
   Intermetallics, **30** (2012) 51.

Presentations

International conferences

1. Min Su Kim, Shota Yamamoto, Hiroaki Tsuchiya, Shinji Fujimoto,
   Oxide Nanotube Coating of Ti-Ni Alloy by Self-organizing Anodization
   International Symposium on EcoTopia Science 2013, NAgoya, Japan, December, 2013

2. Min Su Kim, Hiroaki Tsuchiya, Shinji Fujimoto,
   Growth of oxide nanotube arrays on Ti-Ni alloy
   The 225th Electrochemical Society Meeting, Orlando, USA, May, 2014

3. Min Su Kim, Shota Yamamoto, Hiroaki Tsuchiya, Shinji Fujimoto,
   Growth of TiO_2 nanotube layers on Ti substrates with different microstructures
   The 227th Electrochemical Society Meeting, Chicago, USA, May, 2015

Acknowledgements

The author would like to express his grateful gratitude to ***Prof. Shinji Fujimoto*** of The Division of Material and Manufacturing Science, Osaka University, for his kind guidance, helpful suggestions, constructive discussion and invaluable encouragements throughout this work and then offering constant assistance during the doctor's course in Osaka University.

The author is greatly indebted to ***Prof. Makio Naito*** at Joining and Welding Research Institute, Osaka University and ***Prof. Hiromi Yamashita*** of The Division of Material and Manufacturing Science, Osaka University, for reviewing this thesis and their valuable comments.

The author is very grateful to ***Dr. Hiroaki Tsuchuya*** of The Division of Material and Manufacturing Science, Osaka University, for his helpful suggestion, discussion and guidance throughout this work.

The author is very grateful to ***Mr. Junji Nakata*** of Osaka University for the technical assistance and also for his kind help and constructive comments. The author also would like to thank all members of Prof. Fujimoto's Group for their helpful suggestions and collaborations during my study in Japan.

The author would like to take this opportunity to thank ***Prof. Tae-Hyun Nam*** at Gyeongsang national university for his hearty encouragement and helps. Furthermore, the author thanks the members in the Prof. Nam's Group for their friendships, encouragement and helps.

Finally, the author would like to thank family members and loved ones for their patience and advice. And his wife has assisted the author in innumerable ways, whatever the author might say here cannot do full justice to the extent and the value of her contribution. The period during the study in Japan, will remain associated with the birth of son, *se-yun*. The author has dedicated this dissertation to him.

Min-Su Kim

December 2015